Research advances in the macromolecules of tomorrow through synergistic research in the NSF Center for Sustainable Polymers

Farihah M. Haque, **, * Jacob S. A. Ishibashi, **, * Claire A. L. Lidston, **, * Huiling Shao, **, * Frank Bates, * Alice B. Chang, * Geoffrey W. Coates, * Christopher J. Cramer, * Paul J. Dauenhauer, * William R. Dichtel, * Christopher J. Ellison, * Ethan A. Gormong, * Leslie S. Hamachi, * Thomas R. Hoye, * Mengyuan Jin, * Julia A. Kalow, * Hee Joong Kim, * Gaurav Kumar, * Christopher J. LaSalle, * Stephanie Liffland, * Bryce M. Lipinski, * Jennifer McCambridge, * Yutong Pang, * Riffat Parveen, * Xiayu Peng, * Yanay Popowski, * Emily A. Prebihalo, * Yernaidu Reddi, * Theresa Reineke, * Laura Seifert, * Daylan T. Sheppard, * Jeremy L. Swartz, * William B. Tolman, * Bess Vlaisavljevich, * Jane Wissinger, * Shu Xu, * Marc A. Hillmyer*, *

[▽]Department of Chemistry, Washington University in St. Louis, St. Louis, Missouri 63130-4899, United States

Abstract

The mission of the NSF Center for Sustainable Polymers (CSP) is "to transform how plastics are made, unmade, and remade through innovative research, engaging education, and diverse partnerships that together foster environmental stewardship. CSP participants aim to design, prepare, and implement polymers derived from renewable resources for a wide range of advanced applications, and to promote future economic development, energy efficiency, and environmental sustainability in the emergent area of biobased products." (https://csp.umn.edu/about/) In this Chemical Reviews contribution we review a curated collection of achievements by CSP participants since the inception of the Center at the University of Minnesota in 2009. The review highlights our signature accomplishments across the broad portfolio and is organized into four research themes: Feedstocks, Polymerization Processes and Techniques, Intended Use, and End of Use. We emphasize those successes that benefitted from collaborative engagements across disciplinary lines, a hallmark of the Center's integrative culture. We also highlight the Center's outreach and data management efforts that are central to our overarching goals.

[†]Department of Chemistry, University of Minnesota, Minneapolis, Minnesota 55455, United States

[‡]Department of Chemical Engineering and Materials Science, University of Minnesota, Minnesota 55455, United States

[§]Department of Chemistry and Chemical Biology, Baker Laboratory, Cornell University, Ithaca, New York 14853-1801, United States

Department of Chemistry, Northwestern University, Evanston, Illinois 60208, United States Department of Chemistry, University of South Dakota, Vermillion, South Dakota 57069, United States

[#] Equal contributions by these lead coauthors; * Corresponding author

TOC graphic



Table of Contents:

1.	Introduction	4
2.	Feedstocks	5
	2.1. Commodity Monomers	6
	2.1.1. Dienes	6
	2.1.2. α-Olefins	11
	2.1.3. Acrylates	18
	2.2. New Monomers	19
	2.2.1. Lactone-type Monomers from Terpenes, Carboxylic Acids, and Lignin	19
	2.2.2. Acrylate-type Monomers from Lignin and Sugar	22
	2.2.3. Olefin-type Monomers from Sugar	28
	2.2.4. Multifunctional Alcohols and Carboxylic Acids	29
	2.2.5. Bifunctional Silyl Alcohols	31
3.	Polymerization Techniques and Processes	32
	3.1. Ring-opening Copolymerization of Epoxides with Cyclic Anhydrides and CO ₂	32
	3.2. Ring-Opening Transesterification Polymerization of Lactones	40
	3.3. Other Polymerization Processes to Produce Sustainable Polymers	51
4.	Intended Use	54
	4.1. Thermoplastic Elastomers	54
	4.2. Thermoplastics	61
	4.3. Thermosets	66
	4.4. Elastomers	69
	4.5. Green Applications	71
5.	End of Use	74
	5.1. Degradation	75
	5.2. Compatibilization	79
	5.3. Reprocessable Materials	82
6.	Outreach of CSP	89
7.	Data Management	93
8.	Conclusion	94
9	References	94

1. Introduction

The National Science Foundation (NSF) Center for Sustainable Polymers (CSP) was established in 2009 at the University of Minnesota and initially supported by the Initiative for Renewable Energy and the Environment through an award for a project titled "Sustainable polymers: Tomorrow's advanced materials." Over the decade since that initial award, our interest, activity, commitment, and contributions to sustainable polymer research and technology has grown substantially. NSF support for the Center began in 2011 through its Centers for Chemical Innovation program, and researchers in the Center continued to pursue transformational, basic research in a broad range of topics within the field of sustainable polymer science. New technologies and innovations are built from a strong foundation of basic research that establishes in-depth understanding of fundamental principles and an associated molecular-level comprehension. In a field as vast as sustainable polymers, this approach requires broad-ranging efforts in the chemical sciences. The breadth of this scope in turn necessitates a collaborative approach that integrates different disciplinary expertise and brings together scientists and engineers from diverse backgrounds to solve one of the most vexing problems of our generation: we need plastics in modern society, but their non-renewable origins and indiscriminate disposal result in environmental damage. This damage is likely irreparable and intensifying. New ideas, understanding, approaches, and technologies are paramount for the plastics industry to shift from its current unsustainable paradigm. A more sustainable enterprise, addressing environmental, societal, and economic needs, will assure future generations can build on these practices. This central tenet of sustainability drives the research in the CSP, and it is through collaborative efforts and the integration of our complementary sets of research expertise that we have been able to make the progress reported in this review.

The research of the CSP is summarized in our three Grand Challenge Project Areas: (a) efficient and sustainable conversion of biomass to polymer ingredients, (b) high-performance sustainable plastics and elastomers, and (c) sustainable polymer degradation, chemical recycling, and compatibilization. This structure illustrates what we view as the main priorities for sustainable polymers: sustainable resources, highly effective in their intended use, and sustainable solutions after use. To further contextualize our research, we recently developed a Sustainable Polymer Framework to highlight the relevant sustainability principles and help our researchers and others clearly see how our research efforts are aimed at particular areas that could all contribute to a sustainable polymer future. A graphic that summarizes our efforts and contributions is shown in **Figure 1**, and we summarize this new framework as follows: "Overall, the Sustainable Polymer Framework is meant to encourage focused advancement in fundamental research in the various sub-categories while maintaining a broader vision of the interconnected systems that define a sustainable polymer."

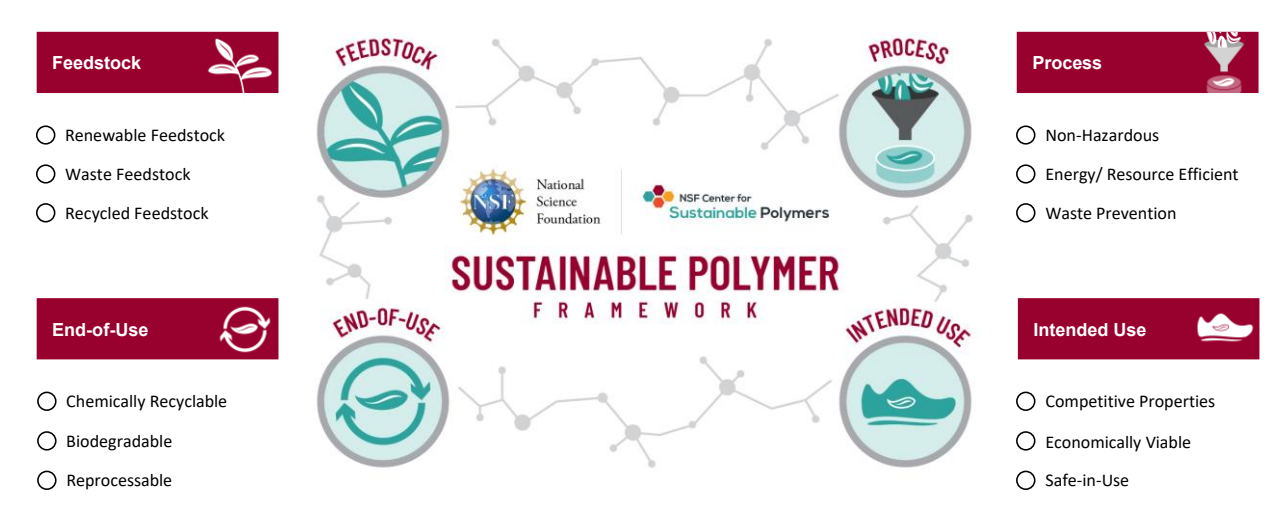


Figure 1. The CSP Sustainable Polymer Framework

In this review of the CSP's accomplishments to date, we have organized our research according to the CSP Sustainable Polymer Framework.² The four sections describing research activity align with the Framework to codify our newly established categorization and lead the way for others. By design, many CSP projects bridge several categories, and they will be described in detail in the most relevant sections. The fifth section of the review covers some of our important contributions to outreach, education, and data management. We intend this last section to provide the reader with a sense of the broader mission of the CSP. Here we highlight our efforts with i) sustainable polymer education for young learners through 4-H, ii) educational initiatives for CSP members that help broaden our scientific understanding outside our more-narrow disciplinary training, iii) teaching laboratories that translate sustainable polymer research can be translated into teaching laboratories for undergraduate students, and iv) data accessibility as it pertains to our published research.

2. Feedstocks

To avoid depleting non-renewable resources, the CSP has sought to develop efficient and sustainable methods to convert biomass or waste feedstocks to polymer products. To date, monomers used in the synthesis of established commodity polymers are largely derived from fossil fuels. Plants provide a renewable source of macromolecules (*e.g.*, cellulose and lignin) and small molecules (*e.g.*, sugars, terpenes, and fatty acids) that may be transformed into polymer feedstocks. Alternatively, valorization of industrial byproducts (*e.g.*, CO₂, limonene, milk permeate) into monomer feeds could mitigate pollution and recover embedded value. To this end, the CSP has endeavored to develop sustainable routes to both established commodity monomers for commercial products and alternative monomers for new polymeric materials (**Figure 2**). In addition to establishing renewable sources, sustainable monomer syntheses should implement nontoxic, low waste, and energy efficient transformations; the CSP has therefore focused on atom economy, catalysis, green or minimal solvents, and biosynthetic pathways. Finally, it is essential to assess the economic viability of these routes in absolute terms and/or relative to existing processes.

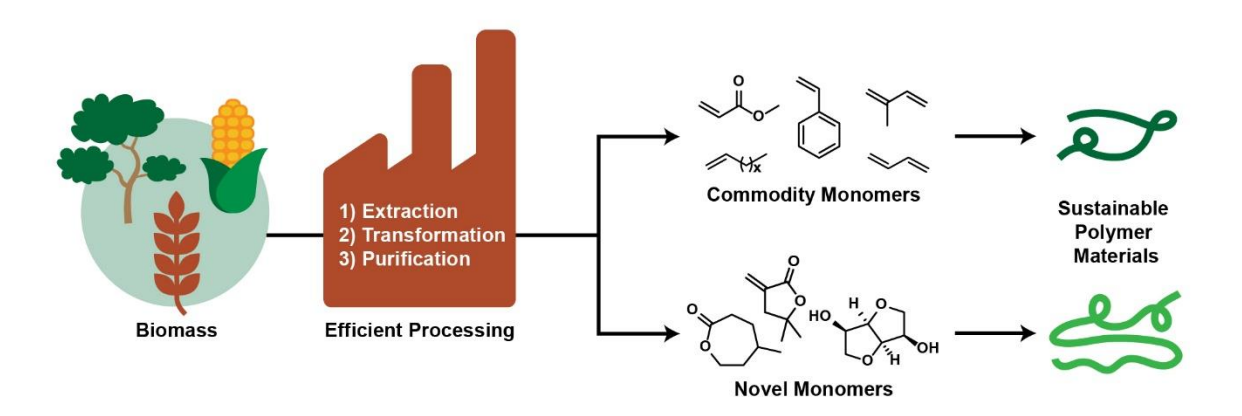


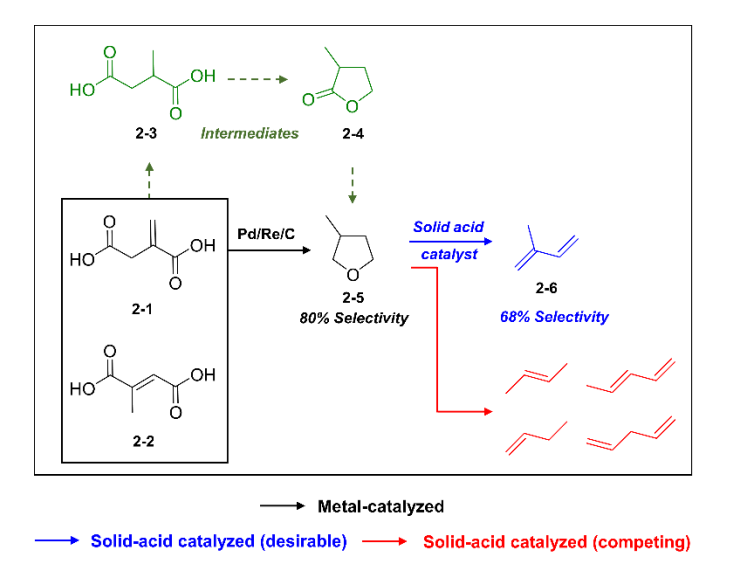
Figure 2. Conversion of biomass to commodity or novel monomers for sustainable polymers.

2.1. Commodity Monomers

Significant research efforts have been dedicated to converting biomass feedstocks into commodity monomers, such as isoprene, styrene, and methyl acrylate. Ideally, sufficiently pure bio-sourced commodity monomers could be directly incorporated into existing polymer industry infrastructure.⁴ Yet large-scale commodity chemicals produced from fossil fuels are typically less expensive than their biomass-derived counterparts.⁵ In addition to significant differences in feedstock costs, conversion inefficiencies further increase the price of biomass-derived monomers.³ Research in the CSP has therefore focused on developing highly active and selective catalysts and high-yielding, atom-efficient pathways to commodity monomers from biomass. Deoxygenation reactions of acids, esters, and phenols have emerged as common methods to obtain largely hydrocarbon products from heteroatom-containing feedstocks.

2.1.1. Dienes

While natural rubber can be sourced from a variety of plants, ^{6,7,8} synthetic variants are obtained from polymerizing fossil-fuel-derived dienes. ^{9,10,11} CSP researchers designed a cascade thermocatalytic process to convert itaconic acid (2-1), a fermentation product of glucose, to isoprene (2-6) in two stages (Scheme 1). ^{12,13} In the upstream condensed-phase process, 2-1 first undergoes hydrodeoxygenation to the methyl-γ-butyrolactone (2-4) intermediate via 2-methylsuccinic acid (2-3). Supported metal catalysts then effect hydrogenation/dehydration under high pressure (50–120 bar) to afford 3-methyltetrahydrofuran (2-5). ¹³ The second downstream ambient pressure process comprises the tandem ring-opening dehydration (*i.e.*, dehydradecyclization) of 2-5 to 2-6 in the vapor-phase on solid-acid catalysts. ¹²



Scheme 1. The cascade thermocatalytic process to convert itaconic acid (2-1) or mesaconic acid (2-2) to isoprene (2-6) via intermediates 2-methylsuccinic acid (2-3) and methyl- γ -butyrolactone (2-4) (green). ^{12,13}

For the upstream processing step, Abdelrahman et al. found that 10 wt% Pd/C catalyzed the complete conversion of **2-1** to **2-4** under mild temperatures (<240 °C). ¹² However, the authors observed negligible formation of 2-5. Remarkably, adding Re to the Pd/C catalyst (10 wt% Pd-10 wt% Re)/C significantly improved the yield of 2-5 (~80%) at complete 2-1 consumption, presumably due to enhanced 2-4 conversion. To probe the mechanism of the multistep catalysis and investigate the need for a bimetallic catalyst (Pd-Re) for producing 2-4, Park et al. investigated the kinetics of individual process steps in the absence of Re on 10 wt % Pd/C. 13 The hydrogenation of 2-1 to 2-3 and subsequent hydrodeoxygenation to 2-4 occurred at rates over an order of magnitude higher than the subsequent ring-opening of 2-4. This result corroborates the notion that **2-4** conversion is the kinetic bottleneck, as observed by Abdelrahman *et al.* using the Pd catalyst in the absence of Re. 12 Park et al. conjectured that Pd likely facilitates dissociative adsorption of hydrogen to reduce the carbonyl, while Re promotes ring-opening of 2-4 via C-O activation. Moreover, due to its oxophilicity, Re may extract oxygen from the feed to form Brønsted acidic Re-OH moieties in the hydrogen atmosphere; these species would further accelerate conversion of the hydrogenated intermediate (namely, 2-methyl-1,4-butanediol) to 2-5. By optimizing the ratio of Pd and Re in the bimetallic catalyst (Pd:Re molar ratio 3.5:1), the researchers achieved a twentyfive-fold increase in 2-5 formation rates from 2-4.

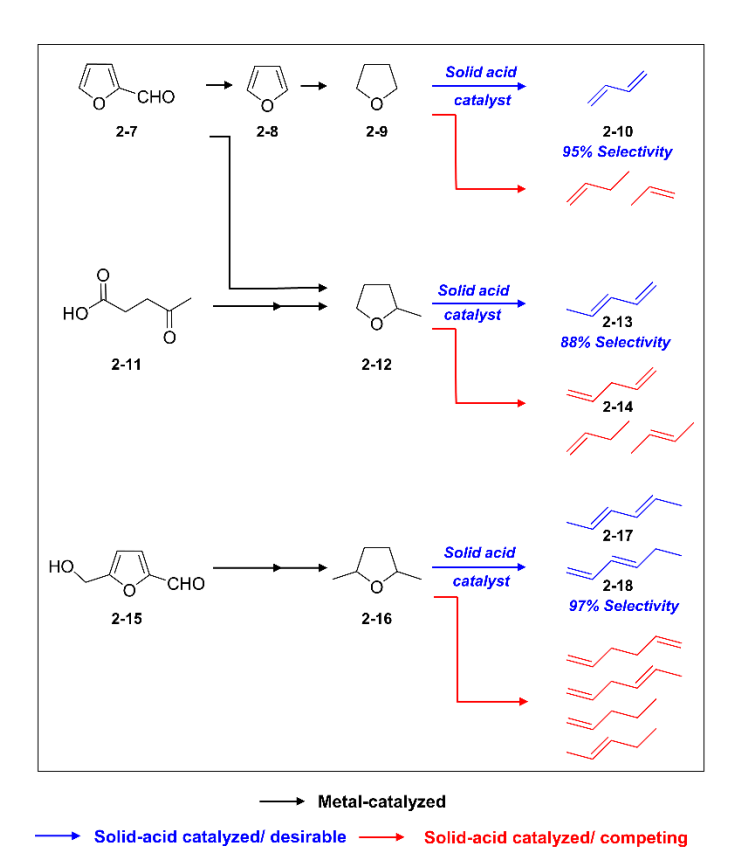
To investigate downstream vapor-phase deoxygenation strategies, Abdelrahman *et al.* screened solid acid catalysts using a high-throughput micro-catalytic pulsed reactor to assess **2-6** formation from a **2-5** feed. Saturated furans, including **2-5**, undergo rate-limiting ring opening on Brønsted acidic sites to form surface alkoxides prior to dehydration to dienes. The predominant competing pathway is a retro-Prins condensation, which results from fragmentation of the adsorbed C_n ether/alkoxide to the C_{n-1} olefin and formaldehyde in equimolar amounts. Accordingly, the main byproducts of the **2-5** pathway comprised butenes and formaldehyde. Among the catalysts tested, a phosphorus-containing solid acid catalyst exhibited moderately high selectivity of \sim 70% for **2-6**

under optimized reaction conditions (\sim 320 °C, space velocity \sim 1 s⁻¹). Linear pentadiene byproducts were formed via a methyl shift to the extent of \sim 20%.

Lundberg *et al.* performed a technoeconomic evaluation to assess the feasibility and challenges of implementing the conversion of sugar-derived acids to **2-6** on an industrial scale. Starting from **2-1** or **2-2**, hydrodeoxygenation with H₂ is expected to achieve multiple reduction steps in a single, multi-phase reactor over the optimized Pd-Re/C catalyst (*vide supra*). Azeotropic distillation over two columns would next separate the resulting **2-5** from water with a recovery of >99.7%. A phosphorus-containing solid acid catalyst would be used to effect dehydra-decyclization, yielding **2-6** and water, in addition to pentadienes, butene, propylene, and formaldehyde byproducts. Molecular sieves may be used to remove water before two distillation steps to first recover and recycle **2-5** and then remove the low molecular weight components. Heating the recovered mixture of pentadienes over a Mo hexacarbonyl zeolite catalyst should afford a single high-boiling isomer, facilitating the final distillation step to provide **2-6** in 99% purity.

For a plant processing 50 kton yr⁻¹ of **2-2** to 13.6 kton yr⁻¹ of isoprene (**2-6**), Lundberg *et al.* estimated a total capital investment of \$63.5 million: roughly half of this value arises from costs associated with the Pd hydrodeoxygenation catalyst. Based on a 35% tax rate and a 10% minimum annual rate of return over 30 years, the authors calculated a minimum selling price (MSP) of \$4.24 kg⁻¹ for **2-6**. Nearly 90% of the MSP arises from feedstock cost, accounting for the purchase price of **2-2** and **2-1**, the mass lost to water, and the moderate molar selectivity (~50%). Consequently, acid purchase price and catalyst selectivity strongly impact the MSP, while changes in operating cost, byproduct sale price, and Pd and H₂ prices had negligible influence. Further optimizing the selectivity of hydrodeoxygenation and dehydra-decyclization has the potential to decrease the MSP of **2-6** to \$2.50 kg⁻¹, which is competitive with its current production costs. The authors determined the total carbon efficiency (moles of product C per moles of feed C) to be ~60%. The ratio of waste to products (E factor) is high (4.7) considering only the **2-6** monomer; accounting for valuable byproducts decreases the E factor to 0.8. Notably, the overall environmental impact of the proposed process also depends on efficient glucose fermentation from sustainable crops to provide the **2-1** and **2-2** acid feedstocks.

The prevalence of linear diene byproducts formed during **2-6** production suggests dehydradecyclization may be a useful strategy for production of linear butadiene and pentadiene monomers. To develop conditions that favor linear diene formation, Abdelrahman *et al.* first investigated the transformation of unsubstituted tetrahydrofuran (**2-9**) to a single dehydradecyclization product, 1,3-butadiene (**2-10**) (**Scheme 2**). Because **2-10** is currently obtained from *n*-butane dehydrogenation or isolated as a byproduct of ethylene production during naphtha cracking; this alternative approach would represent a renewable source for synthetic rubber. Abdelrahman *et al.* achieved high selectivity for **2-10** (85–99%) on a phosphorus-containing solid acid at both low (9%) and high (89%) conversions.



Scheme 2. The catalytic conversion of other biomass-derived saturated furans (2-9), (2-12), and (2-16) to the corresponding dienes. ^{19,23,25}

Kuznetsov *et al.* assessed the viability of a modified process starting from furfural (2-7) on an industrial plant scale (**Scheme 2**).²³ After decarbonylation of **2-7** to furan (**2-8**) and hydrogenation to **2-9**, dehydra-decyclization provided high purity butadiene (**2-10**) monomer. The authors predicted that the gas phase decarbonylation could be performed under ambient pressure at 280 °C over two Pd/alumina catalyst reactors. Two distillation columns first removed unreacted **2-7** and furfuryl alcohol from a mixture of **2-8**, H₂, and carbon monoxide, followed by separation into gaseous and liquid components. The isolated **2-8** intermediate may be fed to a three-phase bubble-column reactor for hydrogenation over a 5% Pd/C catalyst with anticipated quantitative conversion. Dehydra-decyclization of the resulting **2-9** at 425 °C would yield **2-10** and water as the major products, with minor amounts of higher molar mass species, butene, and propene byproducts. The similar boiling points of **2-10** and 1-butene would likely necessitate downstream distillation and absorption columns to finally provide **2-15** in high purity (99.5%) on a production scale.

Kuznetsov *et al.* next evaluated the economic feasibility of the industrial scale conversion of **2-7** to **2-10** (**Scheme 2**). The proposed transformation of biomass-derived **2-7** to **2-10** requires a capital investment of \$61.5 million, including equipment, installation, catalyst syntheses, engineering, and contingency expenses. Of the three transformations, **2-7** decarbonylation accounts for 64% of the capital investment cost. Kuznetsov *et al.* determined the MSP of **2-10** to afford zero net present value over 30 years to be \$5.43 kg⁻¹. The **2-7** purchase price accounts for 83% of this amount, and

a sensitivity analysis corroborated that feedstock cost is the driving factor in setting the MSP. Because the maximum reported price of **2-10** to date is only \$2.40 kg⁻¹, the proposed process is not profitable in the current market. Kuznetsov *et al.* therefore identified possible routes towards economic viability: decreased cost of the **2-7** feedstock, increased demand for **2-10**, or increased costs associated with petroleum-based processes. While biomass offers a sustainable alternative to fossil fuel feedstocks, it is imperative to consider the energetic costs and greenhouse gas emissions associated with any industrial process. The authors determined the total carbon efficiency to be 58.4% for the conversion of **2-7** to **2-10**, with an E factor of 1.5, which is comparable to other bulk chemical processes.

In their original report, Abdelrahman et al. extended their dehydra-decyclization methodology to other methylated furanoic species: 2-methyltetrahydrofuran (2-12), which can be derived from 2-7 or levulinic acid (2-11), and 2,5-dimethyltetrahydrofuran (2-16), which can be derived from 5-(hydroxymethyl)furfural (2-15).¹⁹ Both 2-12 and 2-16 produced linear pentadienes and hexadienes, respectively, with high selectivity (>85%) at conversions below 50% on phosphoruscontaining solid acid catalysts (Scheme 2). While these results were promising, the active site structure of catalytic phosphorus species remained unclear. Cho et al. recently proposed that the active sites in these heterogeneous catalysts are weakly Brønsted acidic.²⁴ To assess the generality of this finding. Kumar et al. sought to test if other weakly Brønsted acidic materials could catalyze diene-selective dehydra-decyclization of saturated furans. 25 To that end, Kumar et al. employed borosilicate zeolites to convert 2-12 to linear pentadienes. Weakly acidic boron sites in different microporous environments consistently exhibited 10-30% higher diene selectivities than the strongly acidic aluminosilicate analogue, albeit at about 5-60-fold lower turnover frequencies (TOF) (Figure 3). The apparent kinetic parameters remained unaltered, with activation energy barriers within 5 kcal mol⁻¹ among all boro- or alumino-silicates as determined through Arrhenius studies. Moreover, borosilicate catalysts were exceptionally stable under the reaction conditions, deactivating ca. ten times more slowly than aluminosilicates under identical reaction conditions. Taken together, these results validate the hypothesis that decreasing the Brønsted acidity of the catalyst active site can enhance diene selectivities in furanic dehydra-decyclization.

Active site structure of solid acid catalysts

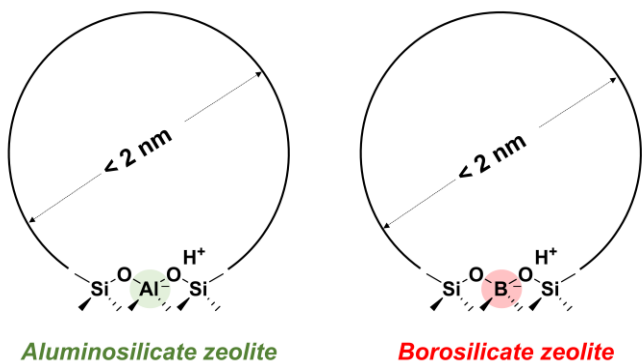


Figure 3. The active site structure of microporous aluminosilicate zeolites (left) and proposed active site structure of borosilicate zeolites (right).²⁵

Because conjugated dienes are typically more valuable for polymer applications, the authors next sought to minimize formation of the non-conjugated component during dehydra-decyclization from 2-12. The significantly higher thermodynamic stability of 2-13 prevents selectivity for this product from being equilibrium-limited under the investigated conditions. The authors therefore sought to promote 2-14 isomerization to 2-13 by operating the reactor under high bed residence times. On the microscale, these isomerization events were enhanced by increasing the crystallite sizes and volume density of active sites to promote longer diffusion lengths. Combining these improvements, the authors achieved an unprecedented 2-13 yield (86%) with near quantitative conversion (~98%) of 2-12 on a borosilicate solid acid.

2.1.2. α-Olefins

Decarbonylation of biomass-derived carboxylic acids to terminal α -olefins represents another promising route to renewable feedstocks for the polymer industry. The CSP has studied carboxylic acid decarbonylation reactions to understand the reaction mechanism and improve transition-metal catalysis.²⁶ It is often necessary to activate the weakly reactive carboxylic acid substrate to afford an anhydride^{27,28,29,30} or ester^{31,32,33} derivative, which may then enter the catalytic cycle. The cycle consists of three major steps: i) oxidative addition, ii) decarbonylative alkene formation, and iii) catalyst regeneration. Experimental and theoretical studies of the catalyst structure and reaction mechanisms have helped to optimize transition-metal complexes to achieve high α -olefin selectivity and yield (**Figure 4**).

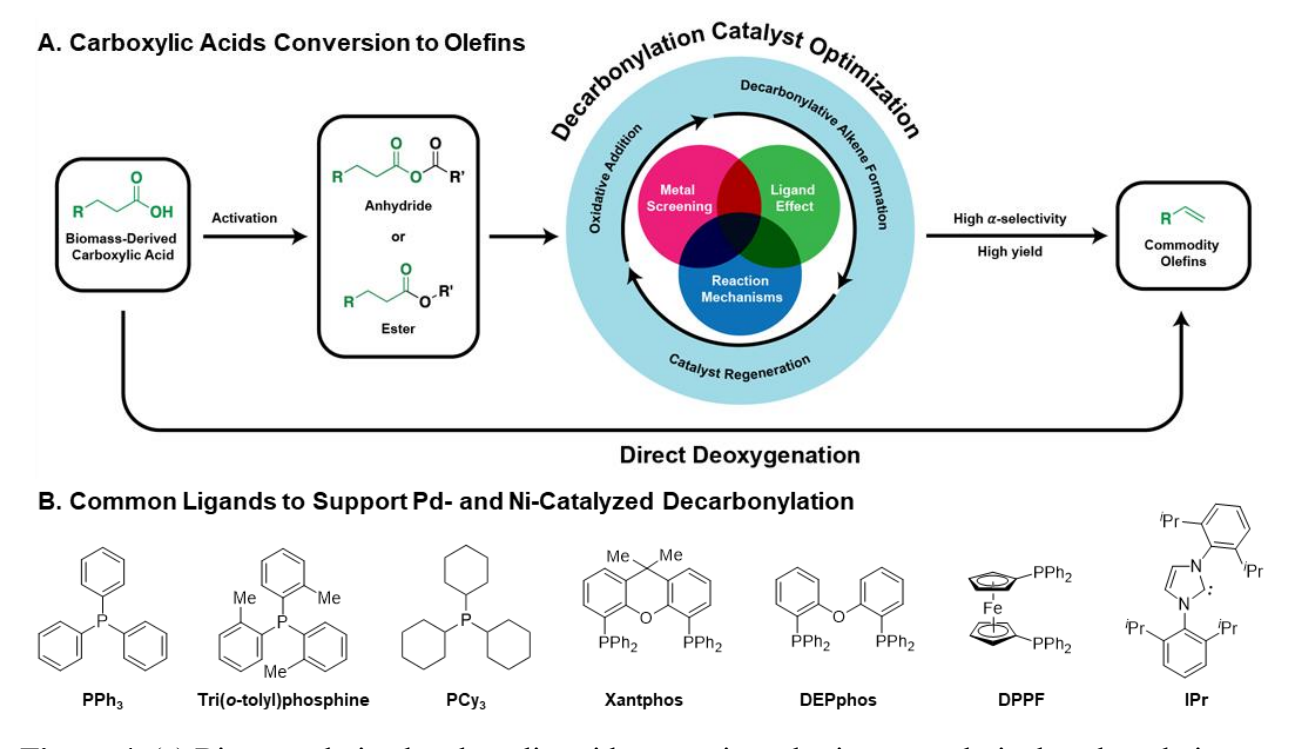
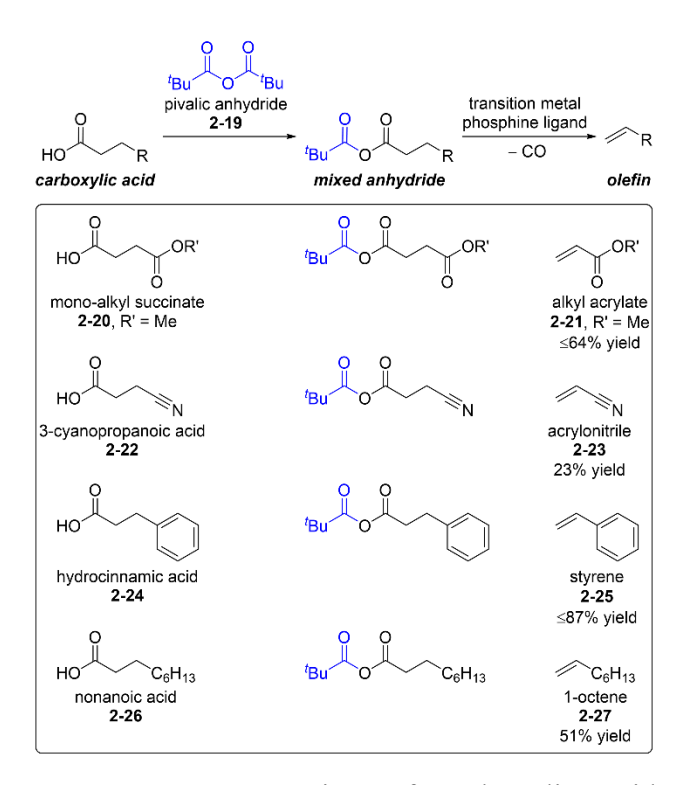


Figure 4. (a) Biomass-derived carboxylic acids are activated prior to catalytic decarbonylation to afford commodity olefins with high α -selectivity and yield (top pathway). Direct deoxygenation of carboxylic acids bypasses the activation and decarbonylation steps (bottom pathway). (b) Common ligands used to support decarbonylation and deoxygenation catalysts.

Miranda *et al.* studied the conversion of various bio-derived carboxylic acids to commodity monomers, including acrylates, styrene, and acrylonitrile, using pivalic anhydride (**2-19**) as the activating agent and palladium complexes as catalysts under moderate reaction conditions (**Scheme 3**). The high boiling point of **2-19** relative to that of the previously used acetic anhydride eliminates the need for multiple reagent addition steps during the reaction. Mono-alkyl succinates from renewable succinic anhydride react with **2-19** to form the activated intermediate. Pd(II)-catalyzed decarbonylation of the generated anhydride forms alkyl acrylates. Miranda *et al.* reported the highest yield of methyl acrylate (**2-21**) (64%) from methyl succinate (**2-20**) at 190 °C under N₂ using PdCl₂ and a bis[(2-diphenylphosphino)phenyl] ether (DPEphos) ligand. However, activation and decarbonylation of bio-derived 3-cyanopropanoic acid (**2-22**) using PdCl₂/PPh₃ afforded only 23% yield of acrylonitrile (**2-23**) due to competing polymerization under the reaction conditions.

Decarbonylation of hydrocinnamic acid (2-24) to styrene (2-25) produced more promising results: PdCl₂ (0.25 mol%) and bidentate phosphine ligands such as DPEphos and 4,6-bis(diphenylphosphino)-9,9-dimethylxanthene (Xantphos) (2.2 mol%) catalyzed the decarbonylation reaction with high yield (80%) and good selectivity (~80%) at 190 °C under N₂. Formation of CO corroborated a decarbonylation pathway. Doubling the phosphine ligand loading (4.4 mol%) increased the yield (87%) and selectivity (92%) for 2-25. Scaling the process to 25 g of 2-24 afforded 70% yield at a significantly lower Pd loading (0.01 mol%). Miranda *et al.* also evaluated the robustness of the 2-24 decarbonylation system. Changing the carrier gas from N₂ to air decreased the styrene yield by only 9%, while omitting rigorous drying procedures produced similar yields (78% with 2.2 mol% DPEphos).



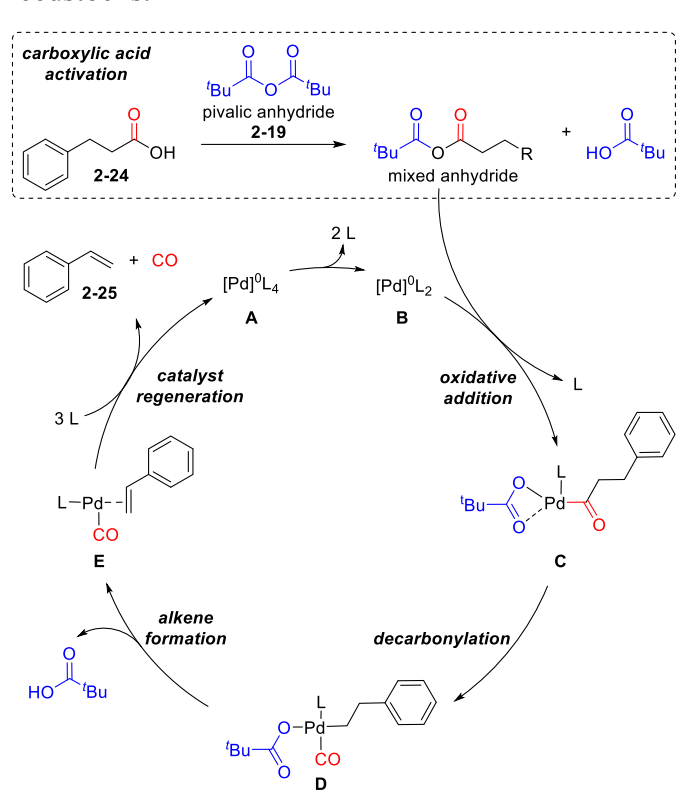
Scheme 3. Conversion of carboxylic acids to olefins via anhydride activation and decarbonylation. ^{28,30}

Ortuño *et al.* studied the reaction mechanism of Pd-catalyzed decarbonylation of **2-24** using density functional theory (DFT) calculations.²⁹ The authors evaluated different competing pathways to identify the most favored reaction pathway and studied the catalyst features controlling reaction rate and selectivity, all with the aim of designing a better catalyst (**Scheme 4**). The PdL4 complex (**A**) first loses two coordinated phosphines, forming complex **B**, which undergoes oxidative addition with the mixed anhydride C–OC(O)/Bu bond to form complex **C**. The κ^2 coordination of the pivalate moiety occupies an additional coordination site. Subsequent decarbonylation generates a CO ligand bound to the Pd-alkyl (complex **D**). Calculations suggested that the pivalate oxygen facilitates deprotonation of the Pd-alkyl, forming free pivalic acid and styrene-bound Pd (complex **E**). Dissociation of styrene and CO and re-coordination of the phosphine ligands regenerate the PdL4 catalyst (complex **A**).

Calculations also suggested that alkene formation is rate-limiting, with a free energy of activation of 34.6 kcal mol⁻¹. The PdL₃–CO species (en route from complexes **E** to **A**) is the free energy sink (-5.6 kcal mol⁻¹) of the entire catalytic cycle, and loss of CO and re-coordination of one phosphine ligand to regenerate PdL₄ (complex **A**) is endergonic by 7.6 kcal mol⁻¹. Overall, under standard state conditions with 1 atm CO pressure, the decarbonylation reaction is predicted to be slightly endergonic (2 kcal mol⁻¹). Taking into consideration removal of CO under experimental conditions, the authors calculated that the decarbonylation reaction with 10⁻⁵ atm CO pressure is exergonic by 8.6 kcal mol⁻¹.²¹ The stability of the PdL₃(CO) complex poses a problem in the absence of CO removal, because a different catalytic cycle becomes prevalent that involves

PdL(CO) after the loss of two phosphine ligands. Following oxidative addition to that species, the activation free energy for alkene formation (45.7 kcal mol⁻¹) is 11.1 kcal mol⁻¹ higher than that of the phosphine-ligated Pd analogue. Ortuño *et al.* thus emphasized that CO poisons the Pd catalyst, such that its efficient removal is crucial for productive decarbonylation.

Ortuño *et al.* also explored the effect of the anhydride additive and phosphine ligand on reaction performance. Although the pivalate moiety contributes to deprotonation of the Pd-alkyl (*vide supra*), the authors were not able to identify any significant correlation between the energy barrier to alkene formation and carboxylate basicity. Bulkier phosphine ligands, by contrast, were computed to significantly decrease the reaction energy barrier: replacing substituting phenyl groups with tri(*ortho*-tolyl) groups decreased the predicted barrier to alkene formation by 8.6 kcal mol⁻¹. These insights into the decarbonylation mechanism and factors governing catalyst performance may enable more efficient decarbonylative transformations of biomass to olefin feedstocks.



Scheme 4. Proposed reaction mechanism for decarbonylation of hydrocinnamic acid (2-24) to styrene (2-25) over Pd catalyst.²⁹ L stands for phosphine ligand.

Expanding these efforts, John *et al.* investigated first-row transition metals as earth abundant and inexpensive alternatives to Pd catalysts for the decarbonylation of activated carboxylic acids.³⁰ Using high-throughput screening, the authors evaluated Fe(II), Co(II), Cu(I), Ni(0), Ni(II), Mn(II), Pd(II), and Zn(II) metal precursors with various ligands for the decarbonylation of **2-24** activated by **2-19**. Initial screens revealed phosphine ligands supporting Ni centers to be the most promising catalysts. Using a Ni(PPh₃)₄ metal precursor and DPEphos ligand afforded the highest **2-25** yield

(34%) at 180 °C. Addition of KI improved conversion and decreased the amount of ethylbenzene byproduct but had no effect on the ultimate **2-25** yield. John *et al.* showed that decarbonylation of nonanoic acid (**2-26**) to 1-octene (**2-27**) proceeded with moderate yield (51%) and high α -selectivity (91%) in 2 hours using Ni(PPh₃)₄/DPEphos at 180–190 °C (**Scheme 3**). A Ni(COD)₂/bis(diphenylphosphino)ferrocene (DPPF) complex improved the yield of **2-27** to 78% with similar α -selectivity (90%) under the same reaction conditions.

John *et al.* analyzed the mechanism of **2-24** decarbonylation with a Ni(PPh₃)₄ catalyst using complementary experiments and DFT calculations. The authors observed that 51% of **2-24** dimerized to hydrocinnamic anhydride; only 35% reacted with **2-19** to generate the mixed anhydride, partially explaining the low conversion to **2-25**. Increasing the reaction temperature improved reaction rates with Ni(PPh₃)₂(CO)₂, indicating CO dissociation to regenerate the catalyst may be rate-limiting. DFT calculations further elucidated the reaction mechanism of Ni-catalyzed decarbonylation of **2-24**. In general, the reaction mechanism using the Ni catalyst is very similar to its Pd-catalyzed counterpart investigated by Ortuño *et al.*²⁹ (*vide supra*). Calculations predicted NiL₃(CO) to be the most stable complex. Loss of CO and phosphine coordination to regenerate NiL₄ was computed to be endergonic by 26.2 kcal mol⁻¹ under standard-state conditions. Similar to the Pd case, Ni catalyst regeneration becomes rate limiting at high CO pressure (1 atm), and the poisoning effect is considerably stronger for Ni than for Pd. Under reaction conditions that maintain sufficiently low CO pressures, alkene formation becomes the rate-limiting step (activation energy of ~25.8 kcal mol⁻¹).

As an alternative to forming a mixed anhydride, carboxylic acids can also be activated via conversion to esters. CSP researchers have worked to understand the decarbonylation mechanism beginning from the ester-activated species to develop highly active catalysts for such transformations. In an early report, John et al. reported that conversion to the corresponding paranitrophenyl ester facilitates decarbonylation to the desired olefin, CO, and para-nitrophenol (2-28) (Scheme 5).³¹ After activating 2-24 by reaction with 2-28, the researchers screened nickel and palladium salts for the decarbonylation reaction. In the presence of phosphine ligands, the ester instead hydrolyzed to the carboxylic acid. Omitting the phosphine ligand afforded moderate conversion to 2-25, 46% yield in 16 h, while stoichiometric amounts of alkali and alkaline-earth metal halides (such as LiCl or CaCl₂) further improved reaction efficiency. Applying the optimized conditions to an expanded substrate scope afforded 2-25, tert-butyl acrylate (2-29), and 2-23 products in moderate yields. Decarbonylation of para-nitrophenyl-2-phenylbutanoate (2-31) or para-nitrophenyl-4-phenylbutanoate (2-33) produced mixtures of β -methylstyrene (2-32) trans and cis isomers (8:1) via chain-walking. Longer chain fatty acid precursors afforded mixtures of olefin isomers. Extending this methodology, the authors performed the decarbonylation in tandem with a Heck-type coupling with aromatic esters; this approach represents the first report of a carboxylic acid being used as a masked olefin.

Scheme 5. Conversion of carboxylic acids to olefins via ester activation and decarbonylation. 31,32

Despite these advances, improvement in α -selectivity is desirable for mass production of commodity olefins from fatty acids. One method to control α -selectivity is to further tune the ancillary ligands. John *et al.* developed a decarbonylation methodology using a Pd(II) catalyst and mixed Xantphos and DPEphos ancillary ligands, yielding high conversion and high selectivity for linear α -olefins. Decarbonylation of *para*-nitrophenyl nonanoate (2-30) to 2-27 using PdCl₂ and LiCl proceeded with low α -selectivity (14%) at 160 °C. The addition of a bidentate phosphine ligand such as DPEphos increased the α -selectivity to 70% under the same reaction conditions. Increasing the reaction temperature to 190 °C and exchanging the DPEphos ligand for the more rigid Xantphos resulted in 82% α -selectivity and >95% conversion. The ability of the phosphine ligand to promote α -selectivity was further studied with substrates whose products would be prone to isomerization to form more stable internal olefins. For example, a 1:1 molar mixture of Xantphos and PPh₃ supported Pd-catalyzed decarbonylation of 2-33 with 92% α -selectivity to

allylbenzene (**2-34**) over the conjugated isomer **2-32**; without the addition of ligands, the α -selectivity was lower than 5%. Using Xantphos/PPh₃ improved the α -selectivity of **2-30** to >98%. Moreover, the *N*-heterocyclic carbene ligand 1,3-bis(2,6-diisopropylphenyl)imidazole-2-ylidene (IPr) was more effective than PPh₃ for decarbonylation of longer-chain fatty acid esters, achieving 85–90% conversion and >98% α -selectivity with a wide range of fatty acid esters. The authors proposed that the different ancillary ligands facilitate distinct elementary steps. Xantphos facilitates rapid olefin dissociation from the metal center, preventing Pd-catalyzed isomerization to preserve α -selectivity. Alternatively, IPr facilitates oxidative addition and stabilizes reaction intermediates, improving ultimate conversion.

John et al. further investigated this mixed ligand effect using DFT calculations.³² The authors proposed that olefin isomerization occurs immediately after the alkene formation step: prior to dissociation from Pd, the alkene may rotate and reinsert at a different carbon before β -hydride elimination to the undesired internal olefin. John et al. first simulated the decarbonylation of paranitrophenyl esters with single ligands. The rate-limiting step of the Pd/Xantphos-catalyzed reaction is alkene formation, which has a free energy of activation of 42.9 kcal mol⁻¹. With the Pd-IPr catalyst, oxidative addition was rate-limiting, with a free energy barrier of 32.3 kcal mol⁻¹. The lower activation free energy with IPr is consistent with the higher experimental conversions. However, the IPr system exhibited a lower free energy barrier to isomerization (5.4 kcal mol⁻¹). By contrast, the Xantphos ligand increased the isomerization energy barrier to 8.4 kcal mol⁻¹. favoring alkene dissociation and stabilizing the low-coordinated Pd-complex after alkene dissociation. The authors next considered decarbonylation catalyzed by Pd complexes with mixed ligands. The calculations suggested that formation of mixed ligand complexes in which both IPr and Xantphos coordinate to the Pd center is feasible, with free energies of intermediates and transition states comparable to those in the Xantphos system. Additionally, steric constraints in the mixed ligand system prevented alkene rotation at Pd. Computing the potential energy as a function of distance between the alkene and the Pd center revealed a significantly slower increase in potential energy for the Xantphos and mixed-ligand systems relative to that for the IPr system. This result demonstrated that alkene dissociation from Pd is facilitated in the mixed ligand system, consistent with suppressed isomerization and high α -selectivity. Because Xantphos controls α selectivity and IPr maintains high conversion, the combination of both ligands supporting a single Pd center enables the transformation of a wide range of carboxylic acids to olefin products with high yield and selectivity.

Activation of the carboxylic acid starting material necessitates an additional synthetic transformation and purification step before decarbonylation to the desired olefin product. In an effort to circumvent isolation of the activated ester intermediate, Fieser *et al.* established a dual-catalytic method to convert fatty acid methyl esters to a mixture of olefins (**Scheme 6**). Methyl palmitate (**2-35**) first undergoes ZnCl₂-catalyzed transesterification with 2-pyridinemethanol (**2-36**) to form the activated palmitic ester (**2-37**) in 67% yield. Subsequent decarbonylation using Ru₃(CO)₁₂ and tricyclohexylphosphine (PCy₃) ligand provided a mixture of olefin products in up to 95% yield. Combining the ZnCl₂ and Ru₃(CO)₁₂/PCy₃ catalysts enabled a simple one-pot olefin synthesis from **2-35** and **2-36** with a final yield of 64%.

HO R =
$$C_{13}H_{27}$$
 methyl palmitate 2-35 Proposition activated palmitic ester 2-37 Ru3(CO)₁₂ PCy₃ $\overline{}$ $\overline{}$

Scheme 6. Dual catalytic method to activate and decarbonylate fatty acid methyl esters to olefin products.³³

To bypass the stoichiometric activation step entirely, John et al. developed the direct deoxygenation of aliphatic carboxylic acids using stoichiometric PPh3 reductant and catalytic earth-abundant nickel salts at modest temperatures (<200 °C) (Scheme 7).³⁴ Of the first row transition metals screened, Ni(II) salts afforded the highest yields (<86%), although Ni(0)(PPh₃)₄ increased selectivity for the α -olefin product (<70%). Deoxygenation of various long-chain carboxylic acids under reduced pressure afforded the corresponding olefins in good yields (51– 88%) and modest selectivity (17–71% α -product). The authors sought to avoid the challenging removal of the OPPh₃ byproduct by regenerating PPh₃ in situ using 1,1,3,3-tetramethyldisiloxane (TMDS) and Cu(OTf)2. This approach enabled the use of substoichiometric amounts of PPh3; however, the volatility of TMDS required a closed system. These conditions precluded removal of the α -olefin by distillation and thus led to significant isomerization to internal olefin products. The methodology can therefore be adapted according to the system requirements: low NiI₂ loadings (0.1 mol%) and stoichiometric PPh₃ reductant primarily afford α -olefins, while less stringent selectivity requirements permit a fully catalytic transformation (2.8 mol% each of NiI₂, PPh₃, TMDS, and Cu(OTf)₂). This atom economical methodology represents an advance towards direct deoxygenation of carboxylic acids to olefin feedstocks.

$$\begin{array}{c} & 10 \text{ mol}\% \text{ Nil}_2 \\ \text{PPh}_3 \\ \\ & \\ \text{HO} \\ & \\ \text{X} = 3-13 \\ & \\ \text{X} \\ & \\ \text{X} = 3-13 \\ & \\ \text{X} \\ & \\ \text{Z.8 mol}\% \text{ Nil}_2 \\ & \\ \text{2.8 mol}\% \text{ Cu(OTf)}_2 \\ & \\ \text{5-14 mol}\% \text{ PPh}_3 \\ & \\ & \\ \text{TMDS} \\ & \\ & \\ \text{mixtures of internal olefin isomers} \end{array}$$

Scheme 7. Direct deoxygenation of long chain carboxylic acids.³⁴

2.1.3. Acrylates

Yee *et al.* sought to convert biomass-derived methyl and ethyl lactates (2-38 and 2-39, respectively) into the corresponding acrylates (2-42 and 2-43, Scheme 8).³⁵ The authors therefore developed Pd-catalyzed hydroesterification of 2-38 and 2-39 with CO and ethylene to form methyl or ethyl 2-(propanoyloxy)propanoate intermediates (2-40 and 2-41, respectively), which could then undergo pyrolysis. By optimizing Pd loading, as well as ligand and acid concentrations, the authors reported good yields of 2-40 (79%) and 2-41 (91%) in EtOAc. In accordance with green chemistry principles, the reaction could be carried out under neat conditions without compromising the ester yield (~84% of 2-40). High temperature (550–560 °C) pyrolysis of esters 2-40 and 2-41 yielded modest amounts of 2-42 (~59%) and small quantities of 2-43 (~10%). In both cases, propanoic acid and propanoic anhydride were the only byproducts. The low product yields were

largely due to incomplete mass recovery (\sim 70% and \sim 30% for the methyl and ethyl cases, respectively) arising from deficiencies associated with the pyrolysis reactor, rather than the intrinsic pyrolysis chemistry.

Scheme 8. Conversion of biomass-derived methyl and ethyl lactates into the corresponding acrylates.³⁵

2.2. New Monomers

An alternate approach to convert biomass feedstocks to commodity materials is to develop alternative monomer classes. Monomers that closely resemble their biomass source may require fewer chemical transformations, increasing atom efficiency and minimizing mass lost to byproducts and waste. Moreover, biomass readily imparts heteroatom functionality, stereochemical features, and reactive units; these complex architectures may afford desirable properties distinct from those of hydrocarbon-derived materials.³ The CSP's efforts to develop novel monomer feeds from lignin, terpenes, sugars, and carboxylic acids, among other promising biomass sources are described in this section.

2.2.1. Lactone-type Monomers from Terpenes, Carboxylic Acids, and Lignin

Significant efforts have focused on developing biorenewable lactone monomers for degradable or hydrolyzable polyester materials. Lowe *et al.* converted the terpenoid natural product carvone (2-44) into two ε -caprolactone derivatives, olefin-substituted dihydrocarvide (2-45) and isopropyl-substituted carvomenthide (2-46) (Scheme 9). ³⁶ The multi-gram scale syntheses of these monomers involved hydrogenation and Baeyer-Villiger oxidation protocols. For the synthesis of 2-45, the authors also explored the use of Oxone® as an environmentally friendly Baeyer-Villiger reagent, which resulted in 86% conversion and 42% yield on a 10 g scale. Ring-opening transesterification polymerization (ROTEP) of these two lactones using Et₂Zn as precatalyst yielded polyesters poly(2-45) and poly(2-46) with good molar mass control (\leq 50 kg mol⁻¹), low D (\leq 1.3), and low glass transition temperatures T_g (\leq -20 °C). The controlled copolymerization of 2-45 with 2-46 in various ratios gave copolymers with varied olefin functional group content. The pendant olefin units enabled post-polymerization epoxidation and radical-induced crosslinking.

Scheme 9. Synthesis of renewable polyesters and polyols from carvone (2-44).³⁶

Xiong *et al.* reported an artificial biosynthetic pathway to produce β -methyl- δ -valerolactone (**2-49**) in a scalable fashion from biosynthetic mevalonate (**2-47**) (**Scheme 10**). ³⁷ Facilitated by engineered *E. coli*, the process comprises three steps: i) overexpression of mevalonate-producing enzymes, ii) introduction of fungal proteins that lead to anhydromevalonolactone (**2-48**), and iii) reduction to (**2-49**) by enoate reductases. The authors also conducted a refined semisynthesis where fermentation of an engineered *E. coli* strain first gave mevalonate, which was then subjected to direct acid-catalyzed dehydration and hydrogenation to yield polymerization grade (*i.e.*, high purity) β-methyl-δ-valerolactone monomer (**2-49**) after distillation. Polymerization of **2-49** gave a low T_g hydroxytelechelic polyester. Copolymerization of **2-49** with lactide formed well-defined triblock copolymers whose mechanical properties could be tuned by varying the molar mass, architecture, and endblock tacticity.

Scheme 10. Conversion of bio-engineered mevalonate (2-47) to β -methyl- δ -valerolactone (2-49).³⁷

Trotta *et al.* reported the facile synthesis of two monomers for radical polymerization, α -methylene- γ , γ -dimethyl- γ -butyrolactone (2-51) and α -methylene- γ -butyrolactone (2-52), from itaconic acid (2-1), an inexpensive monomer extracted from fermentation of corn or rice (Scheme 11). The monomethyl itaconate (2-50) starting material is commercially available. A Grignard addition to 2-50 and an acid work-up afford 2-51 in a one-pot reaction. Although the isolated yield after distillation was modest (39%), the single-step transformation to monomer is economically advantageous. The authors applied a similar one-pot strategy to refine the synthesis of the well-studied monomer 2-52. Subsequent reversible addition-fragmentation chain-transfer (RAFT) polymerization of 2-51 and 2-52 was controlled, producing polymers with low *D* values whose M_n correlated with conversion. Poly(2-51) exhibited high T_g (209 °C) and decomposition temperature (T_d) (>300 °C) values and a similar refractive index to commercial poly(methyl methacrylate), suggesting a variety of possible applications. The poly(2-51) material was also more soluble than poly(2-52) in tetrahydrofuran, which may improve processability.

Scheme 11. Synthesis of α -methylene- γ , γ -dimethyl- γ -butyrolactone (2-51) and α -methylene- γ -butyrolactone (2-52) from itaconic acid (2-1). ³⁸

Xu *et al.* synthesized the valerolactone derivative 4-ketovalerolactone (**2-55**) in two steps from levulinic acid (**2-53**) (**Scheme 12**), ³⁹ which may be obtained in high yield from acid-catalyzed hydrolysis of lignocellulose. ^{40,41,42,43,44,45,46} The two-step synthesis involves bromination of the enol tautomer of **2-53** with a Br₂-urea complex, affording 2:1 selectivity for the desired 5-bromolevulinic acid product (**2-54**) relative to 3-bromo-levulinic acid. The crude product mixture was treated directly with triethylamine to induce cyclization to **2-55**. Ring-opening transesterification polymerization (ROTEP) of this lactone proceeded to high equilibrium monomer conversion (96% in bulk). The resulting semicrystalline poly(4-ketovalerolactone) (poly(**2-55**)) exhibited a low glass transition (7 °C) and high melting (132 and 148 °C) temperatures. Using ¹H NMR spectroscopy, the researchers monitored hydrolysis of this polyketoester. Basic conditions accelerated hydrolysis to afford the ring-opened, hydrated form of the monomer, 5-hydroxylevulinic acid (**2-56**). The researchers propose hydrolysis of the polyketoester proceeds through a ketone-assisted mid-chain cleavage pathway. Under Brønsted acidic conditions, the authors observed the degradation of the polyketoester into a naturally occurring, bis-spirocyclic dilactone (**2-57**), which is a dimer form of the 4-ketovalerolactone monomer.

Scheme 12. Synthesis of 4-ketovalerolactone (2-55) from levulinic acid (2-53). Polymerization via ROTEP affords poly(2-55), which may be chemically recycled under basic or acidic conditions.

Lundberg *et al.* examined the economic feasibility of synthesizing γ-methyl-ε-caprolactone (**2-61**) from lignin biomass via the hydrogenation of alkyl-phenols to alkyl-cyclohexanones, followed by Baeyer-Villiger oxidation to alkyl-caprolactones (**Scheme 13**). This technoeconomic analysis suggested that partial hydrogenation of *para*-cresol (**2-58**) over a Pd/hydroxyapatite catalyst would afford an enol that would tautomerize to 4-methyl-cyclohexanone (**2-59**) in high conversion and chemoselectivity. The ketone intermediate **2-59** must be purified via distillation: *n*-dodecane solvent and unreacted **2-58** may be recovered and recycled, while a second distillation is necessary to remove the 4-methyl-cyclohexanol over-reduction byproduct (**2-60**) from the desired **2-59**. Baeyer-Villiger oxidation using inexpensive hydrogen peroxide over a Sn-BEA catalyst in a flow reactor furnishes **2-61**. As a single pass over the catalyst is likely to lead to only 20% conversion to product **2-61**, residual **2-59** may be recovered, dried, and re-fed. Full conversion is expected to afford 90% **2-61** and 10% hydrolyzed 4-methyl-6-hydroxyhexanoic acid (**2-62**). Finally, two vacuum distillations were necessary to obtain **2-61** in polymerization grade purity (>99.9 mol%).

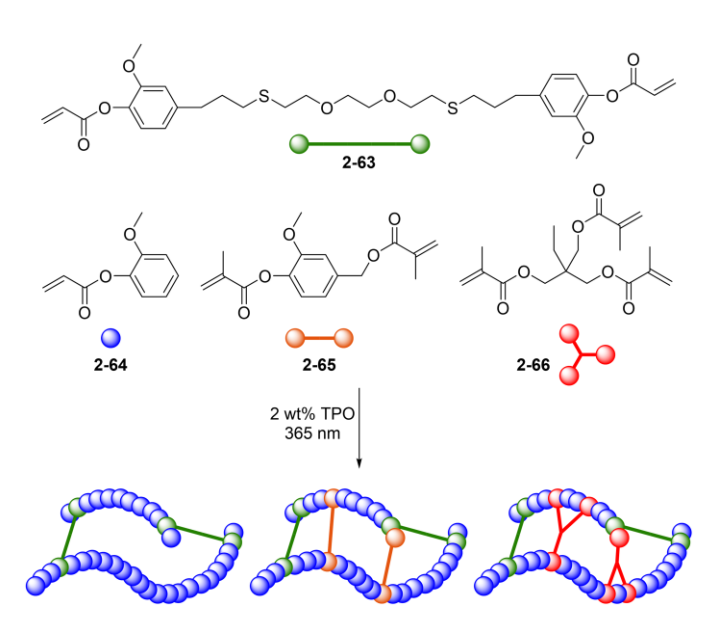
Scheme 13. Proposed industrial scale process to convert *para*-cresol (2-58) to γ -methyl- ε -lactone (2-61).⁴⁷

The proposed process requires a total capital investment of \$25 million for a 10 kton yr⁻¹ plant over 30 years. At this capacity, **2-61** could be sold at a minimum price of \$3.52 kg⁻¹ to achieve zero net present value over the duration of the project. At 60 kton yr⁻¹ this price approaches \$2.50 kg⁻¹. Feedstock and capital costs (\$1.53 and 1.35 kg⁻¹, respectively) comprise the bulk of the MSP; capital costs primarily arise from high-volume purifications of the ketone intermediate **2-59** and **2-61** lactone product. Because the MSP proved most sensitive to variations in molar yield from **2-58**, future improvements should focus on increasing the single-pass conversion of **2-59** to **2-61** above 20%. The authors anticipated that this approach to convert **2-58** to **2-61** can be extended to other lignin-derived aromatics with minimum processing changes to afford the corresponding lactones. Indeed, recent work from Batiste *et al.* demonstrated that mixtures of methyl-substituted caprolactones derived from *meta*- and *para*-cresol afford copolymers with comparable thermal and rheological properties to the established homopolymer analogue from **2-61** (*vide infra*, Section 3.2). ⁴⁸ Preserved polymer performance despite a mixed monomer feed may render expensive separation of *meta*- and *para*-cresol isomers unnecessary, improving the economic viability of renewable lignin feedstocks.

2.2.2. Acrylate-type Monomers from Lignin and Sugar

Functionalized acrylates from lignin feedstocks offer a versatile and sustainable option to replace commercial petroleum-derived monomers. Ding *et al.* studied natural phenolic meth(acrylate)

formulations as degradable photoinitiated thermosets for 3D printing (**Scheme 14**). ⁴⁹ The authors studied two acrylate monomers to assess their viability as sustainable alternatives to the petrochemical-derived bisphenol A glycolate dimethacrylate. 3,6-Dioxa-1,8-octane-dithiol eugenol acrylate (**2-63**) was prepared via thiol-ene click chemistry followed by coupling to acryloyl chloride on large scale (53 g, 78% yield). The di-acrylate functionality of **2-63** permits polymer crosslinking. For a monofunctional comonomer, the authors selected guaiacyl methacrylate (**2-64**), which is derived from guaiacol found in softwood lignin-based oils. Although bifunctional **2-63** readily polymerized via free radical photopolymerization, incorporating **2-64** as a comonomer reduced the reaction rate. To achieve the high photo-reactivity required for printing applications, Ding *et al.* introduced photoreactive acrylate cross-linkers: bifunctional vanillin alcohol dimethacrylate (**2-65**) is derived from naturally-occurring vanillin, while trifunctional trimethylolpropane methacrylate (**2-66**) is used commercially. Copolymerization of **2-63** and **2-64** with **2-65** or **2-66** afforded a library of photo-curable 3D printing formulations with diverse properties (*vide infra*, Section 4.3).



Scheme 14. Thermoset materials synthesized from lignin-derived acrylate monomers (TPO = diphenyl(2,4,6-trimethylbenzoyl) phosphine oxide).⁴⁹ [waiting on permission from RSC]

Fonseca *et al.* used commercial α -lactose (**2-67**) or lactose-rich milk permeate as the raw material to produce lactose methacrylate-based hydrogels (**Scheme 15**). ⁵⁰ By reacting lactose with different amounts of methacrylic anhydride, the authors prepared mixtures of mono-, di-, or tri-lactose methacrylates (**2-68**) and methacrylic acid (**2-69**) as hydrogel precursor mixtures in an atom-economical fashion. In accordance with green chemistry principles, photopolymerization (UV light, 365 nm) under aqueous conditions produced sugar-based hydrogels. The authors characterized the mechanical, rheological, and water uptake behavior of these hydrogels. Different ratios of **2-68** comonomers can impact the compressive elastic moduli (12 to 735 kPa), plateau moduli (5 to 400 kPa), gel fractions (39 to 55%), and equilibrium water contents (80 to 260%) of

the product hydrogels. These results indicate that novel materials from less than pristine biomass-derived monomers can exhibit a range of desirable properties.

Scheme 15. Synthesis of hydrogels based on lactose methacrylates (2-68) from commercial α -lactose (2-67) or milk permeate.⁵⁰

Lactose, which is abundant in whey byproducts of the dairy industry, showed potential as a useful chemical feedstock. Therefore, the authors also considered using milk permeate directly to prepare hydrogels using a similar approach. Using H NMR spectroscopy to compare milk permeate with lactose solutions of various concentrations, the authors determined that the milk permeate contained 83% lactose (40% α -anomer, 60% β -anomer). They adjusted the amount of methacrylic anhydride and reaction temperature accordingly to produce comonomer mixtures using a similar procedure as starting with commercial α -lactose of a higher grade of purity. The hydrogels prepared *in situ* from milk permeate and those prepared from commercial **2-67** showed comparable properties, demonstrating the potential utility of this waste feedstock.

Glucose and trehalose have been used as saccharide-derived monomer feedstocks by researchers in the CSP. In 2016, Nasiri, et al. reported the synthesis and polymerization of a glucose-derived monomer, glucose-6-acrylate-1,2,3,4-tetraacetate (2-73) as a glassy component of block copolymers. 52 Because glucose (2-70) is readily abundant and inexpensive, this direct functionalization is an attractive approach to monomer synthesis (Scheme 16). The primary hydroxyl group was first protected with a trityl unit before acetylation of the remaining hydroxyl units to form 2-71. Deprotection revealed the primary alcohol moiety of 2-72 for reaction with acryloyl chloride to afford 2-73. Using 4-cyano-4-[(ethylsulfanylthiocarbonyl)sulfanyl] pentanoic acid (CEP) as a CTA, the researchers performed RAFT polymerization of the 2-73monomer to create a first glassy block. Chain extension with *n*-butyl acrylate installed the rubbery midblock. However, efforts to install a third 2-73-derived block were unsuccessful. As an alternative approach, Nasiri, et al. employed a symmetric CTA to permit construction of the ABA triblock in two steps. Using this strategy, the authors synthesized polymers with tunable quantities of 2-73 and low dispersities. However, the central trithiocarbonate unit may reduce the thermal stability of these materials. To circumvent potential issues during thermal processing, the authors employed a bifunctional CTA to synthesize the ABA triblocks, leaving the trithiocarbonate moieties at the ends of the A blocks. Analysis of the peel strength of the various ABA triblock polymers in the presence and absence of a tackifier revealed peel strengths of 1.05–2.31 N cm⁻¹, within the range of values observed for common commercial products. 53 Increasing the 2-73content of the endblocks was associated with a decrease in tack, though materials incorporating up to 14% revealed good adhesive properties. The authors have further explored triblock polymers

incorporating 2-73 or poly(acetylated acrylic isosorbide) endblocks and poly(*n*-butyl acrylate) midblocks, demonstrating the effects of non-covalent interactions on adhesion and mechanical properties (*vide infra*, Section 4.1). Zhang, *et al.* have further expanded saccharide-derived monomers for renewable materials, developing trehalose- and beta-cyclodextrin-based hardeners for epoxy resins (*vide infra*, Section 4.3).

Scheme 16. Synthesis of glucose-derived glucose-6-acrylate-1,2,3,4-tetraacetate (2-73).

The bioengineered fermentation of glucose can produce mevalonate (2-47) efficiently,³⁷ and further chemical transformations can give the renewable anhydromevalonolactone (2-48) (*vide supra*, Scheme 10).⁵⁴ Using this sugar-derived lactone, Ball-Jones *et al.* synthesized a series of four glucose-derived isoprenecarboxylic acid esters (2-74, R = Me, Et, "Bu, 'Bu, 45–60% yield, \leq 20 g) and their homopolymers (Scheme 17).⁵⁵ The one-pot synthesis of 2-74 involved base-catalyzed ring opening of 2-48 and consecutive esterification *in situ*. Free radical and reversible addition-fragmentation chain-transfer (RAFT) polymerizations of 2-74 afforded homopolymer poly(isoprenecarboxylates) poly(2-74) with $M_{\rm n}$ up to 150 kg mol⁻¹. Analysis of ¹H and ¹³C NMR spectral data revealed that competing 1,4- and 1,2-addition occurred in approximately a 1.5:1 ratio during the radical polymerizations of 2-74 via both free radical and RAFT techniques. The $T_{\rm g}$ and entanglement molecular weights of poly(2-74) with different ester alkyl moieties revealed similar trends to those of the analogous poly(acrylate esters): increasing alkyl substitution decreased the $T_{\rm g}$ value and increased the $M_{\rm e}$ value for poly(2-74).

Scheme 17. Transformation of anhydromevalonolactone (**2-48**) to renewable polyacrylate analogs (poly(**2-74**), R = Me, Et, nBu , tBu). 55

Further bioengineered derivatives of glucose include triacetic acid lactone (2-76), which has been functionalized and used as a feedstock for sustainable polymers by Sajjad, *et al.*⁵⁶ The authors sought to develop biorenewable high-performance pressure-sensitive adhesives using 2-76 and lauryl acrylate. Lauryl acrylate is readily derived from vegetable oils, including coconut and palm

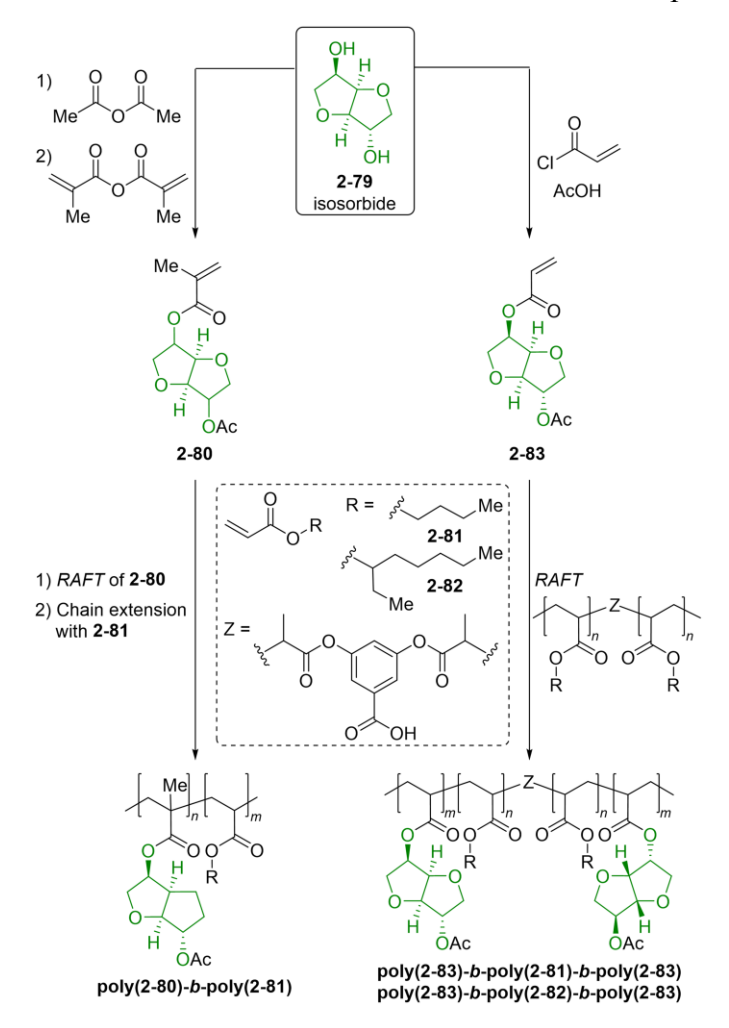
kernel oils^{57,58} and was investigated as an alternative to *n*-butyl acrylate as a rubbery midblock in ABA triblock copolymers. To replace frequently styrenic glassy endblocks, the authors investigated derivatives of 4-hydroxy-6-methyl-2-pyrone (2-75), which is produced as a secondary metabolite of glucose and other sugars by some microbes^{59–61} or may be synthesized from acetic acid. 62-64 Catalytic hydrogenation of the pyrone proceeded over a period of two to three days; the authors attribute the extended reaction time to slow internal keto-enol tautomerization following partial reduction (Scheme 18). Nonetheless, the transformation afforded the corresponding lactone (2-76) in near quantitative yields. Esterification of the hydroxyl substituents of either 2-75 or 2-76 with acryloyl chloride afforded the polymerizable acrylates 2-77 and 2-78, respectively. The authors first confirmed that each of the three monomers could be homopolymerized in a controlled fashion. Sajjad, et al. then synthesized midblocks comprised of either n-butyl acrylate or lauryl acrylate with living chain ends for chain extension with 2-78. The resulting high molecular weight materials were assessed as pressure sensitive adhesives (PSAs) in conjunction with an ester-based tackifier. By varying the tackifier content, the peel adhesion values of the polymers could be tuned from 2–6 N cm⁻¹, competitive with those of commodity adhesive products.⁵³ These results suggest that fully bio-sourced ABA triblock polymers from long-chain lauryl acrylate and 2-76 may be viable high-performance PSAs.

Scheme 18. Synthesis of acrylated-pyrone (2-77) and acrylated-lactone (2-78) monomers.

Sugar-derived isosorbide (2-79) is an attractive potential monomer unit due to its rigid structure and rich functionality. It may therefore serve as a potential alternative to bisphenol A, ⁶⁵ which is an endocrine disruptor that is particularly harmful to infants and children. ^{66,67} Until recently, however, isosorbide was not an economically feasible feedstock. In 2015, Roquette launched a new production facility with an annual capacity of 20,000 tons, decreasing isosorbide cost and increasing availability. ⁶⁸ The use of isosorbide as a functional monomer has been recently reviewed. ⁶⁵ To further develop sustainable acrylate polymers, Gallagher *et al.* synthesized and studied a methacrylate isosorbide monomer (2-80). ⁶⁹ Isosorbide's *endo* and *exo* secondary alcohols exhibit a known difference in reactivity. ⁶⁵ Gallagher *et al.* observed that acetylation of isosorbide with acetic anhydride favored monoacetylation of the *endo* hydroxy group (*endo*-acetate:*exo*-acetate, 4.2:1). ⁶⁹ Reaction with methacrylic anhydride installed the polymerizable methacrylate unit, yielding an isomeric mixture of 2-80 (~20 g, 44% yield, Scheme 19, left). Both the acetylation and methacrylation steps used Sc(OTf)₃ in the first reported use of this catalyst for

isosorbide esterification, affording excellent reactivity with acetic anhydride under ambient conditions.

Gallagher *et al.* then polymerized the regioisomeric mixture of **2-80** under thermal free radical conditions, producing homopolymers with high T_g values of ~130 °C attributed to the rigidity and bulkiness of the pendant isosorbide group. ⁶⁹ These high T_g values make these samples attractive sustainable hard components for block copolymers. Gallagher *et al.* then used RAFT to polymerize **2-80** and maintain a functional end group for chain extension. Molar mass and dispersity were best controlled with dithiobenzoate chain transfer agents (CTAs), affording poly(**2-80**)-CTA polymers with >92% conversion and D < 1.09. Chain extension with *n*-butyl acrylate (**2-81**) yielded the block copolymer, poly(**2-80**)-*b*-poly(**2-81**) (**Scheme 19**, left). The properties of the block copolymer derived from the mixture of monomers versus one pure isomer of the monomer were very similar.



Scheme 19. Isosorbide (2-79)-derived acrylates for block copolymer materials.^{69,70}

Expanding on this work, Gallagher *et al.* replaced the methacrylate unit in **2-80** with an acrylate group to yield acetylated acrylic isosorbide (**2-83**) in 38% yield (**Scheme 19**, right). To Eliminating the methyl substitution in the backbone moderately decreased the T_g value of the homopolymer

poly(2-83) (95 °C) due to increased backbone flexibility. The authors next sought to incorporate poly(2-83) as a hard block component in triblock thermoplastic elastomers. Butyl acrylate and 2-ethylhexyl acrylate (2-82) were selected as comonomers for the soft blocks due to their low cost and flexible structure. RAFT polymerization using a bifunctional CTA-enabled chain extension with poly(2-83) to form triblocks incorporating 8–24 wt% of hard block poly(2-70). The researchers evaluated the poly(2-83)-b-poly(2-81)-b-poly(2-83) and poly(2-83)-b-poly(2-82)-b-(2-83) triblock copolymers as PSAs. Dynamic mechanical thermal analysis (DMTA) and 180° peel, loop tack, and static shear testing demonstrated that poly(2-83)-b-poly(2-82)-b-(2-83) triblock did not perform well, while the poly(2-83)-b-poly(2-81)-b-poly(2-83) triblock exhibited PSA characteristics.

2.2.3. Olefin-type Monomers from Saccharides

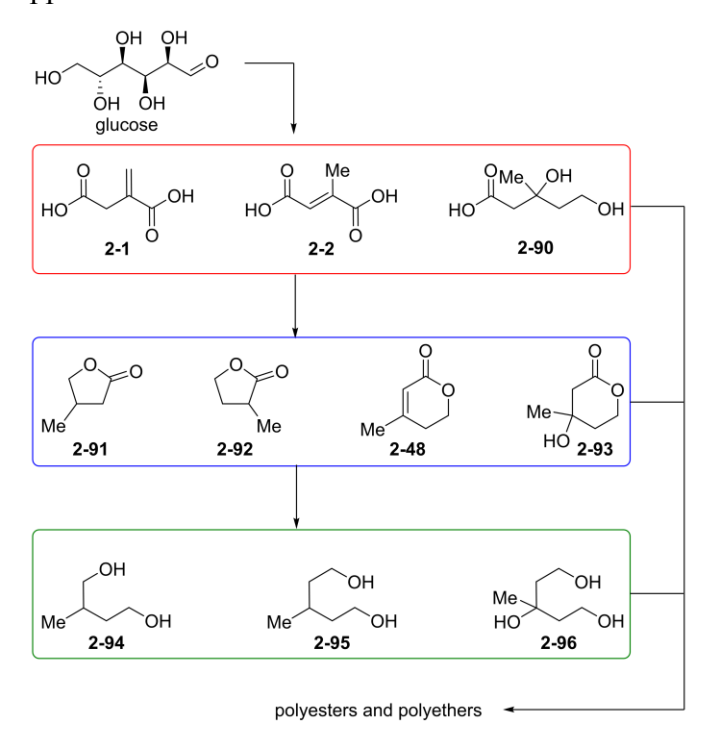
Shearouse et al. explored sustainable polyesters incorporating internal isosorbide or glucarodilactone units. 71 Targeting a fully renewable monomer with a terminal olefin, these researchers reacted these bicyclic heterocycles with 10-undecenovl chloride (2-84), which can be sustainably sourced from castor oil (Scheme 20, left). Addition of dimethylaminopyridine to the coupling reaction prevented ring-opening of the isosorbide or glucarodilactone moieties, affording the isosorbide undecanoate (2-85) and glucarodilactone undecenoate (2-86) in good yields (70– 78%). Acyclic diene metathesis (ADMET) polymerization of monomers 2-85 and 2-86 with Grubbs' second-generation pre-catalyst afforded two homopolymers and two copolymers (poly(2-85)-co-poly(2-86)) of varied comonomer incorporation (46:54 and 52:48). While the two homopolymers were brittle, semicrystalline materials, the copolymers poly(2-85)-co-poly(2-86) were tougher, rubbery, and amorphous. After uniaxial extension, the copolymers gradually returned to their original length, demonstrating shape-memory behavior. Interestingly, Shearouse et al. also observed a lower T_d for polymers incorporating greater amounts of the **2-86** monomer. The authors therefore proposed that polymer stability depended on incorporation of ester linkages. Under basic conditions, the poly(2-86) homopolymer rapidly degraded, while the copolymers hydrolyzed within a day to produce isosorbide, fatty carboxylate salts, and glucarate salts. These results demonstrate the potential for sugar-derived copolymers to serve as degradable shapememory materials.

Scheme 20. Polymers incorporating an internal isosorbide unit for shape-memory and thermoset materials. ^{71,72}

2.2.4. Multifunctional Alcohols and Carboxylic Acids

Wilbon *et al.* developed a facile microwave-assisted condensation method to ring-open two equivalents of succinic anhydride (2-87) with 2-79 and catalytic tin(II) octoate to form the isosorbide disuccinic acid (2-88) (Scheme 20, right). This microwave-assisted method dramatically reduced reaction time (~5 min) relative to previous condensation reactions that required 24 h at 120 °C to reach full conversion. The same tin(II) octoate catalyst also promoted condensation polymerization using 2-88, glycerol (2-89), and hydroxy-terminated polyethylene oxide (PEO). Varying the content of these multifunctional alcohols affected both the mechanical properties (*vide infra*, Section 4.3) and rate of hydrolytic degradation of the polyester materials. Subjecting the polymers to aqueous salt solutions or basic conditions resulted in hydrolytic degradation within hours, and even deionized, unbuffered water produced full degradation within a month. Recovering the degradation products and re-subjecting them to polymerization conditions with exogenous tin(II) octoate did produce polyester, albeit with somewhat different optical and tensile properties.

Spanjers et al. designed and demonstrated a synthesis of renewable multifunctional alcohols from glucose-derived five- or six-carbon acids via lactone intermediates (Scheme 21).74 The authors proposed an efficient synthesis of these glucose-derived alcohols utilizing a heterogeneous catalytic system in aqueous solution. The synthetic route comprised two sequential steps of highpressure hydrogenation: i) the high temperature reduction of acids to lactones, and ii) a low temperature reduction of the lactone to the corresponding diol or triol. DFT calculations of thermodynamic parameters guided the design of this reaction sequence and revealed optimal reaction temperatures for substrates 2-1 and 2-2. Calculations indicated that alkene hydrogenation, carbonyl reduction, and intramolecular esterification to form α -methyl- γ -butyrolactone (2-92) are exergonic under high temperature (80–220 °C) and low H₂ pressure (50–200 bar). Under these conditions, conversion of 2-92 to 2-methyl-1,4-butanediol (2-94) is unfavorable; however, lower temperatures (<140 °C) and high H₂ pressure (200 bar) render this reaction exergonic. Experimentally, a commercially available Pd/C catalyst provided the highest selectivity and TOF to convert 2-1 or 2-2 to β -methyl- γ -butyrolactone (2-91) and 2-92, but for the second hydrogenation Ru/C was superior to give diol 2-94 in 80% yield. Similar conditions were used to convert 2-48 to 3-methyl-1,5-pentanediol (2-95) or mevalonolactone (2-93) to 3-methyl-1,3,5pentanetriol (2-95). This process is efficient for producing valuable lactone, diol, and triol monomers for the synthesis of bio-derived branched polyesters. In a subsequent report, the authors used these branched alcohols in condensation polymerizations with diacids to prepare a series of methyl-substituted aliphatic polyesters with amorphous, rubbery character for various applications.⁷⁵



Scheme 21. Synthesis of renewable multifunctional alcohols from glucose-derived five- or six-carbon acids via lactone intermediates for polyester and polyether materials. Adapted with permission from John Wiley and Sons.⁷⁴

Dipicolinic acid (**2-97**), a natural diacid that composes 5-15% of the dry weight of bacterial spores, serves as a monomer substitute for fossil fuel-derived phthalic acid, and gives rise to polymers that exhibit biodegradability via hydrolysis. McClintock *et al.* successfully engineered a green process to obtain **2-97** on decagram scale from the gene-refined workhorse organism *E. coli* (Figure 5). After strain optimization of the nutrient feed concentration, the authors achieved 5.2 g L⁻¹ of **2-97** when 5 g L⁻¹ of aspartate was supplied.

Blaisse *et al.* also took advantage of cell-based synthesis by telescoping multiple reactions into a single fermentation step. ⁷⁷ α -Substituted acids are widely used in copolymerizations and may improve the processability and thermal stability of the corresponding polyesters relative to unsubstituted analogues. ^{78,79} Roundworms (*A. suum*) have been reported to accumulate short branched organic acids, indicating a biosynthetic thiolase-based pathway that can incorporate both acetate and propionate units. Blaisse *et al.* characterized a thiolase-ketoreductase pathway to produce α -branched acids from glucose and propionate (**Figure 5**). Then, screening of different thiolases and enzymes revealed the best candidates for selective formation of α -branched products over linear products. The authors also used these enzymes in *E. coli* to produce α -methyl acids, enoic acids and 3-hydroxy acids with acceptable yields. This accomplishment encourages the use of this potential biosynthetic pathway to produce a variety of branched acids as precursors for polymers.

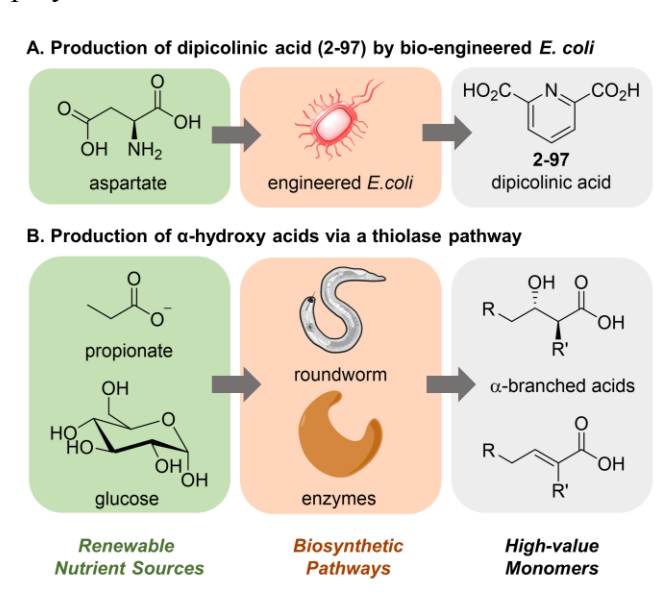


Figure 5. Biosynthesis of acid monomers. ^{76,77}

2.2.5. Bifunctional Silyl Alcohols

Polylsilylethers (PSEs) are recognized as degradable polymers due to the cleavable Si–O bonds present in the backbone. Cheng *et al.* synthesized a novel AB type monomer containing Si–H and O–H functionalities from a renewable bio-feedstock. ⁸⁰ The undecenoic acid starting material was derived from ricinoleic acid, a fatty acid component derived from castor oil. The authors report a two-step monomer via metal-catalyzed hydrosilylation using Karstedt's catalyst (10 ppm) followed by a lithium aluminum hydride reduction. The polymerization proceeded via

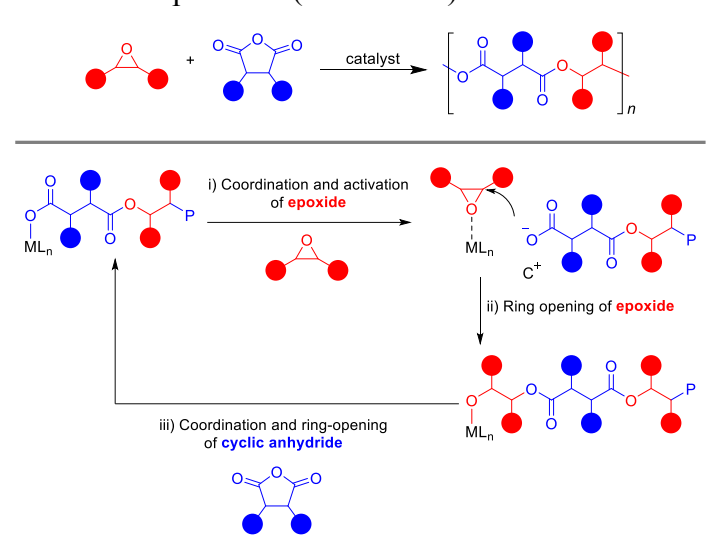
hydrosilylation catalyzed by alkaline bases such as CsOH and KH (0.2–2.5 mol%), yielding PSE materials with high thermal stabilities. The authors intentionally avoided Si–Cl and O–H condensation polymerization methods because these require an equimolar amount of base. The new PSE material degraded via hydrolysis under mild aqueous conditions.

3. Polymerization Processes and Techniques

CSP researchers have a keen interest in developing high-efficiency catalysts for the preparation of sustainable polymers. The cooperative environment within the CSP has enabled collaborations between computational and experimental groups to elucidate reaction mechanisms and to rationally design next-generation catalysts with higher reactivity and improved control over polymer architecture. The CSP has emphasized the study of two important polymerization reactions, namely the ring-opening copolymerization (ROCOP) of epoxides with cyclic anhydrides or CO₂ and the ROTEP of lactones and lactides. ROCOP of epoxides and cyclic anhydrides is an attractive route toward sustainable polyesters because of the scope of accessible monomers. ROTEP of cyclic esters represents another highly efficient approach to obtain biodegradable and sustainable polyesters with good molar mass control under mild reaction conditions. ROTEP of cyclic esters review some of the CSP researchers' achievements in understanding and developing efficient catalytic processes to prepare sustainable polymers.

3.1. Ring-opening Copolymerization of Epoxides with Cyclic Anhydrides and CO2

ROCOP of epoxides and cyclic anhydrides are typically catalyzed by a Lewis acid catalyst in conjunction with a nucleophilic or cationic cocatalyst. The ROCOP propagation cycle involves three elementary steps: i) epoxide activation by binding to a Lewis acidic metal center; ii) epoxide ring-opening by nucleophilic attack of a carboxylate chain end to form a metal-alkoxide; iii) reaction of the metal-alkoxide with cyclic anhydride to form a new ester linkage, enchaining one additional repeat unit (**Scheme 22**). 84,88



Scheme 22. The generalized propagation reaction mechanism of the ROCOP (C^+ = counter ion). ^{84,88}

Chart 1a presents a collection of Lewis acidic metal catalysts used in ROCOP reactions described in this review. Typically, these metal-salph (salph = N,N'-bis(salicylidene)phenylenediamine) catalysts require the addition of a cocatalyst such as bis(triphenylphosphine)iminium chloride ([PPN]Cl) to attain high catalytic activity (Chart 1b). The large comonomer scope (Chart 2) enables preparation of polymers with a wide range of properties and applications, which also can be enhanced by post-polymerization modification.⁸⁹

Chart 1. Catalysts and cocatalysts used for ROCOP.

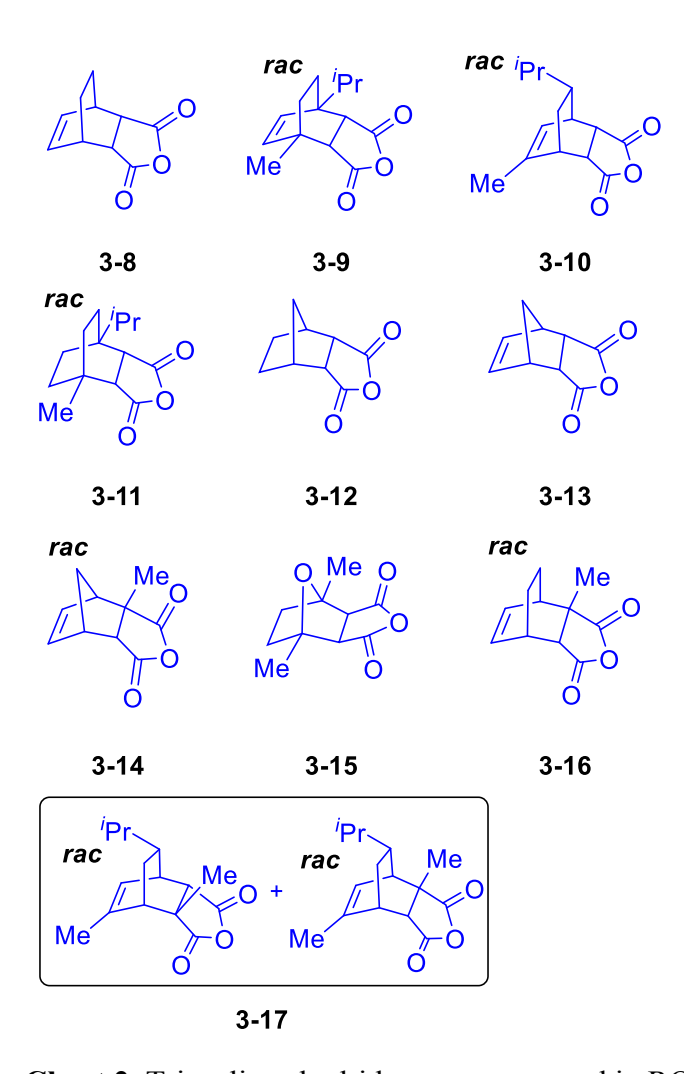
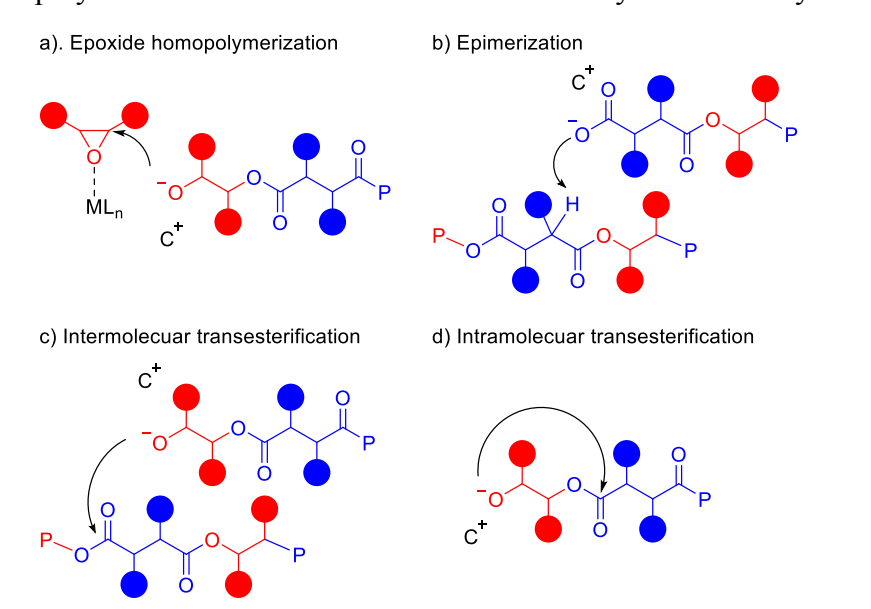


Chart 2. Tricyclic anhydride monomers used in ROCOP reactions.

Van Zee *et al.* aimed to prepare sustainable polyesters with high T_g values as an alternative to glassy petroleum-based polymers. ⁹⁰ Initial studies performed by other members of the CSP demonstrated that copolymerization of bicyclic anhydrides with epoxides results in aliphatic polyesters with high T_g values. ^{91,92} Capitalizing on these prior results, the researchers synthesized a series of terpene-based tricyclic anhydrides (3-8 to 3-11) by Diels-Alder additions of terpenes with maleic anhydride. This straightforward synthesis contrasts with multi-step syntheses required for bicyclic monomers used in earlier studies. ⁸⁸ Copolymerization of the cyclic anhydride monomers (3-8 to 3-11) and propylene oxide (PO) with Cr(salph)Cl (3-1) catalyst and [PPN]Cl cocatalyst provided polymers with moderate M_n , narrow D, and high T_g values. The copolymer microstructure was determined by copolymerization of the tricyclic anhydride with enantiomerically-pure (S)-PO and reductive degradation of the resulting copolymers. Analysis by NMR spectroscopy revealed that the Cr(salph)Cl-catalyzed epoxide ring-opening is highly regioselective for the unsubstituted position, as evidenced by retained stereochemical relationships. Conversely, the orientation of the ester units was found to be regio- and stereo-

irregular, inhibiting the formation of polymer crystallites and resulting in the observed high $T_{\rm g}$ value.

Interestingly, broader \mathcal{D} and lower regio- and stereo-regularities were observed for reactions performed in excess PO upon complete conversion of the cyclic anhydride. The researchers ascribed this degradation of the polymer architecture to side reactions such as transesterification and epimerization of diester units induced by the reactive metal alkoxide species formed at the end of the reaction (**Scheme 23**). These side reactions result in mixtures of polymer architectures and microstructures that can be detrimental to the bulk material properties. The researchers hypothesized that increasing the Lewis acidity of the catalyst would promote stronger binding of the active alkoxide chain ends to minimize these side reactions. They therefore prepared the corresponding Co and Al complexes (**3-2** and **3-3**, respectively) and studied their ROCOP catalytic activity. While **3-2** exhibited lower copolymerization selectivity and permitted substantial epimerization, **3-3** displayed comparable activity to **3-1** without significant transesterification and epimerization even under extended reaction times. Overall, the Al catalyst **3-3** led to controlled polymerization rate that could be conveniently monitored by ¹H NMR spectroscopy.



Scheme 23 Possible side reactions in the ROCOP of epoxides and cyclic anhydrides.⁹⁰

In a continuing study, Van Zee *et al.* reported the copolymerization of tricyclic anhydrides (3-8, 3-9, and 3-12 to 3-14) with excess PO using a Al(salph)Cl catalyst, 3-3, with [PPN]Cl cocatalyst. ⁹³ The authors investigated various factors influencing the rates of undesirable side reactions, such as the structure of the tricyclic anhydride, the molar ratio of catalyst to cocatalyst, and the Lewis acidity of the catalyst. Copolymers derived from tricyclic anhydrides (3-12, 3-13, 3-8) were more susceptible to transesterification and epimerization side reactions (Scheme 23) than copolymers prepared from the bulkier monomer 3-9, a terpene-based cyclic anhydride. Using 3-13 as a model monomer, the authors further demonstrated that decreasing the molar ratio of [PPN]Cl cocatalyst to the Al catalyst minimized side reactions by reducing the concentration of highly reactive alkoxide chain ends at the end of the copolymerization. Moreover, by tuning the Lewis acidity of

the Al center, the researchers showed that the electronic properties of the salph ligand significantly impacted the extent of side reactions. Although catalysts with electron withdrawing substituents at the *para* position (R^1) promote a lower rate of ROCOP (TOF = 88, 80, and 49 h⁻¹ for **3-3**, **3-4**, and **3-5**, with $R = {}^tBu$, H, and F respectively), fluorination of the R *para*-position in **3-5** suppresses side reactions when used in combination with a sub-stoichiometric amount of [PPN]Cl.

Sanford *et al.* continued to study the ROCOP of tricyclic anhydrides with PO and cyclohexene oxide (CHO), ⁹⁴ which has the potential to be renewably sourced. ⁹⁵ The researchers synthesized six tricyclic anhydrides from partially (50–63 wt %; 3-9, 3-10, and 3-14 to 3-16) or fully renewable sources (3-17). In addition to Al(salph)Cl catalysts 3-3 and 3-6, they explored a more geometrically flexible aminotriphenolate Fe complex 3-7 (Chart 1). ⁹⁶ With all three catalysts tested, ROCOP of PO produced polymers with higher M_n and T_g values, as well as lower D values when compared to polylactic acids (PLAs). The iron complex (3-7) exhibited similar reactivity to 3-3 and 3-6, but it produced materials with lower M_n . The more Lewis acidic catalyst 3-6 suppressed side reactions at high conversion with less bulky tricyclic anhydrides (3-10 and 3-15), whereas bulkier anhydrides (3-9, 3-14, 3-16, and 3-17) were copolymerized using 3-3 without significant side reactions.

These researchers then studied the effects of monomer steric bulk on the T_g value of the resulting polymers. Using **3-3** as the catalyst, they observed that poly(PO-alt-**3-9**) has a higher T_g value than poly(PO-alt-**3-16**), 108 °C and 86 °C, respectively. The authors surmised that bulkier monomers could increase the T_g value of the polymer product. To further increase the T_g value, they replaced PO with the bulkier CHO. Indeed, ROCOP of CHO leads to poly(CHO-alt-**3-9**) and poly(CHO-alt-**3-16**) with T_g values of 184 °C and 162 °C, respectively. The T_g values of these CHO-containing polymers are among the highest reported for aliphatic polyesters synthesized through chain-growth polymerization. ROCOP of CHO and cyclic anhydrides proceeds at a slower rate and produces copolymers with lower M_n and higher D values when compared to those incorporating PO.

Access to well-defined structures often relies on the formation of (co)polymers with narrow unimodal molecular weight distributions, a common issue in ROCOP due to the presence of diacid impurities and adventitious water leading to bimodal molar mass distributions. 93,97,98 To address this issue, Sanford *et al.* designed a metal complex/bifunctional cocatalyst system comprising Al catalyst 3-18 and [PPN]₂ADC (Chart 3) to which 1,3-adamantane dicarboxylic acid (AdA) was added as a bifunctional CTA. 99 The authors surmised that in the presence of CTAs, ROCOP of epoxides and cyclic anhydrides proceeds via reversible deactivation chain transfer, which has previously been reported to offer excellent control over M_n and D, facilitating the synthesis of block polymers. 100

Chart 3. Al(salph) catalyst and the bifunctional cocatalyst.

The researchers then modified catalyst **3-19** in which the chloride initiating ligand in **3-18** was replaced with a weakly nucleophilic triflate ligand that does not initiate polymerization in the absence of cocatalyst. ⁹⁹ Copolymerizations of PO and anhydride **3-14** by catalyst **3-19** and the [PPN]₂ADC binary system yielded unimodal polymers with narrow \mathcal{D} . The polymerization exhibited a linear correlation between M_n and monomer conversion, as well as for the ratio of cyclic anhydride monomer to initiating groups (total equivalents of cocatalyst and CTA), reflecting a controlled reversible deactivation chain transfer process. The use of a bifunctional cocatalyst (and CTAs) affords bis-hydroxy-telechelic polyesters following complete consumption of **3-14**. Feeding a second cyclic anhydride into the polymerization system permitted the preparation of well-defined ABA-type triblock copolymers. The resulting copolymers underwent orthogonal post-polymerization modification using thiol-ene and amine condensation reactions that could be performed in tandem, thus providing the first example of a one-pot double post-polymerization modification on an aliphatic polyester.

Aiming to better understand the ROCOP mechanism, Fieser *et al.* carried out a mechanistic study on ROCOP of 1-butene oxide (BO) and **3-13** using a **3-3**/[PPN]Cl binary catalytic system. Within the framework of the general reaction mechanism outlined earlier in **Scheme 22**, the researchers observed a first-order dependence on the epoxide concentration and a zero-order dependence on the cyclic anhydride concentration. There is a first-order dependence on the concentration of the Al/PPN pair when varied together while keeping their relative concentrations the same (in 1:1 ratio). This observation suggests that the Al catalyst **3-3** and the [PPN]Cl cocatalyst act as a single catalytic unit rather than as separate components during the copolymerization. Moreover, a maximum rate was observed with the ~1.5:1 ratio of [PPN]Cl to Al catalyst. These results are consistent with pre-equilibrium epoxide binding, followed by rate-limiting epoxide ring-opening by the carboxylate chain end.

The researchers also conducted DFT calculations to study the reaction mechanism with model PO and succinic anhydride substrates. These studies demonstrated that initiation proceeds via epoxide ring-opening to form intermediate **AA** (**Scheme 24**). Cyclic anhydride ring-opening by **AA** forms the other key intermediate **AC**, a mixed alkoxide/carboxylate aluminum complex. From **AC**, two competing catalytic cycles can take place. In cycle 1, the propagation mechanism from the mixed **AC** intermediate first involves ring-opening of epoxide to form **AA**, followed by cyclic anhydride ring-opening to regenerate **AC**. Alternatively, in cycle 2, **AC** ring-opens the cyclic anhydride to form the dicarboxylate intermediate **CC** prior to ring-opening of the epoxide. The subsequent rate-

limiting epoxide ring-opening step regenerates **AC**. Experimental and DFT studies both suggested that cycle 2 is kinetically favored over cycle 1; namely, **AC** ring-opens the cyclic anhydride faster than the epoxide. Significantly, the authors concluded that the kinetic barrier of the rate-limiting epoxide opening in cycle 2 is low enough for this step to out-compete the epimerization and transesterification side reactions before full conversion.

Scheme 24. Proposed mechanism for ROCOP of PO and succinic anhydride. 101

The above mechanistic insights gained from the collaborative efforts of CSP-affiliated groups¹⁰¹ prompted the investigation of a new catalytic system by Abel *et al.* in 2019.¹⁰² Attempting to overcome the anticipated decrease in the activity of a binary catalyst/cocatalyst system under high dilution (*i.e.*, low catalyst concentration), the researchers designed a bifunctional catalytic system. Contrary to the traditional binary systems (catalyst and cocatalyst), the bifunctional systems comprised a cocatalyst unit covalently tethered to the salph/salen backbone of the ligands (**Chart 4**). The authors proposed that covalently tethering the Lewis acid catalyst and nucleophile cocatalyst would facilitate intramolecular rate-limiting epoxide ring-opening and consequently enhance the rate of ROCOP. They developed a modular synthetic route to avoid linear synthetic strategies, which allowed them to readily vary the steric and electronic properties of the catalyst. ^{103,104,105,106} Use of a tris(dialkylamino)-cyclopropenium (TDAC) salt as the tethered moiety capitalized on the effectiveness of weakly ion-pairing onium salts as cocatalysts for ROCOP and ease of synthesis to improve activity as an effective catalyst for coupling of epoxides with CO₂. ¹⁰⁷ The TDAC salts exhibit comparable catalytic activity to the widely-employed [PPN]Cl cocatalyst when used in conjunction with **3-3** in a binary catalytic system.

The complexes bearing a tethered TDAC cocatalyst (3-20 to 3-22) exhibited excellent molar mass control and low D for the resulting polymers, despite slightly lower activity at high catalyst loadings relative to the analogous binary catalyst system. Nevertheless, polymerization activity is maintained at low catalyst loadings, in striking contrast to the binary analogues. Kinetic measurements validated the hypothesis that the bifunctional complex facilitates intramolecular

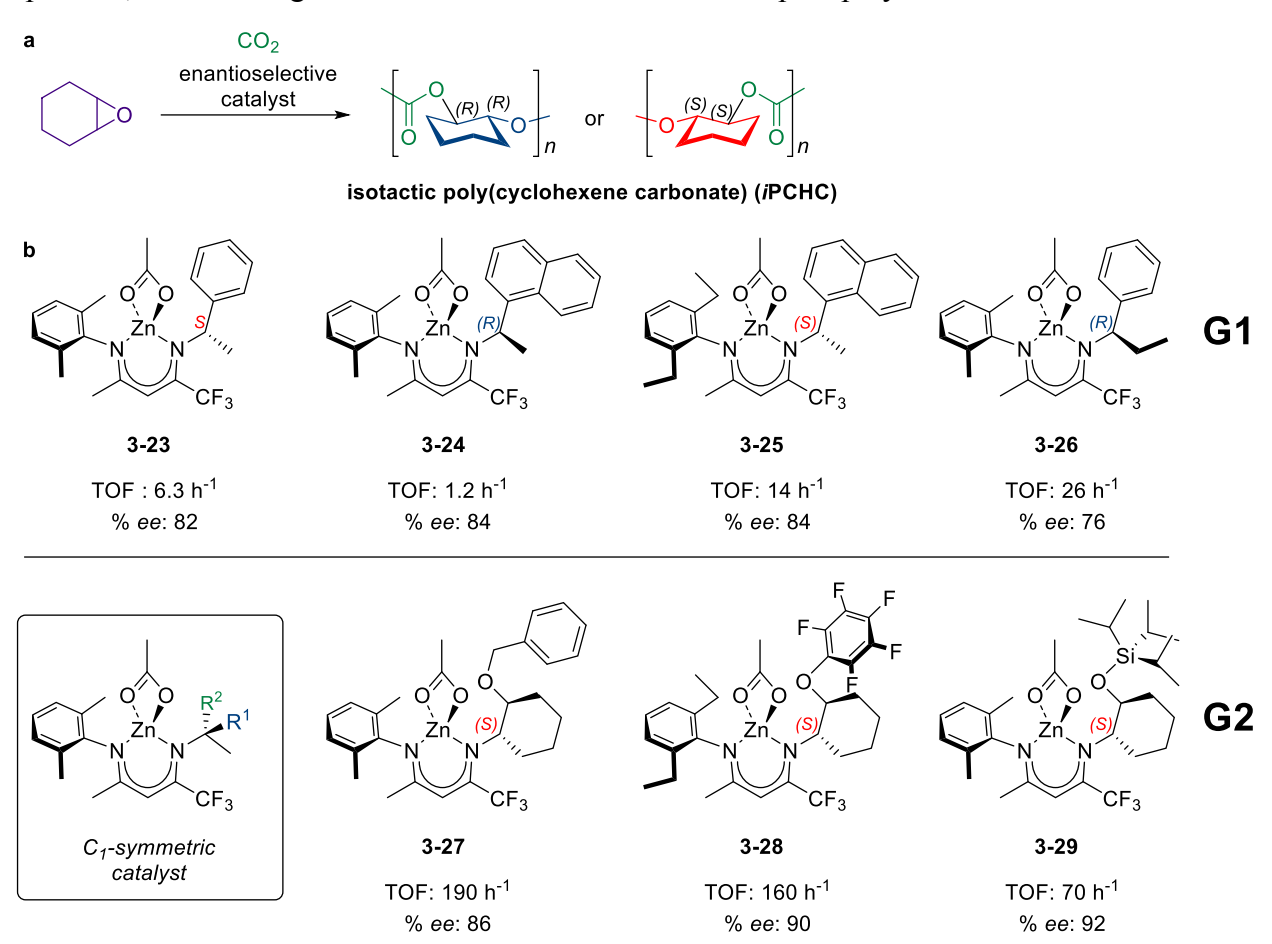
epoxide ring-opening: the polymerization rate depended linearly on the concentration of the catalyst at both high and extremely low catalyst loadings. Interestingly, the aminocyclopropenium cocatalyst also suppresses transesterification and epimerization side reactions commonly observed in ROCOP catalyzed by PPN-based binary systems at high cyclic anhydride conversion. However, some chain coupling is observed after full conversion of the anhydride, suggesting that the TDAC cocatalyst permits S_N2-type chemistry between chloride and persistent alkoxide chain-ends. When using the bifunctional catalyst, the researchers ascribed the relatively low amount of chain-end coupling to the proximity of the cocatalyst and Lewis acid, which keeps alkoxide chain-ends associated with the metal center, reducing their nucleophilicity.

Chart 4. Bifunctional Al-catalysts with tethered TDAC cocatalyst. 102

Copolymerization of epoxides and CO₂ is another essential reaction for the construction of chemically degradable polycarbonate thermoplastics, such as isotactic poly(cyclohexene carbonate) (*i*PCHC).¹⁰⁸ Ellis *et al.* developed a new class of Zn catalysts for the preparation of highly isotactic polycarbonates by the alternating copolymerization of CO₂ and *meso*-CHO.¹⁰⁹ Stereoselective S_N2-type epoxide ring-opening leads to desymmetrization during polymerization and affords an isotactic polymer (**Scheme 25a**). Motivated by previously investigated Zn-based catalytic systems for copolymerization of CO₂ and epoxides, ^{110,111,112,113,114} the authors focused on designing enantioselective zinc β -diiminate (BDI) catalysts. ^{115,116,117,118} Based on previous mechanistic knowledge, the researchers targeted a new class of hybrid C_I -symmetric ligands featuring a single stereocenter, which upon coordination to Zn afforded a series of reactive and stereoselective catalysts (**3-23** to **3-29**, **Scheme 25b**). ¹¹⁹

Significantly, the steric properties of ligand substituents effectively controlled the polymer tacticity. A preliminary screening of catalysts 3-23 to 3-26 revealed that steric bulk at the stereocenter improves both activity and stereoselectivity. The researchers therefore designed the second-generation catalysts 3-27, 3-28, and 3-29, which exhibited high TOF, enantioselectivity, and narrow molar mass distribution in polymerizations performed at 0 °C. Characterization of the pre-catalysts by solid-state X-ray crystallography and by NMR spectroscopic analysis in solution suggested a dimeric catalytic system. The authors therefore proposed that higher dimer lability leads to favorable reactivity. Subsequent computational modeling by Shao *et al.* confirmed that the turnover-limiting step is ring-opening of the epoxide coordinated to a binuclear catalyst. 120

CO₂ insertion, by contrast, occurs with the catalyst dissociated in *mono*nuclear form, and is computed to be kinetically facile by comparison. The modeling attributed the stereochemical preference observed with catalyst **3-27** to differential distortions associated with key non-bonded interactions in competing transition-state structures. The living nature of the new class of catalysts enabled Moore et al. to prepare block copolymers by sequential feeding of different alicyclic epoxides, thus offering an attractive route toward more complex polymer architectures. ¹¹⁹



Scheme 25. a) Stereoselective copolymerization of *meso* CHO and CO₂ and b) structures of the first-generation (G1) and second-generation (G2) catalysts; TOF and % *ee* are given for reactions at 22 °C and 8 atm CO₂ in toluene. 119

3.2. Ring-Opening Transesterification Polymerization of Lactones

Cyclic esters are excellent building blocks for polyesters, which can be prepared under less harsh conditions than those required for condensation polymerization of diols and diacids. Moreover, the "coordination-insertion" mechanism (facilitated by a Brønsted or Lewis acid catalyst) typically observed in ROTEP tends to demonstrate more control over polymer molar mass than condensation polymerization strategies. **Scheme 26** depicts a generic coordination-insertion mechanism of the metal alkoxide-catalyzed ROTEP of ε-caprolactone (ε-CL), which involves three productive elementary steps: i) coordination of the ε-CL monomer to the Lewis acidic metal

center to activate the ester; ii) insertion of the nucleophilic alkoxide into the activated ester bond to form a tetrahedral intermediate; iii) ring-opening by C–O bond cleavage to extend the polymer chain and regenerate the metal alkoxide propagating species. There also exist one competing unproductive coordination step (iv). Because these sequential independent steps are affected differently by the steric and electronic properties of the catalyst, various groups in the CSP have performed mechanistic studies to elucidate structure-activity relationships in the ROTEP of lactones, many of which are discussed next.

Scheme 26. Proposed mechanism of ROTEP of ε -CL.

Ding *et al.* studied the effects of ligand variation on the rate of ε -CL ROTEP catalyzed by Alalkoxide complexes bearing ligands with electron donating (R = OMe) and withdrawing (R = Br, NO₂) substituents in **3-30** to **3-32** (**Chart 5**). The researchers first studied the kinetics of ROTEP of ε -CL catalyzed by **3-30** to **3-32** using ¹H NMR spectroscopy. They then analyzed the thermodynamic parameters associated with substrate coordination and the kinetic data of the insertion step. The experimental mechanistic studies demonstrated that the electronic properties of the ligand have different effects on both the thermodynamic parameters of the coordination step and the rate of the insertion step. Hammett plot analysis and DFT calculations suggested that monomer binding (K_{eq}) is unaffected by varying the electronic properties of the ligand. However, the rate of alkoxide insertion (k_2) is strongly enhanced by electron-donating R substituents.

Chart 5. Al-catalysts with varying remote substituents. 122

In 2013, Miranda *et al.* conducted kinetic experiments on the polymerization of ε -CL catalyzed by monomeric Al(salen) complexes comprising ligands with similar steric properties but different

electron donating characteristics (**3-33** to **3-35**, R¹ = OMe, Br, and NO₂ respectively) (**Chart 6**). This kinetic study demonstrated that the equilibrium of monomer binding (K_{eq}) is not altered significantly by increasing the electronic-withdrawing character of the ligand. Alternatively, k_2 of the insertion step showed a much more significant enhancement of the rate with an increase in electron withdrawing character. Further, the authors evaluated thermodynamic parameters (obtained from the Eyring equation) associated with K_{eq} (ΔG°) and k_2 (ΔG^{\ddagger}). They reported that the ΔG° values for all catalysts studied are close to zero, and that the equilibrium for monomer binding is not affected by the ligand substitutions. The free energy of alkoxide insertion (ΔG^{\ddagger}) decreases as the electron-withdrawing character increases, which is consistent with the rate of polymerization of ε -CL being higher with catalysts bearing electron withdrawing groups (**3-34** and **3-35**) than with catalysts bearing electron-donating substitutions (**3-33**).

Miranda *et al.* performed DFT calculations to rationalize the experimental kinetics and understand the origin of ligand-controlled reactivity. The authors found that alkoxide insertion is the rate-limiting step. DFT calculations predicted that free energies of activation decrease with an increase in the electron-withdrawing character of ligand substituents, which agreed well with the experimental results. Furthermore, Charge Model 5¹²⁴ (CM5) analysis on the initial rate-limiting alkoxide insertion step revealed that the calculated CM5 charge of the Al atom increases with increasing electron withdrawing character of the R substituent in complexes **3-33** to **3-35**. The authors concluded that the higher Lewis acidity of the electron deficient metal center enhances the ROTEP reaction rate through the stabilization of the alkoxide insertion transition state.

R
$$\longrightarrow$$
 N \longrightarrow N \longrightarrow

Chart 6. Al(salen) catalysts used in studies of ROTEP. 123,125

Marlier *et al.* continued the mechanistic study of ligand-rate relationships in ROTEP of lactones using complexes **3-33** to **3-35** (R=OMe, Br, and NO₂) and **3-36** to **3-38** (R=OMe, Br, and NO₂). The authors obtained thermodynamic and kinetic parameters using 1 H NMR spectroscopy. Consistent with previous studies, 123 differences in K_{eq} for the investigated catalysts were relatively small, suggesting that the electronic properties of the ligand do not significantly affect the equilibrium of monomer binding. The authors evaluated the activation parameters (k_2) of the ϵ -CL polymerization reaction using both Eyring plots and DFT calculations for all six catalysts. These studies yielded three pieces of mechanistic information: i) the binding of ϵ -CL can take place *trans* to the alkoxide to form an off-cycle intermediate, which can potentially lead to an unproductive pathway (see iv in **Scheme 26**); ii) catalysts with more electron-withdrawing R substituents (**3-35** and **3-38**) are more active than those with more electron-donating R substituents (**3-33** and **3-36**);

and iii) catalysts **3-36** to **3-38** with longer backbone linkers better facilitate the insertion step, which consequently leads to higher polymerization rates compared to catalysts **3-33** to **3-35**. A linear relationship was found between the computed ΔG^{\ddagger} (and consequently the rate of ROTEP) and the computed framework distortion energies (FDE), where the latter refers to the energy required to take the metal-ligand framework from the resting catalyst geometry to that in the transition-state structure *without* any coordinating reactants in either case, *i.e.*, it is a measure of the intrinsic deformability of the catalyst with respect to achieving a geometry that promotes nucleophilic ring-opening. DFT calculations demonstrated that the smaller FDEs accompanying the structural changes in catalysts **3-36** to **3-38** are the key contributors to the lower kinetic barrier of the insertion step.

In 2017, Stasiw *et al.* hypothesized that a new Al-alkoxide catalyst (3-39) may prevent the unproductive *trans*-binding of ε -CL and lead to higher reactivity in the ROTEP of ε -CL (Chart 7). However, they found that 3-39 is significantly less active ($t_{1/2} = 1920$ min) than other aluminum alkyl catalysts 3-41 (10 min), have 127 3-42 (104 min), have 127 3-43 (332 min), have 128 and alkoxide (3-38) (R = Et), the authors conducted DFT calculations using a truncated model complex 3-40 (R = Me). The calculated free energy of activation of the ε -CL ring-opening step is high, consistent with the experimentally observed low rate of ROTEP. Although the computational studies identified that 3-42 suppresses the *trans*-binding of ε -CL as hypothesized, the high FDE, associated with the very "stiff" cyclic ligand, was found to be more important, leading to the observed low activity of model catalyst 3-40, and by extension 3-39.

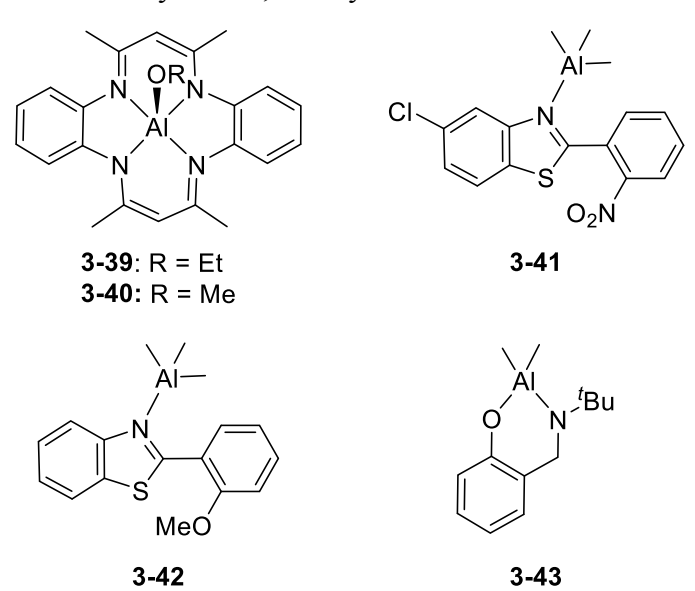


Chart 7. Al catalysts designed to study effects of FDE on rate of ROTEP. 126

In an effort to design more efficient Al(salen) catalysts with smaller FDEs, and a consequently higher rate of ROTEP, Macaranas *et al.* incorporated sterically bulkier and more rigid adamantyl (Ad) substitutions at the *ortho* aryl position of the ligand (3-44 and 3-45 in Chart 8). ¹²⁹ The experimental kinetic studies suggested that the polymerization rate has little dependence on the monomer binding, regardless of the catalyst studied. Conversely, the rate of ε -CL ring-opening

increases by two (3-45 vs 3-37) to five (3-44 vs 3-34) orders of magnitude when incorporating Ad instead of 'Bu *ortho* substituents. Consistent with the hypothesis, the *ortho*-Ad-substituted catalysts 3-44 and 3-45 lead to pre-distorted Al species with calculated low FDEs, thus lowering the kinetic barrier of ε-CL insertion and enhancing the rate of ROTEP.

$$Br \xrightarrow{AI} O \mid O \longrightarrow Br$$

$$Ad Ad Ad Ad Ad$$

$$3-44$$

$$3-45$$

Chart 8. Al(salen) catalysts with sterically bulky Ad substituents. 129

Continuing this work, Mandal *et al.* explored the development of a series of new aluminum alkoxide catalysts for the ROTEP of ε -CL and used the previously employed FDE model to predict their catalytic activity towards the ROTEP of ε -CL (**Chart 9**). The authors first computed free energies of activation for the rate-limiting alkoxide insertion to ε -CL, as well as the associated FDEs. Based on the DFT calculations, they predicted that (N,N,N,N)-aluminum complexes with bis-indolide Schiff-base ligands (3-53 to 3-57) and pyridine-based catalysts (3-50 and 3-51) should be more efficient than other catalysts (3-46 to 3-49 and 3-52) for ROTEP of ε -CL. To validate the theoretical prediction, the authors synthesized a benzyloxy analogue of complex 3-54 (R = Bn), and observed a rate (k_{obs}) that agreed with the predicted ΔG^{\ddagger} . This study exemplifies rational catalyst design inspired by theory in the CSP.

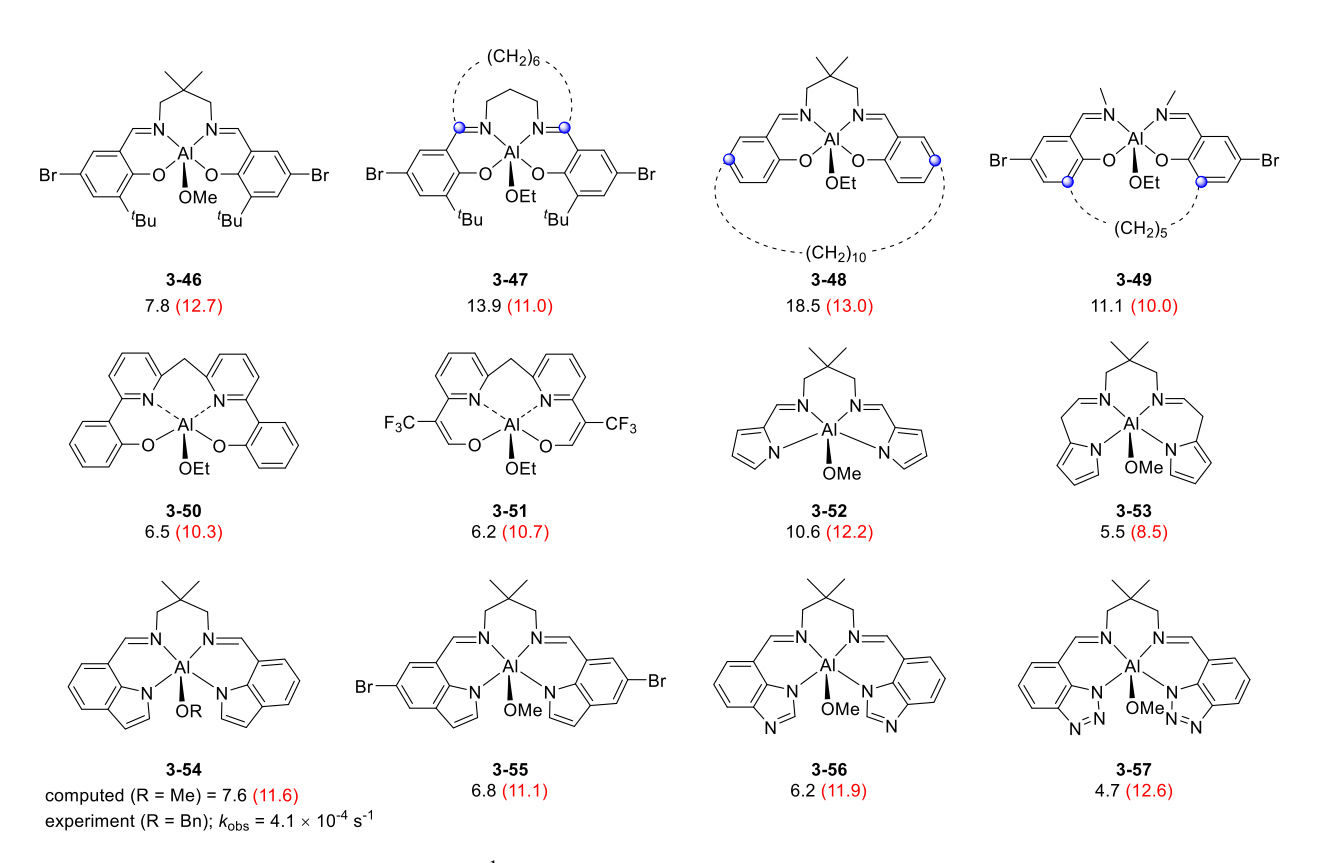
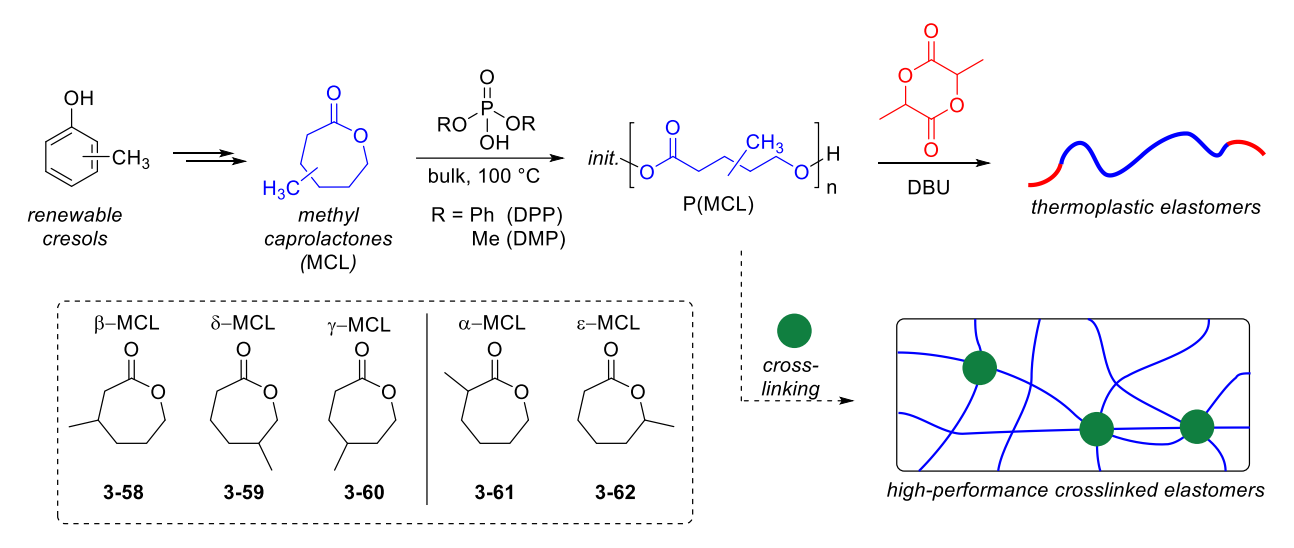


Chart 9. Free energies (kcal mol⁻¹) of activation (black) for alkoxide insertion and associated FDEs (kcal mol⁻¹) (red and in parentheses) of various Al-alkoxide catalysts at the SMD_(CH2Cl2)/M06-2X-D3/6-311+G(d,p) level of theory.¹³⁰

While ε-CL provides a convenient model monomer to study the ROTEP mechanism, researchers at the CSP have also investigated ROTEP of a variety of other lactone derivatives and the properties of the resulting polyesters. Polymers derived from substituted caprolactones are suitable for applications requiring thermoplastic and crosslinked elastomers. thermodynamics of polymerization make y-methylcaprolactone 3-60 a promising building block for low entanglement (M_e) and potentially biodegradable aliphatic polyesters. However, obtaining isomerically pure feedstocks of the requisite para-cresol can be challenging (Scheme 27). As briefly introduced in the previous section, Batiste et al. investigated the use of mixtures of various methyl caprolactone monomers β , δ , and γ -MCL (3-58 to 3-60) in Brønsted acid-catalyzed ROTEP and compared the thermal and rheological properties of the resulting polymers to those obtained from pure 3-60.⁴⁸ These monomers (3-58 to 3-60) can be derived from a mixed stream of *meta*and para-cresol, which represents a significant economic advantage in the processing of raw biomaterials to polymer ingredients. The authors synthesized a range of copolymers and terpolymers from equimolar mixtures of 3-58 to 3-60 (and found the resulting materials to have comparable T_g and M_e values to those of poly-y-methylcaprolactone (poly(3-60)). This observation suggested that polymers from a mixed monomer stream can be used to produce high-performance materials. Also, dimethylphosphoric acid (DMP) was found to be an effective organocatalyst for the ROTEP of cyclic esters, and it enables facile purification by devolatilization under vacuum. However, polymerizations employing DMP proceed with less molar mass control than the

analogous and more commonly used diphenylphosophoric acid (DPP). Nevertheless, the presence of α MCL and ε MCL (**3-61** and **3-62**), which can be prepared from *ortho*-cresol, led to eliminative termination reactions and precluded good molar mass control during the polymerization. Batiste *et al.* demonstrated that polymers synthesized from a mixture of MCL monomers have highly competitive thermal and mechanical properties to poly(**3-60**).



Scheme 28. Brønsted acid-catalyzed formation of poly(MCL) from mixed cresols. ⁴⁸

Fahnhorst *et al.* investigated the polymerization of 4-carbomethoxyvalerolactone **3-63** using the Zn(II) catalyst **3-64** (**Scheme 29**). ROTEP of **3-63** quickly formed the linear polyester **3-65** in high conversion similarly to the DPP catalyzed process previously reported. However, when this linear polyester was subjected to catalyst **3-64** for an extended period, the thermal properties of the obtained amorphous product no longer matched those reported for the linear semicrystalline material. In addition, the HNMR spectrum of the new product featured multiple new resonances for the methyl ester substituent, suggesting that various unexpected microstructural environments were present. The authors proposed that the product material was the highly branched, isostructural, equilibrated polyester **3-66**.

Although tin(II) octoate catalyzed a retro-ROTEP process of the linear polymer **3-65** to produce monomer, subjecting the branched polymer **3-66** to the same conditions had little effect. Moreover, exposing **3-66** to the organobase 1,8-diazabicyclo[5.4.0]undec-7-ene (DBU) produced a series of four methyleneglutarate degradation products, suggesting that multiple transesterification events along the side chain and in the backbone of the linear polymer are present in the highly branched analogue. MALDI-TOF MS and time-dependent SEC measurements of the isomerization from the linear to hyperbranched architectures further corroborated the structure of **3-66**. In a complementary experiment, the isomeric propiolactone monomer **3-67** was subjected to ROTEP conditions to produce the isomeric polyester **3-68**, which also converged to the same highly branched, equilibrated structure **3-66** upon extended exposure to the catalyst **3-64**. This unprecedented transesterification of linear polymers **3-65** and **3-68** to hyperbranched polymer **3-66** was attributed to the presence of carboalkoxy substituents in each repeat unit of the linear polyester precursors.

3-64
$$fast$$
 CO_2Me

3-64
 $fast$
 CO_2Me

3-65

3-66

 CO_2Me

3-64
 $fast$
 CO_2Me

3-65
 $fast$
 CO_2Me

3-64
 $fast$
 CO_2Me

3-65
 $fast$
 CO_2Me

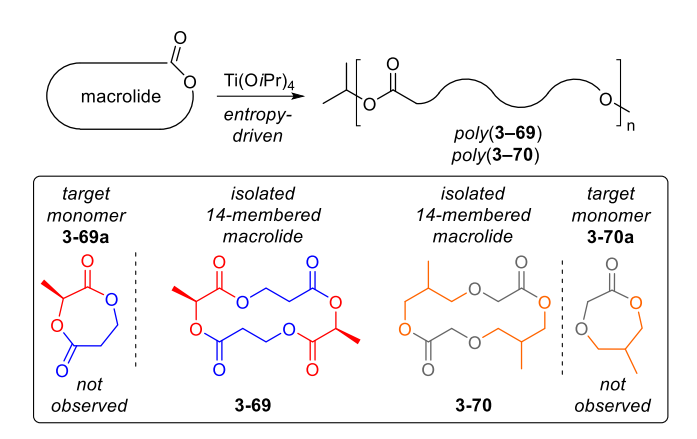
3-66
 $fast$
 CO_2Me

3-64
 $fast$
 CO_2Me

3-68

Scheme 29. Zn-catalyzed transesterification of two isomeric linear polyesters to a hyperbranched structure. ¹³¹

In other related work, Amador et al. reported the polymerization of unstrained cyclic esters (14membered macrolides 3-69 and 3-70) through entropy-driven ROTEP. 133 These researchers attempted to synthesize two distinct 7-membered cyclic esters (Scheme 30), the first comprising a unit of lactic acid and 3-hydroxypropionic acid and the second comprising a unit of glycolic acid and 2-methylpropanediol. Surprisingly, only higher-order macrolides, the 14-membered products 3-69 and 3-70 (Scheme 30) as well as small amounts of analogous 21-membered macrolides were observed. Ring-strain calculations suggested that ROTEP of these macrolides is driven by entropy, as opposed to ring-strain relief as observed in ROTEP of monomers of smaller ring size. The authors used the nontoxic and inexpensive Ti(O'Pr)₄ as catalyst to polymerize the macrolides both in toluene and in bulk to high conversion in a short time period. The molar mass of the resulting polyesters was as high as 70 kg mol⁻¹ with dispersity values D = 1.3-1.7. The macrolide-derived polyesters were thermally stable up to ca. 215 °C. Consistent with the authors' theoretical predictions according to the Fox equation, ¹³⁴ both of the atactic polyesters poly(**3-69**) and poly(**3-**70) were amorphous and demonstrated low T_g values (-30 and 7 °C, respectively). In contrast, a perfectly alternating, semicrystalline variant of poly(3-69), synthesized through condensation polymerization of the stereoregular diols and diacids, exhibited a T_m at 96 °C, suggesting that stereoregularity was necessary for crystallinity in these polymers.



Scheme 30. Entropy-driven ROTEP of unstrained macrolides. 133

Continuing work presented in Section 2, Gurusamy-Thangavelu *et al.* used two terpene-derived lactones, carvomenthide (2-46) and menthide,³⁶ to prepare four renewable polyols with different molar mass for polyurethane film formulations (Scheme 31).¹³⁵ ROTEP of 2-46 or menthide using tin(II) octoate catalyst and diethanolamine initiator (3-71) formed trifunctional polyols (3-72), whose structures were characterized using ¹H NMR spectroscopy. Formulation of the product polyols 3-72 with additional short chain diol components (diethylene glycol, 3-73) and diisocyanate components (diphenylmethane diisocyanate, 3-74) gave polyurethane films. The researchers modified the T_g value of these polyurethane films by introducing polyols 3-72 of varying molar mass from a range of precursor monomers and diisocyanates. They also conducted dynamic mechanical thermal analysis (DMTA) and tensile testing of these polyurethane films. The results (*e.g.*, modulus values) showed that at ambient temperature, the films from lower molar mass polyols show potential as tough biobased plastic materials, and those from higher molar mass polyols behave like crosslinked elastomers.

Scheme 31. a) Preparation of trifunctional polyols **3-72** through ROTEP. b) Preparation of biobased polyurethane films. ¹³⁵

Lactide has also attracted considerable attention in the CSP because ROTEP of D-, L-, and rac-lactides can lead to distinct microstructures and therefore diverse material properties. In 2004, Jensen $et\ al$. developed an indium-based catalytic system (InCl₃, BnOH, and Et₃N) displaying remarkable stereocontrol in the ROTEP of lactide. ¹³⁶ As continuing work, Pietrangelo $et\ al$. investigated the mechanistic features and attempted to elucidate the origin of heterospecifity in the polymerization process despite the absence of a chiral ligand. ¹³⁷ Linear relationships between M_n and monomer conversion suggested that ROTEP of lactide is controlled by the In catalyst.

The authors then characterized the structure of the active catalyst and investigated the reaction mechanism via various experimental approaches. Analyses of polymer samples by MALDI-TOF MS and ¹H NMR spectroscopy validated that BnOH is the initiating species. Kinetic data for the polymerization subsequently revealed a first-order dependence on the concentration of InCl₃ and a zero-order dependence on the concentrations of BnOH and NEt₃. To identify the active catalyst, the authors first varied the halide ligands bound to the active catalytic species. Following a decrease in polymerization rate upon variation of the halide ligands (X = Cl, Br, I), the authors concluded that the ligand is part of the active catalytic species. Furthermore, loss of stereoregularity when using a homoleptic [In(OCH₂CH₂OCH₃)₃] pre-catalyst demonstrated the significance of the halide ligands for both the rate and stereocontrol. To further elucidate the structural features of the active catalyst, the researchers employed a 3-diethylamino-1-propanol (deapH) ligand instead of BnOH and Et₃N. X-ray crystallography analysis showed that [InCl₃(deapH)(H₂O)]₂ (3-75) is dinuclear in the solid state and that its structure is retained in solution, as determined by FTIR and pulsed gradient spin-echo (PGSE) NMR spectroscopies (Chart 10). Despite a slightly lower rate of polymerization, catalyst 3-75 displayed comparable stereocontrol to the InCl₃/BnOH/Et₃N system, leading the authors to suggest that similarly active bimetallic species are formed in both systems. In addition, the crystal structure indicated that the amine merely serves as a base activating the BnOH initiator, which was further validated by tertiary amines, including the non-nucleophilic replacing Et₃N with other bis(dimethylamino)naphthalene (Proton Sponge®). The similarity between polymerization rates of meso-lactide and D,L-lactide suggested a mechanism in which both the rate and selectivity of monomer enchainment are derived from several stereocenters in the monomer and propagating polymer chain.

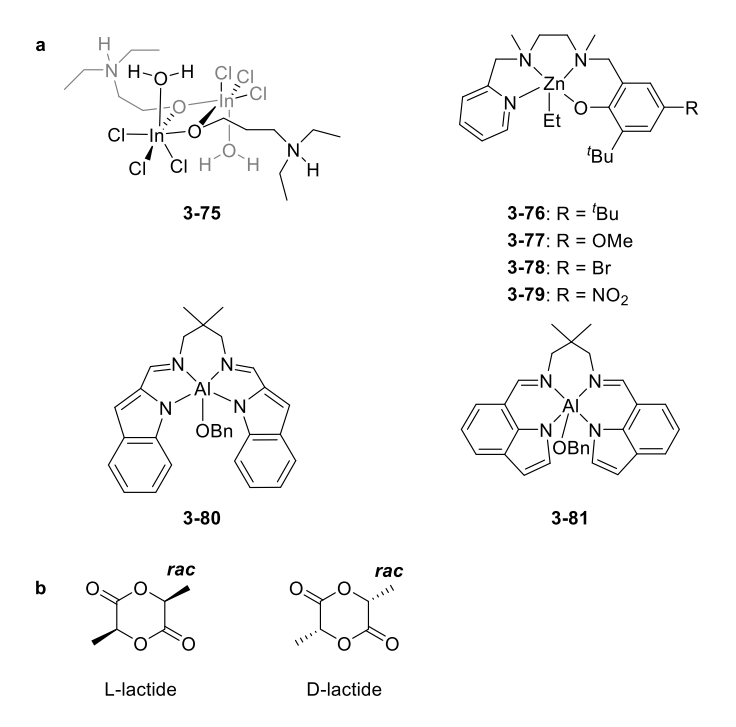


Chart 10. Catalysts and monomers used in ROTEP of lactides. 136,138,139

In 2017, Stasiw et al. performed kinetic experiments on the ROTEP of rac-lactide using Zncatalysts 3-76 to 3-79 (Chart 10) comprising phenolate donors with various para- substituents (R = ^tBu, OMe, Br, and NO₂, respectively). ¹³⁸ The polymerization follows a pseudo-first-order rate expression and the rate of polymerization of rac-lactide was nearly unaffected by varying the electronic properties of the Zn-based catalysts (3-76 to 3-79), as opposed to the aforementioned Al(salen) catalysts (3-33 to 3-35) in the ROTEP of ε -CL. All catalysts studied promoted formation of isotactic polymers with $P_{\rm m} = 0.72 - 0.78$ and narrow θ (1.06–1.17). Subsequently, the authors conducted computational mechanistic studies to understand the electronic effect of the para- substituents on rate and isotacticity of the polymerization. DFT modeling predicted lactide ring-opening to be the rate-limiting step for both enantiomers of rac-lactide. The computed energetics for 3-76 to 3-79 indicated that the free energies of activation for catalysts bearing electron-withdrawing Br and NO₂ substituents (12.9 kcal mol⁻¹ and 13.3 kcal mol⁻¹ for **3-78** and 3-79, respectively) are only slightly lower compared to those for the complexes bearing electrondonating 'Bu and OMe substituents (14.0 kcal mol⁻¹ and 14.0 kcal mol⁻¹ for 3-76 and 3-77, respectively), consistent with the experimental observations. The authors identified that the formation of the S,S enantiomer (15.4 to 16.9 kcal mol⁻¹) requires higher free energies of activation compared to those required to form the $R_{*}R$ enantiomer (12.9 to 14.0 kcal mol⁻¹) in the stereodetermining ring-opening step for the catalysts 3-76 and 3-79. The predicted isotacticities are consistent with the experimental findings, revealing that the origin of isotacticity is governed by steric repulsions between the ligand and lactide.

Recently, Luke *et al.* synthesized and characterized aluminum complexes bearing indolide-imine ligands (3-80 and 3-81) to study the catalyst-controlled stereoselectivity in initiation of ROTEP of *rac*-lactide. ¹³⁹ Using VT-NMR, the authors identified interconversion of the Δ and Λ enantiomers

of pre-catalysts **3-80** and **3-81**. Upon stoichiometric reactions of rac-, L(S,S)-, and D(R,R)-lactide, four possible stereoisomers, classified as two diastereomeric pairs of enantiomers: Δ - $L(S,S)/\Lambda$ -D(R,R) and Δ - $D(R,R)/\Lambda$ -L(S,S) are expected. Interestingly, ¹H NMR spectra of the products of the reaction with rac-, L(S,S)-, and D(R,R)-lactide are nearly identical, which suggested the selective formation of a 1:1 mixture of two symmetric complexes, or a single asymmetric complex. Moreover, X-ray crystallography revealed that the initial ring-opening forms a pair of enantiomers comprising a single diastereomer (Δ -L(S,S) and Λ -D(R,R)). Further NMR exchange spectroscopy (EXSY) experiments and DFT calculation revealed that the stereoselectivity of initiation is thermodynamically controlled rather than kinetically controlled.

3.3. Other Polymerization Processes to Produce Sustainable Polymers

CSP researchers have also investigated a variety of other polymerization strategies for the synthesis of sustainable polymer materials. Ahmed *et al.* investigated the enantioselective polymerization of PO using biaryl-linked bimetallic Co(salen) catalysts using both experimental and theoretical approaches. These bimetallic cobalt(III) complexes (3-82 and 3-83) comprise two salen moieties linked through a chiral binaphthol linker, affording a favorable Co···Co separation for epoxide enchainment. Cocatalyst salts, such as [PPN]OAc 3-82 and 3-83, kinetically resolve racemic epoxides to yield highly isotactic polyethers and unreacted enantioenriched epoxides (Scheme 32). Specifically, the absolute configuration of the binaphthol linker in both 3-82 and 3-83 determines an enantiomeric preference for the S-epoxide. Further computational studies led to the conclusion that the Co(III) centers of these catalysts experienced spin crossover along the most favorable reaction pathway.

Scheme 32 Enantioselective homopolymerization of epoxides catalyzed by bimetallic Co complexes. 140

Carbohydrates are promising sustainable feedstocks for polymer building blocks. Lillie *et al.* selected a series of rigid diols to serve as monomer cores, including isosorbide (2-79), glucarodilactone, and *bis*-(hydroxymethyl)furan. ¹⁴¹ These diols were converted to the corresponding diesters with the castor oil-derived 10-undecenoic acid, resulting in α , ω -diene monomers 3-84, 3-85 (first reported by Shearouse⁷¹ *et al.*, see Section 2 for more details), and 3-86, which are suitable for ruthenium-catalyzed ADMET polymerization (Scheme 33). Although homopolymers poly(3-84) and poly(3-85) were both rather brittle (though the latter was glassier and tougher), a statistical copolymer comprised of an equimolar mixture of the two monomers was an elastic material (ca. 500% strain-at-break) with shape memory capabilities. The authors

prepared a series of copolymers comprising varying ratios of **3-84** and **3-85** to better understand the structure-property relationships of these materials. Polymers rich in **3-85** showed higher T_g (15–32 °C) and T_m (46–59 °C) values than those rich in **3-84**.

Small-amplitude oscillatory shear rheology measurements indicated the presence of transient network points in the material; this observation is supported by the detection of small nanoscale aggregates by X-ray scattering. To probe the source of the transient networking, the authors synthesized an additional set of copolymers containing various fractions of monomers **3-86** and **3-85**. The new copolymers of **3-86** and **3-85** were generally softer and had lower T_g values than copolymers featuring **3-84** and **3-85**. Incorporation of **3-85** was necessary for good mechanical strength and shape memory behavior. Partial decomposition of glucarodilactone in **3-85**-containing materials may result in hydrogen bonding capabilities, responsible for transient network points. Glucarodilactone (**3-85**)-containing polymers also display enhanced degradability under basic conditions. Hydrolysis of the strained dilactone liberates carboxyl and hydroxyl groups, increasing the hydrophilicity of the material. A subsequent study by Kim *et al.* suggested these α , ω -diene monomers, in combination with a degradable tetrathiol crosslinker under UV irradiation, produce electrospun thermoset fibers. 142

Scheme 33. ADMET polymerization of alpha, omega-dienes derived from isosorbide, glucaodilactone, and bis-(hydroxymethyl)furan¹⁴¹

Previous methods for synthesizing polyethers derived from isosorbide offered poor architectural control and resulted in oligomeric and non-linear products. Saxon *et al.* developed a method for producing well-defined polyethers from annulated tricyclic ether monomer **3-87**, which was prepared in good yield from isosorbide using a regioselective strategy. He authors employed high-throughput screening tools to efficiently evaluate polymerization catalysts and initiators under a wide array of conditions. Cationic ring-opening polymerization (cROP) was the only method that resulted in successful homopolymerization of **3-87** to form **3-88**. Because the cationic initiation with methyl triflate resulted in low conversion and degradation of the monomer core through side reactions, the authors investigated the initiation mechanism with the aim of finding a way to favor homopolymerization.

As shown in **Scheme 34**, monomer **3-87** can undergo an electrophilic ring-opening reaction at two positions: ring-opening at the bridgehead ether (red pathway) results in productive propagation toward polyether **3-88**, while ring-opening at the terminal ether (blue pathway) to obtain **3-89** leads to termination and crosslinking. DFT calculations were undertaken to better understand the thermodynamics of polymerization, revealing that one equivalent of PO initiator lowered the

activation barrier for productive ring-opening with the Sc(OTf)₃ catalyst. Although conversion of monomer **3-87** to polymer **3-88** was suboptimal (≤16%), excess monomer could be recovered by sublimation. The solvent dielectric constant played an important role in determining the topology of the polymer product. High dielectric solvents, such as acetonitrile, enhanced the charge separation of the end groups and exclusively formed linear species, while lower dielectric solvents like dichloromethane produced macrocyclic polymers, as corroborated by MALDI-TOF MS and ¹H NMR spectroscopy.

Scheme 34. Architectural control of isosorbide-derived polyethers by polymerization solvent. 144

Schneiderman *et al.* studied the open-to-air enzyme-assisted, reversible addition-fragmentation chain transfer (EnzA-RAFT) polymerization of hydroxyethyl acrylate (**3-90**) in a variety of complex aqueous solvents. The glucose oxidase (GOx) enzyme is essential to deoxygenate the open-to-air aqueous RAFT polymerization reaction, which can improve scalability of the controlled polymerization processes (**Scheme 35**). The kinetic and chain extension experiments on the HEA polymerization reaction in whiskey suggested all the flavor compounds in the whiskey had inconsequential impacts on the polymer molar mass, D, and end-group fidelity. The authors then tested the EnzA-RAFT reaction in a wide range of solvents containing many additives, including commercially available beer, wine, liquor, and fermentation broth. All solvents tested afforded low $D \leq 1.2$ and good conversion (68–97%), with grape juice as the only exception. Their studies demonstrated that EnzA-RAFT polymerization can take place under mild conditions and is resilient towards minor contaminants, which is essential to aid cell survival and growth.

Scheme 35. Enzyme assisted open-to-air RAFT of HEA. 146

CSP researchers have also investigated the biosynthesis of fluoropolymers in living cells from renewable sources. In 2017, Thuronyi *et al.* designed a high-flux organofluorine biosynthetic pathway to produce 2-fluoro-3-hydroxybutyrate (FHB) through organofluorine metabolism. ¹⁴⁷ In the presence of fluoromalonyl coenzyme A (CoA), FHB-CoA monomer polymerized to form novel 2-fluorinated polymers (poly(FHB-*co*-HB)) *in vivo*. The authors have demonstrated that this system can produce biopolymer with up to 15% fluorinated monomers.

4. Intended Use

4.1. Thermoplastic Elastomers

Thermoplastic elastomers (TPEs) are a class of reprocessable copolymers that display both elastic and thermoplastic behavior depending on the temperature of the system. Most commonly, TPEs have a linear ABA triblock molecular architecture (**Figure 6**), where the A endblocks are a hard, rigid (i.e., glassy or semi-crystalline) polymer while the B polymer is a soft, rubbery midblock. If the ABA triblock possesses sufficiently large segregation strength (i.e., the product of the Flory-Huggins interaction parameter and the volume normalized degree of polymerization, χ N), the system microphase separates into an ordered morphology with domains rich in A and B. The selection of polymers for the hard and soft domains and their respective volume fractions affect the tensile strength and stiffness of the material. The ABA TPEs the volume fraction of A (f_A) component is typically <0.5, producing A-rich minority domains dispersed in a B matrix. The hard A endblock domains serve as anchors that physically rather than chemically crosslink the rubbery B matrix to accommodate elastic deformation. This is distinct from a conventional vulcanized rubber that contains covalent sulfide bonds as crosslinks. When the volume fraction of the A blocks is increased such that A becomes the majority component (f_A > 0.50), TPEs begin to behave less like elastomers and more like thermoplastics.

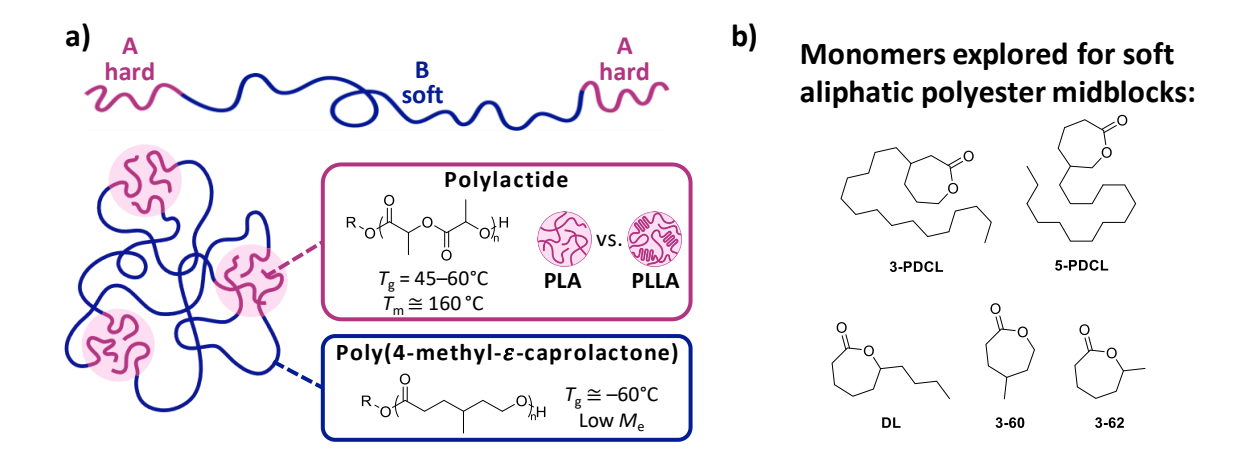


Figure 6. a) Schematic of (top) a typical linear ABA triblock copolymer having a volume fraction $f_A < 0.5$ and (bottom, left) the self-assembled, physically crosslinked domain structure of the corresponding thermoplastic elastomer. The boxed insets show a representative aliphatic polyester TPE comprising (blue) soft poly(3-60) and (pink) crosslinking segregated hard blocks of either glassy amorphous or semi-crystalline PLA. ¹⁵⁰ b) Shown here are additional monomers explored by the Center for use as the midblock component of thermoplastic elastomers. ^{150150,156,158,159}

Unlike the chemical crosslinks found in vulcanized rubbers, the physical crosslinking domains in TPEs are reversible because they can become more liquid like upon heating, allowing easier reprocessing or recycling (**Figure 7**). Additionally, the temperature dependence of χ can be exploited to further promote reprocessability. As the temperature of the system is raised above a critical value (order-disorder temperature T_{ODT}), microphase separated polymers undergo an order-disorder transition. During this transition, the polymer domains are able to more readily mix, which results in a relatively homogenous disordered phase characterized by liquid-like rheological properties. An order-disorder transition can also occur when the polymer is dissolved in a good solvent for both blocks. As temperature is decreased below T_{ODT} or the solvent is removed, the material returns to the original microphase separated morphology.

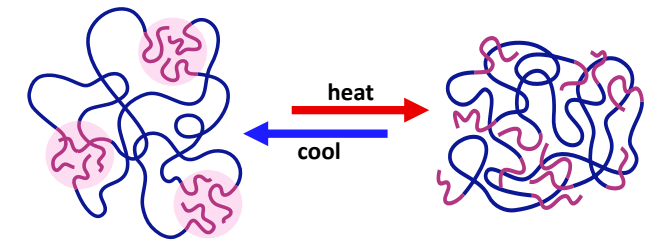


Figure 7. TPEs can be reprocessed by heating them above their order-disorder temperature, resulting in the loss of physical crosslinks and allowing mixing of hard and soft blocks and the formation of a homogenous melt.

The majority of TPEs produced commercially are styrenic ABA triblock polymers. ¹⁵² The Kraton© corporation is one of the most prolific manufacturers of styrenic TPEs, which contain hard polystyrene (PS) endblocks and either a polybutadiene (PB), polyisoprene (PI), or hydrogenated PB or PI rubbery midblocks. ¹⁵³ Unfortunately, these materials are not easily degradable and are completely derived from petroleum feedstocks.

Significant research efforts in the CSP have been devoted to the development of sustainable alternatives to these petrochemical-derived TPEs. Aliphatic polyesters have become an area of focus as they can be prepared from renewable biomass and are amenable to recycling and composting. One method used to synthesize aliphatic polyesters is ROTEP of lactones, as was illustrated in section 3, which enables control over molecular architecture, molar mass, and stereochemical features. The work in the CSP has demonstrated that strategic selection of a rubbery midblock with a low T_g value, in combination with glassy PLA or semi-crystalline poly(L-lactide) (PLLA) endblocks affords sustainable, aliphatic polyester-based thermoplastic elastomers (APTPEs) with mechanical properties similar to styrenic TPEs. PLA is an effective replacement for the hard domains of TPEs due to its low cost, accessibility from renewable resources, and similar mechanical properties to PS, as demonstrated by the following examples. Aliphatic polyester midblocks in PLA-containing TPEs studied by CSP researchers include: poly(ε-methyl-ε-caprolactone) (poly(3-62), poly(ε-caprolactone-co-ε-decalactone) (poly(3-62), poly(ε-decalactone) (poly(3-60)), poly(ε-caprolactone-co-ε-decalactone) (PCD), poly(ε-caprolactone-co-ε-decalactone) (Figure 6).

The ϵ -caprolactone derivative **3-62** was explored as a potential elastomeric midblock for APTPEs using green chemistry principles to synthesize the monomer more safely and efficiently. Using ROTEP, the researchers synthesized a series of PLA-b-poly(**3-62**)-b-PLA triblock polymers with varied molar mass and PLA content. Analysis via small angle X-ray scattering (SAXS) indicated that the polymers were microphase separated at room temperature with low molar mass triblocks displaying ordered cylindrical and lamellar morphologies. Tensile testing of two high molar mass triblocks revealed the effect of PLA content. Both triblock polymers displayed exceptional elastomeric behavior with strains-at-break exceeding those of commercial PS-b-PI-b-PS. Increasing the PLA content in the material from 20 to 34 wt % resulted in a decrease in the strainat-break from 1880 \pm 70 to 1360 \pm 120%. This increase in PLA content also resulted in a 40% increase in the ultimate tensile strength from 10.2 \pm 0.8 to 14 \pm 2 MPa. The materials displayed a high level of elastic recovery, ranging from 88 to 96%, when subjected to 10 loading cycles of 50% strain.

 were mechanically similar to PLA-*b*-poly(3-62)-*b*-PLA materials, displaying large strain-at-break (1310 \pm 44 %) and moderate ultimate tensile strength (9.4 \pm 0.7 MPa).

As another example, Ding *et al.* studied renewable and biodegradable ABA triblock TPEs as pressure-sensitive adhesives (PSA), where the hard A blocks consisted of poly(γ -methyl- α -methylene- γ -butyrolactone) (PMMBL) and the soft B block polymenthide (PM). Tensile tests revealed high strain-at-break values greater than 1600%. Blends of PMMBL-b-PM-b-PMMBL triblocks with rosin ester tackifiers showed high peel adhesion, loop tack, and adhesion failure temperatures. Whereas non-crosslinked styrenic PSAs typically have adhesion-failure temperatures around 100 °C, 161 formulations with PMMBL-b-PM-b-PMMBL displayed failure temperatures greater than 150 °C. The adhesive performance of PMMBL-b-PM-b-PMMBL PSAs was competitive with commercial formulations based on petrochemical polymers.

Expanding on previous work (vide supra, Section 2.2.2), Nasiri et al. investigated the use of ABA triblock polymers as thermoplastic elastomers, using sugar-based poly(glucose-6-acrylate-1,2,3,4tetraacetate) (poly(GATA)) or poly(acetylated acrylic isosorbide) (poly(PAAI)) as endblocks with poly(n-butyl acrylate) ($poly(^nBA)$) as a midblock (Figure 8Figure 8. Sustainable TPEs with applications as pressure sensitive adhesives can be synthesized using poly(n-butyl acrylate) as the soft midblock with sugar-based poly(glucose-6-acrylate-1,2,3,4-tetraacetate) (poly(2-73)) or poly(acetylated acrylic isosorbide) (poly(2-83)) as the hard end blocks.). 162 Poly(n-butyl acrylate)'s large entanglement molar mass (28 kDa) contributes to ideal characteristics as a tacky component in pressure sensitive adhesives. However, an additional tackifier, Sylvalite 80HP, a renewable rosin ester produced by Arizona Chemicals, was added to produce a stronger PSA. Samples of poly(AAI)-b-poly(${}^{n}BA$)-PAAI ($M_{n} = \sim 100 \text{ kDa}$; hard block content = $\sim 10\%$) were prepared with 40 wt % of the rosin ester and exhibited quite impressive adhesion properties as demonstrated by peel (8.74 N cm⁻¹) and loop-tack (2.96 N cm⁻²) tests. They also exhibited no shear failure up to 100 h. The related poly(GATA)-b-poly(BA)-b-poly(GATA) ($M_n = \sim 100 \text{ kDa}$; hard block content = $\sim 10\%$) demonstrated moderate adhesion properties with a shear failure after 844 minutes. To improve the physical properties of this polymer, a partial deacetylation was performed to introduce one hydroxyl group per monomer unit resulting in improved tensile properties, likely due to increased strength in the physical crosslinks through hydrogen bonding. A similar sample of poly(GATA)-b-poly(BA)-b-poly(GATA) ($M_n = \sim 150$ kDa; hard block content = $\sim 25\%$) gave material that showed increased tensile strength (from 0.8 to 1.4 MPa) before and after deacetylation, respectively. Both poly(GATA) and poly(PAAI) demonstrated potential use in TPEs as PSAs. In the case of poly(GATA) a simple post-polymerization deacetylation allowed for a functional group handle to control the physical properties of the material.

$$C_{12}H_{25}$$

$$S$$

$$S$$

$$C_{12}H_{25}$$

$$S$$

$$C_{12}H_{25}$$

$$C_{12}H$$

Figure 8. Sustainable TPEs with applications as pressure sensitive adhesives can be synthesized using poly(*n*-butyl acrylate) as the soft midblock with sugar-based poly(glucose-6-acrylate-1,2,3,4-tetraacetate) (poly(2-73)) or poly(acetylated acrylic isosorbide) (poly(2-83)) as the hard end blocks.

The properties of thermoplastic elastomers depend on the ability of B blocks to bridge the hard (glassy or semi-crystalline) minority domains forming the physical crosslinks. Spencer and Matsen introduced a strategy for calculating the bridging statistics for complex architectures using self-consistent field theory (SCFT). Their study focused on (AB)_n star polymers, in which the hard A blocks at the ends of the star arms form discrete minority domains and the rubbery B blocks in the star's core form a rubbery matrix. High-performance elastomers require the B blocks to bridge different A domains. However, looped B blocks, which force A ends of the same star to reside at the same A/B interface, do not generally contribute to elasticity. SCFT calculations demonstrated that the fraction of bridging molecules increases rapidly with the number of arms, n. For n > 10, nearly all molecules form bridges, resulting in a much larger effective bridging fraction than predicted for conventional linear ABA triblock polymers.

Manipulating the molecular architecture provides control over the fraction of bridging B blocks and therefore the elastomeric performance of a material. While high molar masses are required to achieve beneficial tensile properties in ABA TPEs, which include high ultimate tensile strength and large strain-at-break, the $T_{\rm ODT}$ for these materials also scales with molar mass. Hence, sustainable APTPEs with promising mechanical properties can often display order-disorder transition temperatures above the onset of thermal decomposition ($T_{\rm d}$). The inaccessibility of $T_{\rm ODT}$ values for these high molar mass TPEs poses a problem for facile materials processing, as most industrially relevant melt processing techniques require the low melt viscosity characteristic of block polymers in the disordered state. These challenges have been addressed through (AB)_n multiblock architectures, where the $T_{\rm ODT}$ is influenced by the length of the repeat block more than

the total molar mass (**Figure 9**). ¹⁴⁹ Low molar mass PLA-*b*-PDL-*b*-PLA triblocks displayed low ultimate tensile strengths (0.24 ± 0.01 MPa) and strains-at-break ($218 \pm 9\%$), making them unsuitable for most TPE applications. However, when these telechelic low molar mass triblocks were coupled using 4,4'-methylenebis(phenyl isocyanate) (MDI) to generate high molar mass multiblock polymers, (LDL)_n, the mechanical properties were significantly improved. Compared to the low molar mass precursors, high molar mass multiblock polymers displayed much higher strains-at-break ($1020 \pm 124\%$) and ultimate tensile strengths (6.67 ± 0.37 MPa); however, these values remain lower than those exhibited by PLA-*b*-PDL-*b*-PLA triblocks of analogous total molar mass and composition. Unlike the high molar mass triblocks with inaccessible $T_{\rm ODT}$ values, the linear multiblock polymers were found to disorder at much lower temperatures ($T_{\rm ODT} < 150$ °C), allowing for melt processing via injection molding. This work demonstrates that architecture significantly influences material properties and may be manipulated to facilitate polymer processability.

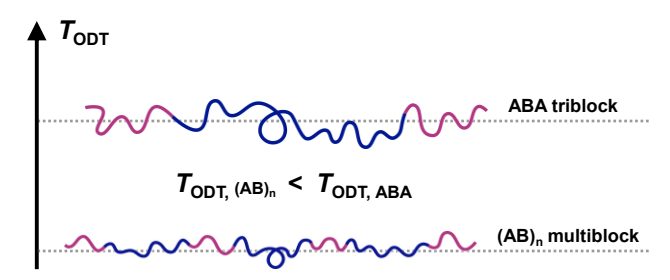


Figure 9. The order disorder transition temperature (T_{ODT}) of multiblock polymers (proportional to the molar mass of the repeat blocks) is lower than the T_{ODT} of an ABA triblock polymer (proportional to polymer molar mass) of analogous overall molar mass. This strategy can enable the T_{ODT} of an initial, telechelic aliphatic ABA triblock polyester to be raised above its inherent T_{d} , dictated by ester pyrolysis cleavage of the backbone.

Given the promising tensile behavior of PLA-*b*-PDL-*b*-PLA materials, researchers further focused on enhancing the rheological and mechanical properties. While the low T_g value and amorphous nature of PDL make it an appealing TPE midblock, the entanglement molar mass (M_e) of the polymer is 5.9 kg mol⁻¹, which can limit the ultimate tensile strength of the material. ¹⁵⁷ To address this, Schneiderman *et al.* explored the use of poly(ε -caprolactone-*co*- ε -decalactone) statistical polymers as the amorphous midblock in APTPEs. ¹⁵⁷ The addition of ε -CL as a co-monomer was found to result in a lowered M_e (3.9 kg mol⁻¹) when compared to PDL homopolymer. Statistical PCD copolymers were synthesized via the bulk melt copolymerization of ε -caprolactone and ε -decalactone with the ε -CL mole fraction ranging from 0.63 to 0.78. The difunctional telechelic PCD copolymers were then used as macroinitiators for the synthesis of PLA-*b*-PCD-*b*-PLA triblock polymers. The tensile properties of the high molar mass triblocks were found to be qualitatively similar to previously reported PLA-containing APTPEs, with increases in the PLA content resulting in an increase in ultimate tensile strength but a decrease in strain-at-break.

Similar to previously discussed PLA-containing APTPEs, the toughness of the PLA-b-PCD-b-PLA triblocks increased dramatically with molar mass at fixed composition, further indicating the need for high molar mass polymers to achieve high performance materials. The PLA-b-PCD-b-PLA materials displayed significantly higher ultimate tensile strength (18 \pm 4 MPa) and similar

strain-at-break ($1200 \pm 100\%$) to PLA-*b*-PDL-*b*-PLA and PLA-*b*-poly(3-62)-*b*-PLA triblocks with analogous compositions. ^{155,156,157} The authors attributed the improvement in the tensile properties to the reduced entanglement molar mass relative to PDL. The facile synthesis methodology and ability to tune mechanical properties with changes in midblock composition make these polymers attractive sustainable materials.

More recently, Watts *et al.* investigated **3-60** as a renewably derived monomer for sustainable TPEs. The polymerizations of substituted ε-caprolactones are thermodynamically favorable, with the methyl group at the γ- rather than ε-position increasing the rate of reaction such that industrial polymerization of **3-60** may be viable. A technoeconomic analysis from Lundberg *et al.* has also shown that **3-60** can be economically manufactured at large scale from cresol (Scheme 12), which can be derived from the renewable resources lignin and sulfate turpentine (*vide supra*, Section 2.2.1). A7,164,165 Similarly to poly(**3-62**), poly(**3-60**) is amorphous, with a low T_g ($T_g = -59$ °C) and low M_e of 2.9 kg mol⁻¹. Given these factors, **3-60** is a promising monomer for the midblock of tough and sustainable APTPEs that are bioderived and scalable for industrial production.

To study the effect of PLA crystallinity on mechanical properties of APTPEs, the authors synthesized a pair of complementary triblock polymers with the same molar mass and volume fraction of PLA: one with atactic, amorphous endblocks (PLA-b-poly(3-60)-b-PLA) and one with isotactic, semi-crystalline endblocks (PLLA-b-poly(3-60)-b-PLLA). Both poly(3-60)-based polymers displayed higher ultimate tensile strengths than previously discussed APTPEs despite having a lower volume fraction of PLA ($f_{LA} = 0.17$). ^{155,156,157} The PLA-b-p(3-60)-b-PLA APTPEs exhibited an ultimate tensile strength of 24 ± 2 MPa. PLLA-b-poly(3-60)-b-PLLA demonstrated an even higher strength of 30 ± 4 MPa, which is comparable to the strength of commercial PS-PI-PS and exceeds that of commercial PS-b-PB-b-PS. 149,157 The high tensile strength of the APTPEs with semi-crystalline PLLA is proposed to result from strain-induced crystallization of the endblocks, which enhances the strain hardening behavior of the materials. In both the PLA and PLLA systems, strains-at-break similar to those of previous APTPEs were observed, indicating that the PLLA endblock TPEs exhibit significantly higher ultimate tensile strength while maintaining almost identical strain-at-break. 155,156,157,158 Similar to previously reported APTPEs containing PLA, these triblock materials demonstrated that an increase in the volume fraction of PLLA produced a corresponding increase in the ultimate tensile strength and a concurrent decrease in the strain-at-break. The PLLA-containing triblocks also exhibit improved elastomeric recovery and lessened permanent deformation, displaying higher percent recoveries (97–98%) than the amorphous PLA analogues (94–96%) and significantly less stress relaxation. The introduction of semi-crystalline PLLA results in APTPEs with minimal permanent deformation and excellent tensile properties, suitable for high-performance applications.

One of the most promising features of the PLLA-poly(**3-60**)-PLLA APTPEs is the reduced permanent deformation after extension, observed in both hysteresis and stress relaxation experiments, as compared to the amorphous PLA analogues. This improvement is hypothesized to be due to the anchoring of chain ends in crystal domains that makes chain pullout more difficult. To explore the effect of crystallinity and secondary bonding interactions on both the tensile and stress relaxation behavior of PLA-containing APTPEs, Watts led an extension of this work to PLA-*b*-poly(**3-60**)-*b*-PLA with ureidopyrimidinone (UPy) hydrogen-bonding endgroups. The authors targeted low molar mass polymers to highlight the impact of the added crystallinity from the UPy groups on mechanical properties and achieve polymers with low *T*_{ODT}

values for mild processing. Both low molar mass PLA-*b*-poly(**3-60**)-*b*-PLA and UPy-PLA-*b*-poly(**3-60**)-*b*-PLA-UPy were found to be microphase separated at room temperature. A clear order-disorder transition was not observed in the samples, but the authors posited that they are disordered at elevated temperatures based on SAXS data.

Given that TPE mechanical performance is highly dependent on molar mass, the tensile properties of these materials are inferior to those of high molar mass variants. Non-end-functionalized triblocks exhibited strain softening behavior with low ultimate tensile strengths (0.11 \pm 0.01 MPa) and only moderate strains-at-break (870 \pm 40%). End-functionalization with UPy groups resulted in significant increases in both ultimate tensile strength (5.4 ± 0.3 MPa) and strain-at-break (1130 ± 30%) with added strain hardening behavior compared to the parent triblocks. The tensile properties were further improved by the inclusion of semi-crystalline PLLA as the endblocks with UPy endgroups. The parent PLLA-b-poly(3-60)-b-PLLA triblocks did not exhibit strain-hardening behavior, leading to low ultimate tensile strength (2.5 \pm 0.1 MPa) and poor strain-at-break (490 \pm 20%). Unlike the parent PLLA-*b*-poly(3-60)-*b*-PLLA polymers and similarly to their amorphous PLA analogues, the UPy-functionalized polymers exhibited strain hardening behavior leading to significantly higher ultimate tensile strength (13 ± 1 MPa) and strain-at-break ($1140 \pm 40\%$). Endfunctionalization with UPy groups also improved the stress relaxation behavior of the materials. In the polymers with PLA endblocks, UPy functionalization resulted in a 500-fold increase in relaxation time; in the polymers with PLLA endblocks and UPv end groups, the authors estimated it would take nearly 6 months for the material to relax the original stress at room temperature. The promising tensile properties and impressive stress relaxation in low molar mass UPy-PLLA-bpoly(3-60)-b-PLLA-UPy APTPEs suggests that high molar mass variants could display even better mechanical properties competitive with those of commercial styrenic TPEs.

To date, researchers in the CSP have uncovered many examples of employing sustainably derived monomers for TPEs with comparable or often improved properties compared to petroleum-based commercial materials. The properties of these sustainable TPEs can easily be tuned through modifications in volume fractions of hard- and soft-block domains, molar mass, and molecular architecture.

4.2. Thermoplastics

Thermoplastics are materials that can be reversibly reshaped using heat. Unlike thermosets, which cannot be reprocessed due to the presence of chemical cross-links, thermoplastics can be continually reprocessed by heating and reshaping above the glass transition or melting temperature. Common processing techniques of thermoplastics include extrusion, injection molding, thermoforming, and film blowing, providing access to a diverse portfolio of commercial products. Thermoplastics represent the largest share of the plastics economy, accounting for 90% of global plastics production since 1950. ¹⁶⁶ The widespread use of thermoplastics in modern society makes the development of sustainable thermoplastics an important challenge for the scientific research community.

Polymer architecture and connectivity have been used to design thermoplastic materials with varying properties. A comprehensive understanding of the relationship between polymer architecture and physical properties can guide the design of sustainable polymers with potentially enhanced properties towards targeted applications. For example, linking two or more chemically distinct polymer blocks can result in nanoscale structured materials, improving the mechanical

properties. ^{167,168} Grafts can amplify shear thinning and strain hardening behavior, improving melt processability. ^{169,170} Understanding how the polymer architecture impacts the physical properties of plastics and elastomers represents an important theme of research in the CSP to design materials with competitive properties.

As shown in **Figure 10**, branching and block connectivity motifs are key architectural parameters for material design. If the volume fraction of hard A blocks is high ($f_A > 0.5$), these materials behave more like thermoplastics than elastomers where the minority B soft midblocks can act as uniformly dispersed, toughening fillers in a continuous, hard matrix (**Figure 10A**). As a result, ABA triblock polymers can be both strong and ductile unlike A homopolymers. In ABABA pentablock polymers (**Figure 10B**), for example, the interior blocks can stitch together multiple domains, facilitating stress transfer and inhibiting the propagation of cracks that lead to macroscopic failure. The multiblock architecture also largely decouples the total molar mass from the $T_{\rm ODT}$ needed to process the material. Despite their attractive properties, these multiblock polymers are limited in several ways by their linear architecture: they exhibit limited conformational mobility of the interior blocks, high viscosity, and only modest strain-hardening ability. Branched block architectures (**Figure 10C** and **D**) can overcome these drawbacks while maintaining the desired toughness and strength.

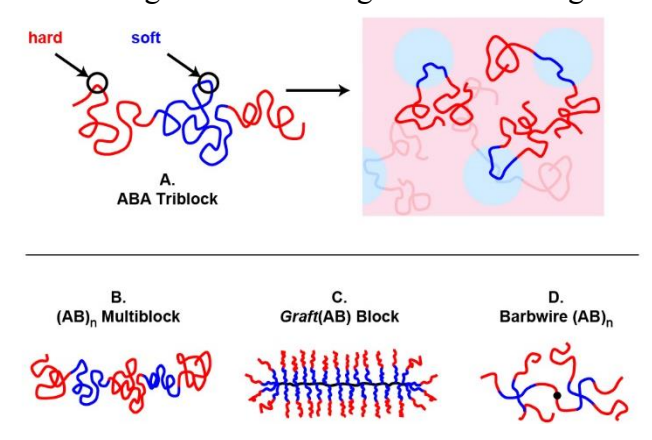


Figure 10. Block polymer architectures studied as sustainable thermoplastics with varied branching and block connectivity motifs, including (A) linear ABA triblocks, (B) linear (AB)_n multiblocks, (C) graft(AB) diblocks, and (D) "barbwire" (AB)_n multiblock polymers.

Toward the goal of developing tough and sustainable thermoplastics, CSP researchers have studied the mechanical and rheological properties of branched block polymers. 177,178,179,180,181,182 In these studies, AB-type block polymers with hard PLA majority blocks (A) and soft aliphatic polyester minority blocks (B) were synthesized and studied. Unlike conventional petrochemical plastics, polyester blocks can be sourced from renewable feedstock 183 and can degrade to environmentally benign products via biodegradation or composting. 184,185 Zhang *et al.* reported graft(AB) polymers featuring methylcellulose backbones and AB diblock side chains, where A is PLLA and B is poly(β -methyl- δ -valerolactone) (poly(2-49)) (Figure 10C). 178 Connecting the rubbery poly(2-49) blocks to the backbone facilitates crystallization of the PLLA endblocks, which in turn promotes microphase separation. Microphase separation toughens the material by uniformly dispersing nanoscopic rubber particles throughout the PLLA matrix. The graft (AB) platform offers several

advantages compared to linear ABA triblocks and linear (AB)_n multiblocks. First, the graft polymer architecture decouples the total molar mass (M) from the melt viscosity (η_0). Introducing grafts increases the molar mass between entanglements (M_e), allowing Rouse scaling ($\eta_0 \sim M$) to persist to higher M before the onset of reptation ($\eta_0 \sim M^{3.4}$). In this way, introducing grafts improves the melt processability of the material compared to linear analogues. Second, using PLLA as the endblocks in the graft architecture facilitates crystallization, which increases the strength and potential use temperature of the material. Lastly, the graft polymer platform is highly modular: varying the backbone length or volume fraction of PLLA allows either thermoplastic or elastomeric behavior to be accessed.

Building on these reports of decoupling molar mass and melt viscosity using graft polymers, Haugan *et al.* studied the linear viscoelastic behavior of PLA graft homopolymers. The linear rheological properties were studied as functions of the backbone degree of polymerization (N_{bb}) and the grafting density, z, defined as the average number of grafts per backbone repeat unit. Well-defined (D < 1.1) graft polymers were synthesized with fixed PLA side chain molar mass (3.5 kg mol⁻¹) and variable $10 < N_{bb} < 3000$ and $0 \le z \le 1$. Dynamic master curves reveal that these polymers display either Rouse-like or reptation dynamics and that increasing grafting density delays the onset of entanglements. The scaling of the entanglement plateau modulus with z was found to conflict with existing theoretical models for graft polymers, but a molecular interpretation was proposed based on thin, flexible chains at low z and thick, semiflexible mesoscopic cylinders at high z.

Mannion *et al.* reported the synthesis and rheological behavior of branched "barbwire" AB multiblock polymers, where A is PLA and B is PDL (**8D**). ¹⁸¹ The branched multiblocks were synthesized by coupling end-functional 4-arm stars, in which each arm is an AB diblock and the rubbery PDL blocks comprise the star's core. The branched multiblocks also underwent microphase separation, forming domains of rubbery PDL bridged by PLA blocks. Consistent with previous work on linear multiblock polymers, the barbwire (PLA-*b*-PDL)_n multiblocks also demonstrated increased tensile toughness as the average block number increased. Direct comparison with a (PLA-*b*-PDL)_n linear multiblock containing similar total molar mass and PLA content suggests that the interior, bridging PLA blocks are most crucial in connecting domains and toughening the material; dangling PLA blocks are proposed to have a smaller effect on toughness. Studies on the extensional rheological behavior of the disordered multiblock melts demonstrated significant strain hardening. Strain hardening is a prized phenomenon in which the extensional viscosity increases above the value predicted based on linear viscoelastic behavior. Increased strain hardening improves the melt processability in extension-dominated processing methods, such as fiber spinning and film blowing.

Turning towards homopolymer systems, Lipinski *et al.* recently reported a high strength semicrystalline thermoplastic polyether with photodegradable properties. ¹⁸⁶ Isotactic polypropylene oxide (*i*PPO) has been a target of stereoselective and enantioselective synthesis for the past two decades, but recent catalyst developments enabled the synthesis of a highly isotactic, high molar mass material. ^{187,188} In this research, the authors measured the mechanical strength of several *i*PPO samples of varying molar mass using uniaxial tensile testing. An upper ultimate tensile strength of 75 MPa was achieved by a 104 kDa polymer (**Figure 11, blue**). This tensile strength far exceeds that of commercial polyolefins (polyethylene and polypropylene, ~26 MPa) and is more comparable to nylon-6,6 (81 MPa). ¹⁸⁷ The polyether linkages in *i*PPO provide increased reactivity to environmental stimuli. Upon being exposed to UVA light (365 nm) for extended periods, the molar mass of *i*PPO steadily decreased. The degradation by auto-oxidation reduced the M_n of a 93 kDa sample to 21 kDa in just 30 days of continuous exposure. Literature precedent suggests the possible biodegradation of *i*PPO, ¹⁸⁹ but further investigation is required. The researchers suggested that *i*PPO could be suitable for environmentally sensitive applications such as commercial fishing nets, where large quantities of the plastic will inevitably escape to the environment.

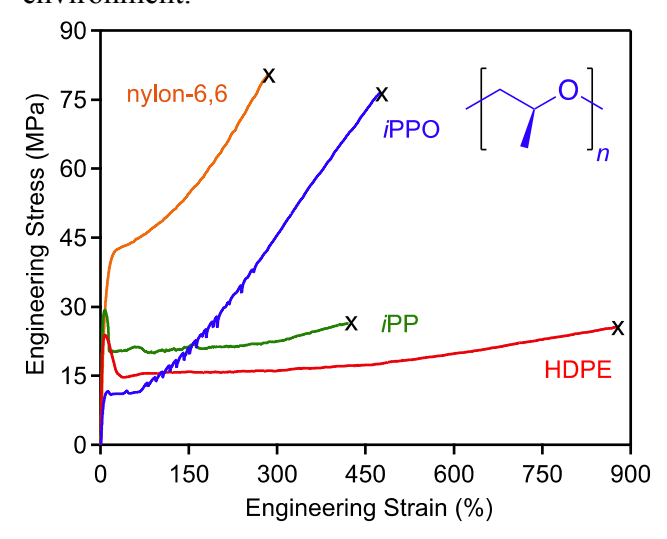
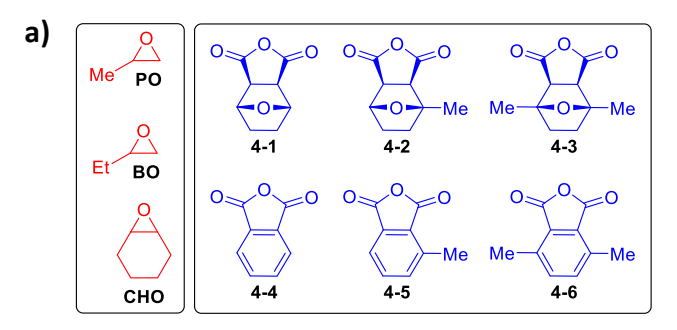


Figure 11. Representative stress-strain data of iPPO and commercial iPP, HDPE, and nylon-6,6 resins. X = sample fracture. Adapted with permission from ref 186. Copyright 2020 American Chemical Society.

Fahnhorst *et al.* reported the synthesis, mechanical testing, and hydrolytic degradation of various poly(4-carboalkoxyvalerolactone)s. ¹⁹⁰ Each CRVL was synthesized from malic acid, a renewable and scalable feedstock for monomer production. The chemical recyclability of PCRVLs is heavily desired in the area of single use plastics. ¹³² Uniaxial tensile tests revealed poly(4-carbomethoxyvalerolactone) (poly(3-63)) as the strongest (34.5 MPa) and toughest (88 MJ m⁻³) of the PCRVLs analyzed. Increasing steric bulk by substituting isopropyl or ethyl groups for the methyl group resulted in significantly lower yield stress, strength, and toughness. The bulkiness of the alkyl groups also played a role in acid- and base-catalyzed hydrolytic degradation. Under both conditions, poly(3-63) was fully degraded (relative to sterically bulkier alkoxy groups), within 1 day in basic media and 13 days in acidic media. ¹H NMR spectroscopy of the acid degradation products revealed the formation of 2-(hydroxymethyl)pentanedioic acid and the corresponding alcohol. With mechanical properties similar to commercial polyethylene, poly(3-63) could potentially be a chemically recyclable, bioderived, polyester for single use plastics.

Yu *et al.* systematically investigated the copolymerization of cyclic anhydrides (**Figure 12**) and epoxide monomers (PO, BO, and CHO) as a means of synthesizing high T_g polymers with potential thermoplastic applications. ¹⁹¹ Due to the bulky nature of tricyclic monomers **4-1**, **4-2**, and **4-3**, the resulting copolymers exhibited higher T_g values than those made from **4-4**, **4-5**, or **4-6** with the same number of methyl substituents (**Figure 12**). When the epoxide monomer was varied, it was observed that the BO-based polymers had lower T_g values than the PO-based polymers, likely

resulting from the longer alkyl groups hindering the polymer chains from packing as densely. 192,193 Furthermore, the CHO-based polymers were characterized with substantially higher $T_{\rm g}$ values relative to both the PO- and BO-based analogues due to the decreased chain flexibility imposed by the cyclohexyl ring. Quite interestingly, the addition of methyl substituents to the cyclic anhydride monomers had a non-linear influence over the observed T_g values, despite the widely accepted notion that T_g increases upon methyl substitution due to the additional steric hindrance near the polymer backbone. 194,195 Polymers with an intermediate number of methyl substituents exhibited the highest T_g values in each series. This understanding was further supported experimentally using positron annihilation lifetime spectroscopy, which demonstrated that monomethyl-substituted polyesters in both the tricyclic and phthalic series indeed have the largest respective average molecular hole volumes 196,197 within a given series (when compared with their unsubstituted and dimethyl-substituted counterparts). These results provide a direct correlation between chain flexibility and the anomalous T_g relationship observed in these polyesters. A detailed theoretical analysis of the nonlinear influence of these methyl substituents on the backbone rotational flexibility of the respective polyesters also confirmed the experimental findings. This work demonstrated the ability to tune thermal properties based on a comprehensive understanding of substituent effect on monomers, which has implications not only for thermoplastics but also other materials in which the T_g value is a defining characteristic.



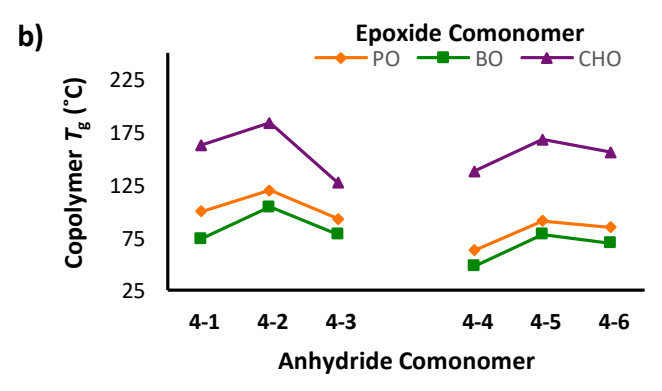


Figure 12. a) Cyclic anhydrides and epoxides monomers were copolymerized and b) their T_g values demonstrated tunable thermal properties. Adapted with permission from ref 191. *Copyright* © 2018, *Springer Nature*.

4.3. Thermosets

Thermosets, commonly used for commercial products like car tires and adhesives, are generally non-reprocessable networks generated from chemically crosslinked polymer chains, which afford high ultimate strengths and moduli. Research efforts in the CSP have demonstrated that sustainable high-performance thermosets can be produced through the use of biomass-derived monomers.

In particular, Zhang et al. demonstrated the fabrication of high-performance bio-based epoxy thermosets using succinylated β -cyclodextrin (4-7) and trehalose (4-8) as carboxylic acid functionalized in epoxy resins. 198 The hardeners were crosslinked with trimethylolpropane triglycidyl ether (TTE) in varying ratios of succinvlated monomer to TTE, forming thermally stable crosslinked thermosets as demonstrated by 5% mass loss by thermogravimetric analysis at around 300 °C. The resins demonstrated high tensile strength. In one example of the functionalized trehalose crosslinked with TTE (45:55 molar ratio), it exhibited a tensile strength up to 47 MPa and a strain of 16%. In the case of cyclodextrin-based resins, tensile strengths up to 64 MPa, likely resulting from the rigid, highly-functionalized monomer were seen, arising presumably from a more densely crosslinked system. In both cases, the epoxy thermosets resulted in materials with high Young's moduli of up to ~1.4 MPa and ~1.8 MPa for resins with trehalose and cyclodextrin, respectively. To further explore adhesion applications, the researchers used the formulations of highest tensile strength (4-7:TTE 50:50 and 4-8 45:55) to crosslink stainless steel strips. The trehalose system resisted much higher force, yielding a high lap shear adhesion of around 3600 psi compared to the cyclodextrin system of around 2100 psi, both comparing well to commercial Loctite two-part epoxy adhesives D609 (2900 psi) and 615 (3800 psi). These results illustrate the potential of these bio-based monomers to be used towards high-performance epoxy resins.

In continuation of this work, Zhang et al. reported the synthesis of sustainable and degradable epoxy resins from functionalized β -cyclodextrin (4-7) or trehalose (4-8), and epoxidized soybean oil (4-9) (Figure 13). 199 These biobased thermosets have potential applications as biomedical plastics. In this work, various resins consisting of 4-9 crosslinked with 4-7 or 4-8 were produced (4-10 and 4-11, respectively). The resulting materials exhibited a distribution of physical and mechanical properties by tuning the monomer feed ratio. The 4-10 resins displayed significantly higher T_g values than the **4-11** materials. However, altering the monomer feed ratio did not strongly affect the properties of the material T_g (4-10: 28–36 °C; 4-11: -3–3 °C). Greater differences between feed ratios were observed during uniaxial tensile elongation analysis. Increasing the content of 4-8 resulted in thermosets 4-11with decreased Young's modulus (0.3-2.4 MPa) and tensile strength (0.5–1.3 MPa). Meanwhile, the relative physical properties of **4-10** thermosets were influenced significantly less by changes in the feed ratio, as demonstrated by characterizing their Young's modulus (~200-300 MPa) and tensile strength (~10 MPa). The **4-10** resins were significantly stronger and stiffer than those sourced from 4-8, revealing that this method can be used as a modular route to thermosets with varying mechanical properties. Furthermore, by using base-catalyzed hydrolysis, the thermosets could be fully degraded, providing evidence of chemical recyclability.

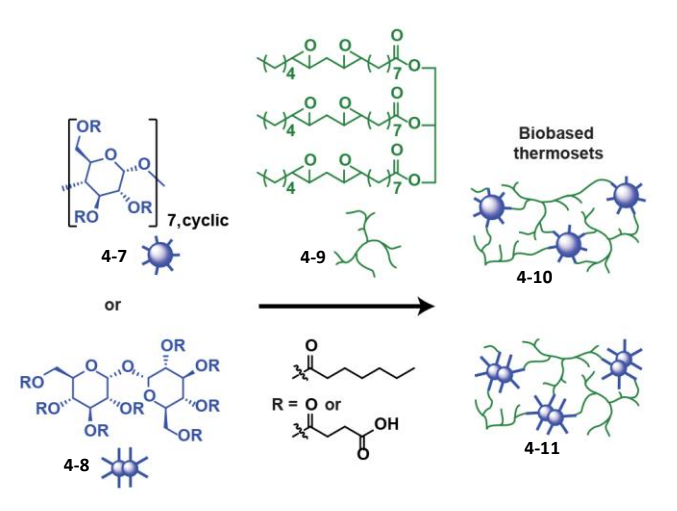


Figure 13. Biobased thermosets have been reported through the crosslinking of degradable epoxy resins (4-9) with functionalized trehalose (4-8) or β -cyclodextrin (4-7). Adapted from Ref. 199. Copyright 2018 American Chemical Society.

Finally, cell adhesion was investigated to assess the biocompatibility of the thermosets. Thermoset **4-11** is notable for mitigating adhesion and proliferation of neonatal human dermal fibroblast cells, advantageous for sterile biomedical plastics. Conversely, **4-10** exhibited excellent cell adhesion and growth on the polymer surface, showing potential for use in biomedical implants. This study demonstrates the use of biobased monomers to design degradable thermosets with tunable thermal, mechanical, and cell adhesion properties for various biomedical applications.

Ding et al. reported the synthesis and mechanical evaluation of sustainable thermosetting resins from natural phenolic (meth)acrylates derived from softwood lignin. ⁴⁹ Photocured polymers have a wide range of applications, such as additive manufacturing, electronics, and medical devices, but most require petroleum-based monomers for desired mechanical properties. Rigid, biobased monomers guaiacol methacrylate (2-64) and octanedithiol eugenol acrylate (2-63) were combined with crosslinkers vanilly alcohol methacrylate (2-65) or trimethylolpropane trimethacrylate (2-66) to form crosslinked networks (Scheme 14). Uniaxial-tensile elongation of the networks showed how the mechanical properties could be tuned by varying the 2-64:2-63 ratio or crosslinker identity. For example, increasing 2-64 content in thermosets composed of 2-63, 2-64, and 2-66 increased the Young's modulus (0.83-1.35 GPa), but also resulted in a lower tensile strength (33.1-38.8 MPa) and toughness (0.5-2.2 MJ m⁻³). Conversely, increasing 2-64 content in thermosets composed of 2-63, 2-64, and 2-65 increased the Young's modulus (1.02–1.23 GPa), tensile strength (44.6–83.4 MPa), and toughness (1.9–5.6 MJ m⁻³). The mechanical properties of a polymer composed of 2-64, 2-63, and 2-65 (monomer composition of 60:20:20), were found to be competitive with commercial prototype resins for stereolithography 3D printing. This work showed that natural phenolics can produce ideal photocuring kinetics to form mechanically robust networks for use in 3D printing.

Wilbon *et al.* described the fabrication of thermosets incorporating isosorbide **2-79**, a monomer that can be sustainably sourced from glucose.⁷² This structurally rigid molecule lends itself to

making high $T_{\rm g}$ and high modulus materials, which are particularly advantageous characteristics for thermosets. Thermosets with tunable mechanical properties were produced by varying the amount of glycerol and short-chained poly(ethylene oxide) (PEO). Increased PEO resulted in a decrease in stiffness and increased elasticity due to a decreased crosslink density and increased ductility of PEO. For example, 0 and 23 wt % PEO samples resulted in ultimate strengths of ~50 MPa and < 5 MPa, respectively. Furthermore, increasing PEO content decreased the $T_{\rm g}$ value of the thermoset ($T_{\rm g} \approx 68$ °C with 0 wt % PEO and $T_{\rm g} = 21$ °C with 23 wt % PEO). Simple changes in the thermoset formulation allowed for varying mechanical and thermal properties, without compromising thermal stability ($T_{\rm d} = \sim 300$ °C). The high thermal stability of these materials makes them promising for applications over a wide range of operating temperatures.

Polyurethanes are an important class of polymers with many commercial applications as both thermosets and thermoplastics. Knight et al. described the ROTEP of 7-membered lactones dihydrocarvide (2-45) and carvomenthide (2-46) to produce polymeric precursors to polyurethane thermosets. 87 These monomers can be sustainably sourced from limonene, a major byproduct of the citrus industry, thereby avoiding resources that would otherwise be used for food. The pendant vinyl group of carvomenthide allowed for post-polymerization modification using thiol-ene click chemistry to install crosslinkable alcohol moieties. Using dihydrocarvide's alkene functionality as a means to tune the crosslink density, short-chained statistical copolymers were synthesized (M_n = 3 kg mol⁻¹) with 1–5 alcohols per chain. Regardless of their post polymerization modifications, these polyesters maintained a constant $T_{\rm g}$ value around -30 °C. Polyurethane films with tunable mechanical and thermal properties were prepared by the reaction of thiol functionalized prepolymer with 1,4-butanediol (BD) and MDI. Initial formulation screening used a constant molar ratio (i.e., 1 OHpolyol: 0.25 OHBD: 1.25 NCOMDI) and resulted in the most reliable, flexible, and durable polyurethane films when polymers consisted of 4-5 OH groups per chain. In one example, a prepolymer with ~4 OH groups per chain resulted in a polyurethane material with ultimate tensile strength and Young's modulus of approximately of 1 MPa and strain-at-break of about 450%. These properties are similar to those of other vegetable oil-based polyurethanes.²⁰⁰

The relative amount of hard segment in polyurethanes is known to have a large influence on the overall stiffness or flexibility of the material. In this work, increased MDI content resulted in increased hard content through pi-pi stacking and H-bonding, promoting a higher *T*_g value. However, increasing the ratio of isocyanates to overall OH groups resulted in a decrease in *T*_g value, likely reflecting the decreased crosslinking and increased chain flexibility. In an optimized polyurethane thermoset, the ratio of isocyanates to total OH groups was kept constant, but the MDI hard segment content was increased to 40 wt%. This resulted in a considerable improvement in the Young's modulus and tensile strength (40 MPa and 11 MPa, respectively). DMTA analysis of the material showed a glassy storage modulus of 2.5 GPa and a rubbery plateau of 10.9 MPa. These values were found to be typical for polyurethanes prepared from soybean-based polyols, ²⁰¹ poly(ε-caprolactone), ²⁰² poly(ethylene adipate), ^{203,204} polytetrahydrofuran, ²⁰⁵ and castor oil. ^{206,207} This work demonstrated that the sustainably sourced monomers dihydrocarvide and carvomenthide can be used for the formulation of polyurethanes while offering competitive properties to many non-sustainable alternatives.

Trotta *et al.* reported the synthesis and mechanical testing of renewable thermosets and thermoplastics derived almost completely from itaconic acid (IA). ²⁰⁸ IA is an economically viable, biorenewable building block produced by the fermentation of biomass. In this work, thiol-ene click

reactions of IA-derived terpolymers composed of dimethyl 2-(4-methylcyclohex-3-ene)succinate (CS), dimethyl 2-methylsuccinate (MS), and 2-methyl-1,4-butanediol (MB) produced thermoset materials. Uniaxial tensile elongation showed that increasing the thermoset crosslinking density results in increased Young's moduli (1.4–6.2 MPa) and tensile strength (0.5–0.9 MPa). Poly(MBCS)-*stat*-poly(MBMS) (with a molar ratio of 0.19 MBCS to 0.81 MBMS), the thermoset of highest cross-linking density, was particularly susceptible to hydrolytic degradation under basic conditions.

These researchers also synthesized a triblock polymer (PMBL-PMBMS-PMBL) by functionalizing and chain-extending PMBMS with α -methylene- γ -butyrolactone (MBL). The resulting thermoplastic showed comparable properties to other MBL materials and increased toughness when compared to PMBMS alone. It is anticipated that increasing the molar mass could further improve the strength of the thermoplastic. Implementation of IA-derived materials could help relieve societal reliance on petroleum feed stocks.

Above, we have described many examples of utilizing sustainably sourced monomers to fabricate thermosets with tunable physical properties for various commercial applications. In many cases, these materials exhibit degradability, which is significantly less common for petroleum-based thermosets.

4.4. Elastomers

Elastomers are a class of materials that are formed through the chemical crosslinking of polymer chains. Unlike thermosets, elastomers are typically characterized as soft, rubbery materials with low $T_{\rm g}$ values, making them highly elastic and flexible. Consequently, these materials can endure high strains without permanent deformation, typically corresponding to low ultimate tensile strength and storage modulus. Due to the chemical crosslinks within elastomers, they are considerably solvent resistant and thermally robust materials, especially when compared to TPEs, their physically crosslinked counterparts. Despite the favorable properties of elastomers, the irreversible nature of most crosslinking chemistry results in recycling and reprocessing challenges. Polyesters are an important class of polymers that help meet the demand for sustainable materials. Their ester linkages allow for the increased possibility of hydrolysis-based degradation, unlike their polyolefin counterparts. In one example of making sustainable elastomers, Brutman et al. describe the crosslinking of poly(2-49) to fabricate elastomers using a one step, one pot copolymerization of 2-49, a difunctional, six-membered cyclic carbonate crosslinker (i.e., 5,5'-[oxybis(methylene)]bis(5-ethyl-1,3-dioxan-2-one)), and a monofunctional alcohol (**Figure 14**). ²⁰⁹ Low amounts of crosslinker (0.25 to 2.0 mol %) resulted in high gel fractions (>89%). The $T_{\rm g}$ value remained constant at approximately -50 °C even with formulation modifications, consistent with the $T_{\rm g}$ value of poly(2-49) (-52 °C). This result demonstrates the minimal influence of the initiator and crosslinker on thermal properties. The elastomers demonstrated desirable elastomeric properties with low amounts of crosslinker (0.25 % or 0.5 mol %), outperforming the tensile behavior of a rubber band with ultimate tensile strengths greater than 5 MPa and strains-at-break of more than 1000%.

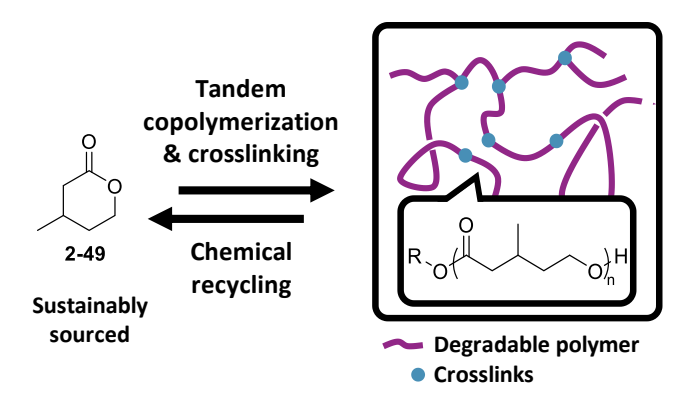


Figure 14. Poly(**2-49**) elastomeric networks were fabricated using a one-step, one-pot synthetic route. The resulting material could be chemically recycled to the monomer **2-49** (β-methyl-δ-valerolactone) in high yield and purity. Adapted from Ref. 209. Copyright 2016 American Chemical Society.

Using an alternative approach, poly(2-49) homopolymer ($M_n = 162 \text{ kg mol}^{-1}$) was crosslinked with a free radical generator resulting in improved tensile properties. With 2–3% crosslinker, ultimate tensile strength and strain-at-break of greater than 10 MPa and 1000% were achieved, outperforming previous samples. To further improve the mechanical properties, physical blends of crosslinked poly(2-49) with fumed silica filler (*i.e.*, FS Aerosil R 812) were fabricated using twin-screw extrusion. Tensile data of the composites demonstrated that the strain-at-break remained consistent even with high filler loading, while tensile strength significantly improved. In the case of 30 wt % filler, the tensile strength improved by 83%. Finally, these materials demonstrated chemical recyclability and hydrolytic degradation in acidic aqueous conditions at elevated temperatures.

De Hoe *et al.* investigated the fabrication of elastomers using poly(**3-60**) (**Figure 15**). ²¹⁰ The monomer, γMCL, can be synthesized cost effectively and sustainably from biorenewable resources using *para*-cresol or *para*-cymene. ^{165,47,211} Crosslinked elastomers were prepared by solvent casting 4-arm poly(**3-60**) with a bis(β-lactone) cross-linker (*i.e.*, 4,4'-(ethane-1,2-diyl)bis(oxetan-2-one)) and tin(II) octoate, affording the desired film with gel fractions greater than 0.9. By DMTA, elastomers exhibit a rubbery plateau modulus between 2–3 MPa, with no evidence of terminal flow up to 200 °C, indicative of a thermally robust material. The crosslinked elastomers displayed desirable elastomeric behavior; using tensile testing, a film crosslinked with 30 kDa prepolymer exhibited a strain-at-break over 900% and ultimate tensile strength of 6 MPa. Furthermore, hysteresis studies of the 30 kDa film showed low permanent deformations and high percent recoveries of over 94% after 20 cycles.

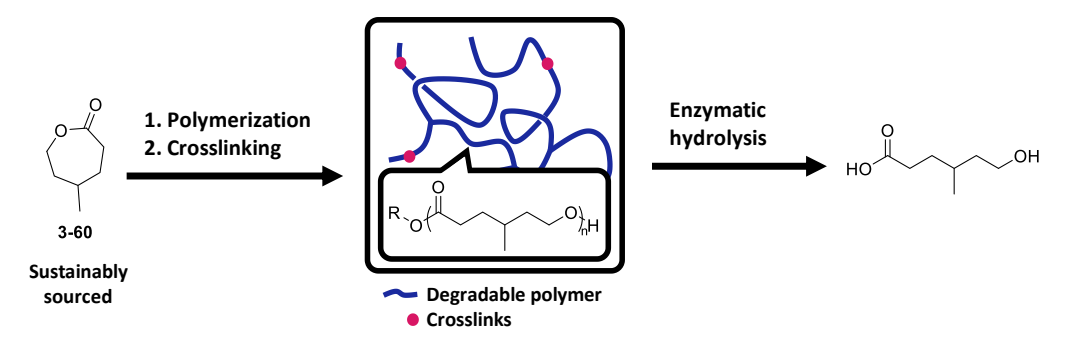


Figure 15. Polymerization of γ-ethyl-ε-caprolactone (**3-60**) and subsequent crosslinking to form elastomeric networks that can be composted via enzymatic hydrolysis. Adapted from Ref. 210. Copyright 2018 American Chemical Society.

Based on the work investigating elastomers within the CSP, there are several different avenues to fabricate these materials sustainably using biorenewable resources with final products that are processable and recyclable.

4.5. Green Applications

The presence of micropollutants (MPs) in water arising from pesticides, pharmaceuticals, and consumer products is a major environmental and health hazard. Oxidation is a common method of removing these pollutants. However due to its inefficiency, oxidation can leave behind toxic, partially oxidized products. ²¹² Environmentally-relevant MPs also have a broad range of properties, such as charge, hydrophobicity, and chemical functionality, making their chemical targeting difficult. ²¹³ Water purification via adsorption is an attractive purification technique as it removes MPs without introducing additional toxicity. The most common commercial adsorption method is the use of activated carbons (ACs). However, ACs have several deficiencies, including slow pollutant uptake, poor removal of anionic fluorinated MPs such as perfluorooctanoic acid, and energy-intensive regeneration. ²¹⁴ Efforts in the CSP have addressed these shortcomings through the development of crosslinked cavitands for MP removal via supramolecular interactions with β-cyclodextrin networks (**Figure 16**).

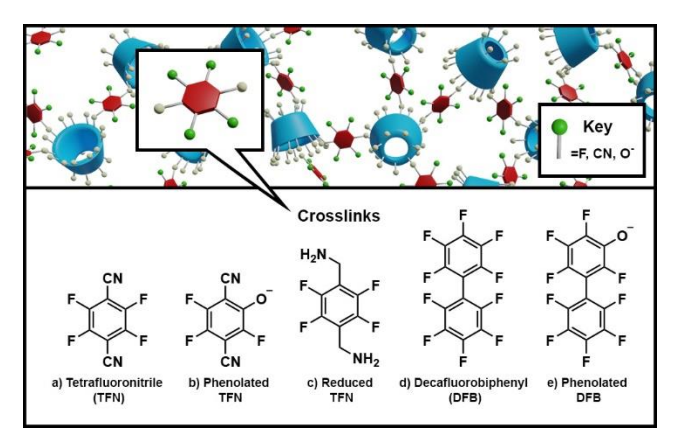


Figure 16. β-Cyclodextrin has been crosslinked with various fluorinated aromatic molecules for the removal of MPs in water. a) Crosslinking with tetrafluoronitrile targets removal of bisphenol-A.²¹⁵ b) Phenolating tetrafluoronitrile increases affinity for cationic MPs, including Pb²⁺ ions.²¹³ c) Reduced tetrafluoronitrile reverses the selectivity and targets anionic MPs.²¹⁴ d) Crosslinking with decafluorobiphenyl targets removal of perfluoroalkyl substances, particularly perfluorooctanoic acid.²¹⁶ e) Phenolated decafluorobiphenyl hinders anionic perfluoroalkyl substances removal, but increases cationic MP affinity.²¹⁷

In 2016, Alsbaiee *et al.* reported a novel system of β-cyclodextrin crosslinked with tetrafluoronitrile (TFN) to form a porous network (**Figure 16a**). These porous cyclodextrin polymers (P-CDPs) synthesized from a TFN:β-CD ratio of 3:1 consistently showed dense crosslinking, high uptake capacity (up to 265% of its weight in water), and minimal swelling, all desirable characteristics for adsorption capabilities. Compared to a non-porous CDP (NP-CDP), β-CD crosslinked with epichlorohydrin (EPI-CDP), and 3 mesoporous ACs, P-CDP removed bisphenol-A (BPA) much more quickly than any other adsorbent, reaching 95% of equilibrium uptake in just 10 seconds. Flow-through uptake revealed that P-CDP removed 80% of BPA in 20 seconds, while ACs removed only 50-60% BPA under the same conditions. A notable advantage of P-CDP systems is their facile regeneration with no loss of performance by rinsing with MeOH at room temperature, compared to the extreme heating (500–900 °C) required for ACs. Fitting adsorption data to a Langmuir model suggested a 1:1 inclusion complex formation between BPA and the β-CD polymer network; however, at higher concentrations of BPA, P-CDP showed BPA:β-CD ratios greater than one, indicating that BPA is also binding through other nonspecific interactions, such as with the crosslinker.

However, inconsistencies in monomer feed:incorporation ratio and diminished polymerization yields suggested a side reaction was taking place. Klemes *et al.* determined this to be phenolation of TFN via S_NAr with K₂CO₃ followed by decarboxylation, and investigated the impact of this phenolation on the uptake of MPs (*e.g.*, Pb²⁺ ions). Model studies demonstrated that phenolated products do not undergo further reactions in the presence of competing electrophiles, thus delaying phenolation is desirable to increase molar mass of the crosslinked networks (**Figure 16b**). Analysis of a library of polymers with varying phenolate concentrations by a Langmuir isotherm model showed strong positive correlations between Pb²⁺ capacity and phenolation, as well as Pb²⁺ capacity and porosity. Of 83 other MPs tested, 81 bound more strongly to the more phenolated

polymer, particularly cationic MPs. However, this TCN-CDP system showed poor affinity for anionic MPs, particularly anionic per- and poly-fluoroalkyl substances (PFASs).

PFASs are widely used in consumer products and are particularly resistant to degradation, making the capability to remove them by adsorption of high importance.²¹⁴ Capitalizing on the strong dependence on secondary interactions of the crosslinker with MPs, Klemes *et al.* reversed the adsorbent selectivity by reducing the nitriles on TFN to primary amines (**Figure 16c**), creating a strong affinity for anionic MPs, including anionic PFASs.²¹⁴ The reduced polymer removed at least 95% of 8 of the 10 PFASs studied, and performed better than the leading granular activated carbon (GAC), similar to powdered activated carbon (PAC) for PFASs, and better than PAC for PFBA (a particularly hard-to-remove MP). Notably, one of the major problems facing the ACs currently in use is their fouling in the presence of natural organic matter (NOM). However, with humic acid (a major component of NOM) present, the β-CD-based polymer showed only a slight reduction in binding affinity to anionic PFASs. It also exhibited increased affinity for cationic MPs, which was attributed to the NOM partially shielding the electrostatic repulsion interactions.

Xiao *et al.* targeted perfluorooctanoic acid (PFOA), which is prevalent in commercial products and has negative environmental and health hazards. To this end, the authors performed crosslinking with decafluorobiphenyl (DFB) (**Figure 16d**). While the resulting DFB-CDP samples were non-porous, a DFB:β-CD feed ratio of 3:1 reduced PFOA levels to <10 ng L⁻¹ after 24 hours and achieved 95% of this removal within 13.5 hours. However, samples with high crosslink density were too heavily substituted to form host-guest complexes, suggesting that optimal performance depends on accessibility of β-CD, crosslinker functionality, and free hydroxyl groups. A kinetic analysis showed performance comparable to the leading PAC (and thus superior to GAC) and P-CDP, likely due to superior PFOA affinity. Like other CDP systems studied, the adsorption by these DFB-CDP polymers was unaffected by humic acid and was easily regenerated by suspension in MeOH for 24 hours with little to no decrease in adsorption performance.

Because phenolation affected the performance of TFN-CDP adsorbents, Xiao et al. proceeded to examine the role of phenolation on the kinetics and thermodynamics of PFAS uptake in DFB-CDP adsorbents (Figure 16e). ²¹⁶ Phenolated DFB-CDP systems were compared to EPI-CDP and β-CD crosslinked with isocyanatoethyl methacrylate (IEM-CDP). Each of the systems adsorbed PFOA; however, the degree of phenolation incorporated was inversely associated with PFOA equilibrium removal percentage, suggesting that the thermodynamics of PFOA uptake are negatively affected by phenolates. All five of the β-CD-based polymers showed a higher affinity for longer-chain PFASs, possibly due to hydrophobic interactions. All five materials showed better removal of perfluorosulfonic acids than perfluorocarboxylic acids with the same carbon number. None of the β-CD-based polymers achieved any significant removal of 2,3,3,3-tetrafluoro-2-(heptafluoropropoxyl)propionate (GenX), an ammonium perfluoroalkyl ether carboxylate developed by Chemours as a potential replacement for PFOA. The authors attributed this difficulty to GenX's branched structure. GenX is known to have lower cyclodextrin binding, confirming β-CD is involved during the adsorption. All of the DFB-CDP systems performed significantly better than EPI-CDP and IEM-CDP, and also showed improved removal for the majority of PFASs when pH was lowered from 7.5 to 5.5.

Alzate-Sánchez *et al.* adapted the CDP adsorbent to a packed-bed column by polymerizing β-CD on the surface of 100 μm long rod-like cellulose microcrystals.²¹⁷ β-CD crosslinked with TFN onto cellulose microcrystals (CD-TFN@CMC) showed (by scanning transmission electron microscopy) a core particle surrounded by a shell of 1.5 μm, suggesting formation of a thin polymer coating around the cellulose. When the capacity of adsorbents per unit mass of β-CD for both CD-TFN and CD-TFN@CMC were compared, they showed similar capacities and that the β-CD in the thin film is completely available to form inclusion complexes with MPs. Importantly, due to the rapid access to β-CD sites from the thin layer, CD-TFN@CMC removed BPA with an equilibration time of 2 minutes, compared to a 20 minute equilibration time for CD-TFN. CD-TFN@CMC packed columns showed only slightly higher back-pressure than unmodified CMC but showed breakthrough volumes nonlinearly dependent on BPA concentration. The column was regenerated with MeOH and the capacity and breakthrough times were unaffected. CD-TFN itself does not degrade and shields the cellulose, introducing increased stability towards bacterial aging during water remediation treatments.

This research within the CSP demonstrated the systematic investigation of crosslinked β -CD for removal of a wide range of MPs. The crosslinking chemistry has been investigated thoroughly through fundamental model reactions, enabling targeted removal of different MPs and maximized efficiency of pollutant uptake at environmentally-relevant concentrations. As a result of these studies, β -CD-based adsorbents have recently been commercialized as the active materials in PFAS-detection products in the consumer and environmental remediation markets. PFAS and micropollutant removal products featuring these materials are under active development.

5. End of Use

Plastics are durable and ubiquitous in modern life, but this durability also impedes degradation when plastics reach the end of their intended use. This longevity, coupled with the inefficiency of recycling, means that plastics persist in landfills and the environment. The "end-of-use" pillar of sustainable polymers addresses ways for potential reduction of plastic pollution, but, importantly, also ways in which the value of end-of-use plastics can be recaptured more efficiently. The CSP has articulated broad categories that describe its approaches: i) degrading polymers back to their constituent monomers or oligomers or other benign compounds ii) identifying new strategies for more effective reuse of high-volume plastics, and iii) developing reprocessable materials (**Figure 17**). Accordingly, Center researchers have focused on i) (pink) designing new, degradable polymers synthesized from biomass-derived monomers that still possess mechanical properties competitive to those sourced from petroleum, ii) (blue) investigating new strategies for compatibilizing thermoplastic waste streams using block polymers, and iii) (green) developing reversible cross-linking chemistry to render thermosetting polymers remoldable.

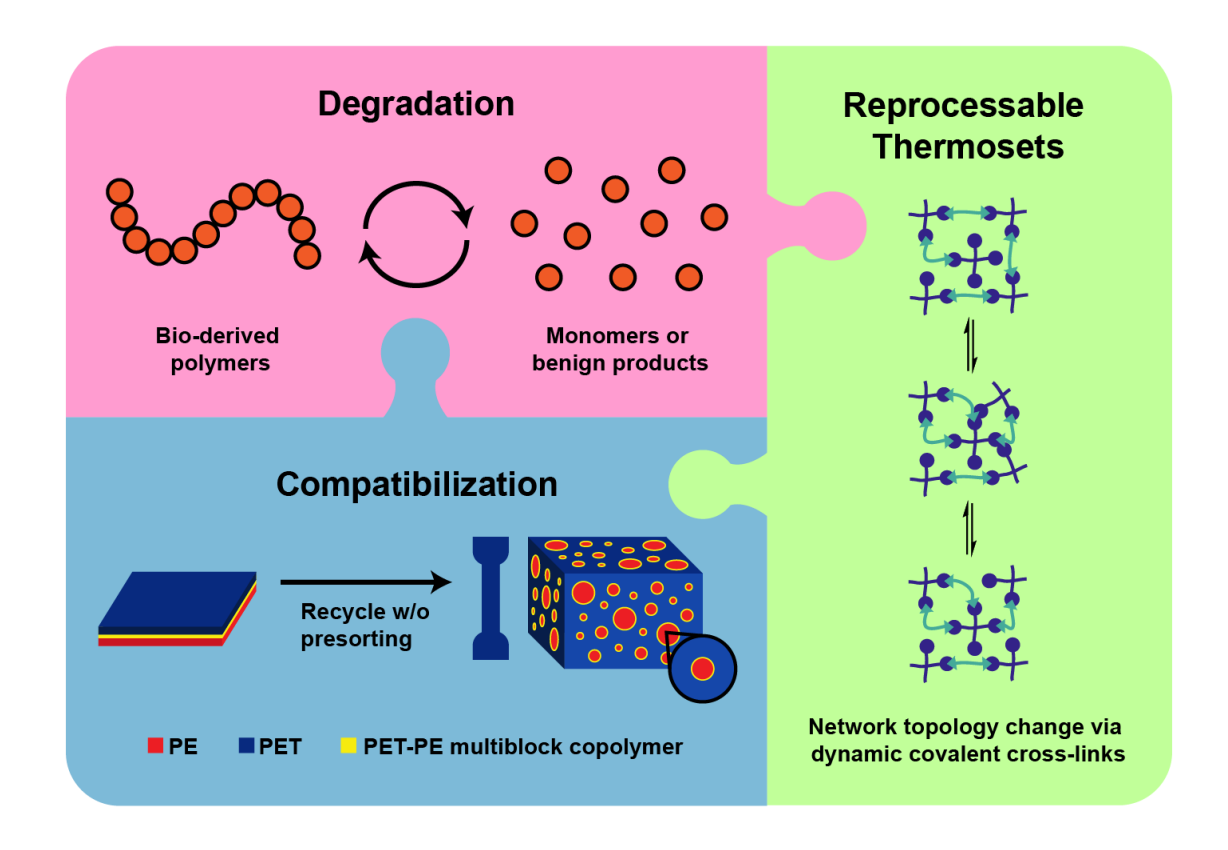


Figure 17. CSP approaches to the end-of-use pillar of sustainable polymers.

5.1. Degradation

Most commercial plastics are derived from fossil fuel resources and are essentially non-degradable. Although degradable alternatives have been successfully developed, some materials marketed as "degradable" are not readily decomposed under environmental conditions. For example, PLA often requires industrial composting conditions such as high humidity and high temperature to undergo degradation. ²¹⁹, ²²⁰ The CSP is designing polymers with competitive properties, made from sustainable feedstocks, that easily degrade under triggered, mild conditions (**Figure 18**).

One of those feedstocks, β -methyl- δ -valerolactone (2-49), was developed as a low-cost, monomer that could be efficiently accessed from sugar using new bio-engineered technology. Its polymer, poly(2-49) (Figure 18), is a low T_g (< -60 °C) polyester that can serve as the soft block together with PLA as the hard block in sustainable TPEs (*vide supra*, Section 4.1). Schneiderman *et al.* synthesized chemically recyclable biorenewable polyurethane (PU) foam from poly(2-49)-based polyols. Thermally-induced degradation is thought to proceed first through the reversion of urethane linkages to isocyanates and chain-end alcohols. Subsequent lactonization then mediates the depolymerization of the poly(2-49) backbone, and distillation pushes the reaction equilibrium toward the monomers and allows for efficient recovery of monomer 2-49 of acceptable purity for

reuse. This example compares favorably to traditional chemical recycling of polyurethane waste, which is typically accomplished using glycolysis or hydrolysis ^{222,223} and would not result in lactone monomer recovery.

Figure 18. Examples of ester-containing degradable polymers developed by the CSP.

Aromatic polyesters such as PET possess desirable mechanical properties due to their high $T_{\rm g}$ and $T_{\rm m}$ values, in addition to rigidity from crystallinity. However, the stability of aromatic ester bonds makes hydrolytic and enzymatic degradation difficult, resulting in plastics that persist in the environment. Aliphatic polyesters are attractive alternatives to aromatic polyesters because the aliphatic ester bond can be more easily biodegraded. Tang *et al.* designed a family of poly(urea esters) (PUEs) (**Figure 18**) which exhibited high T_m (>90 °C) while retaining biodegradability in the presence of *Pseudomonas cepacian* lipase under buffered conditions at pH 7.4. PUEs exhibited similar cold crystallization behavior as aliphatic polyesters.

Despite widespread use of aliphatic polyesters such as PLA, their T_m and T_g values tend to be much lower and their mechanical properties are generally inferior when compared to aromatic polyesters. To improve the degradation of aromatic polyesters, Kim *et al.* introduced substitution on the aromatic rings (**Scheme 33**). Aromatic polyesters derived from salicylic acid, a naturally-occurring benzoic acid derivative, showed thermal and mechanical properties competitive with commercial PLA and PET ($T_g = 85$ °C and Young's modulus = 2.3 GPa). Remarkably, these polyesters readily degraded in conditions mimicking natural environments. Immersing these polymers in seawater at 50 °C induced complete degradation over 2 months whereas PLA and a PET showed no degradation over the same period. In addition to the innately more reactive salicylate ester moiety compared to those in PLA and PET, the more acidic nature of the salicylic acid byproduct provided an autocatalytic enhancement of the degradation rate.

Scheme 36. Hydrolysis of aromatic polyesters described by Kim *et al.* ²²⁹

Hydrolytic degradation of polyesters can be greatly accelerated if the ester linkages are internally activated. Poly(acetal esters) are readily degradable because they incorporate a hydrolytically labile acyl acetal linkage. Neitzel *et al.* polymerized cyclic hemiacetal ester 5-methoxycaprolactone (alternatively 7-methoxyoxepan-2-one "MOPO", **Figure 18**.) ²³⁰ Degradation of the MOPO homopolymers proceeded cleanly under acidic conditions, rapidly giving 5-formylpentanoic acid as the sole product ($t_{1/2} = 3-5$ min.). Under basic conditions, the degradation was noticeably faster ($t_{1/2} < 1$ min). Furthermore, copolymers of isobutyl vinyl ether and small amounts of MOPO were produced under these conditions. The IBVE-MOPO copolymers (**Figure 18**) are degradable polyvinyl ethers; IBVE itself is not base-degradable.

Monomer design can afford multiple degradation options. Fahnhorst et al. reported the synthesis of 4-carbomethoxyvalerolactone (5-1) in two steps from readily available, naturally occurring malic acid. 132 Depolymerization of poly(5-1) was studied by detailed NMR spectroscopic analysis. Treating the polymer with Lewis acidic tin(II) octoate at 150 °C and under reduced pressure triggered depolymerization from the hydroxy-terminus to give a clean distillate of monomer 5-1 (Scheme 37). On the other hand, treatment of poly(5-1) with basic DBU yielded an acrylic monomer, methyl 2-methyleneglutarate (5-2). The authors postulate that depolymerization can proceed from the chain end, with reverse-ROTEP (*via* deprotonation of the acidic ω -end hydroxyl) initially producing 5-1. Further deprotonation of 5-1 at the 4-position adjacent to the exocyclic methyl ester promotes ring-opening retro-oxa-Michael reactions, giving 5-2. Alternatively, the degradation of poly(5-1) under basic conditions can proceed through main-chain cleavage because of the acidic proton adjacent to the pendant methyl esters. Main-chain cleavage leads to the formation of oligomers with acrylic chain ends, which degrade via the same retro-oxa-Michael mechanism to give the acrylic monomer. The resulting acrylic monomers can undergo radical polymerization to form functional polyacrylates with high $T_{\rm g}$ values; this is an example of using chemical degradation to recycle polymers into new materials with distinct properties.

MeO₂C
$$\xrightarrow{\text{Initiator}}$$
 $\xrightarrow{\text{H+ cat.}}$ $\xrightarrow{\text{N(Oct)}_2}$ $\xrightarrow{\text{NeO}_2\text{C}}$ $\xrightarrow{\text{N$

Scheme 37. Reagent-dependent degradation of poly(4-carbomethoxyvalerolactone) described in ref. 132.

In addition to thermoplastics, CSP researchers are developing mechanically robust, chemically degradable thermosets. These contrast with commodity thermosets which typically contain strong covalent cross-links. De Hoe *et al.* reported cross-linked elastomers synthesized from sustainable monomers such as bis(β-lactone) and poly(3-60) that possess properties competitive with commodity rubber bands. These cross-linked elastomers were fully and rapidly degradable by hydrolysis at various temperatures (2–40 °C) when *Fusarium solani* cutinase was added. While the principal role of this enzyme is to degrade the natural polyester cutin, it has been demonstrated to also catalyze hydrolysis of synthetic polyesters such as polycaprolactone. To simulate conditions found in natural soils, the elastomers were exposed to pH 7 and temperatures between 2 and 40 °C. The water-soluble total organic content indicated that the crosslinked polyesters underwent complete hydrolysis in 16 days at 20°C.

Wilbon *et al.* studied polyester thermosets synthesized from isosorbide, succinic anhydride, and glycerol. These bioderived thermosets were thermally stable even in the presence of a PEO plasticizer and yet were hydrolytically degradable in both neutral and acidic water (**Figure 19**).⁷² The hydrolytic degradation of the polyesters was substantially enhanced by heating at 98 °C (in a microwave reactor); the time required for dissolution of the cross-linked network in unbuffered water was decreased from 1 month to 2.5 days using microwave heating.

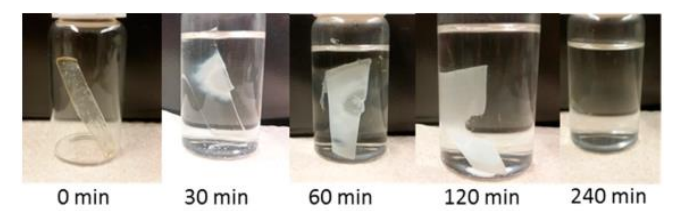


Figure 19. Degradation of a bio-derived thermoset in 1 M HCl at 50 °C as described by Wilbon *et al.*⁷² Image adapted from Ref. 72. Copyright 2017 American Chemical Society.

Brutman *et al.* studied polyester/polycarbonate elastomers derived from **2-49**.²⁰⁹ As mentioned above, poly(**2-49**) can be depolymerized in the presence of the same base catalyst that polymerizes it. Premature depolymerization was prevented by end-capping the chains with acetate groups. After considerable materials evaluation, the researchers were able to produce a material with better toughness than commercial rubber bands (*vide supra*, Section 4.1), and these sustainable materials did not undergo significant hysteresis loss after multiple tensile cycles. These elastomers could be

depolymerized using a catalyst and a tetrol, resulting in a high amount of monomer recovery (>90%). In addition to being chemically degradable to monomers, these elastomers were hydrolytically degradable to the extent of 60–80% over 18 days in 1 M hydrochloric acid at 60 °C. However, at room temperature in 1 M hydrochloric acid or 1 M sodium hydroxide, or under mimicked physiologically relevant conditions (PBS solution at 37 °C), the polymers showed very little hydrolytic degradation. The authors hypothesized that the hydrophobic nature of the poly(2-49) polymer increases its resilience towards hydrolytic degradation, allowing the polymers to be used for a wide range of applications, some of which may be long term applications and under aqueous conditions.

Sugar-derived polymers represent an important opportunity in post-use degradation. For example, Gallagher *et al.* reported the synthesis of polyurethane methacrylate thermosets derived from the renewable dilactone sugar derivatives. ²³² These dilactones formed the core of dimethacrylate monomers, which then underwent polymerization to form networks. Due to the high cross-link density, the rigid nature of the fused dilactone ring and hydrogen bonding between urethane groups, these polymers were brittle. The degradation mechanism likely proceeds via initial dilactone ring opening, followed by urethane bond scission, consistent with previous reports. ²³³

Additional studies from the CSP focused on analogous degradation of thermoplastic polyesters synthesized via ADMET polymerization. Motivated by drawbacks associated with ADMET polymerization, including high synthesis temperatures and expensive ruthenium-based catalysts, Lillie *et al.* synthesized dilactone-based linear polyesters via thiol-ene "click" chemistry while maintaining degradability of the system, finding complete degradation in 1–3 days under basic conditions. ²³⁴

5.2. Compatibilization

Recycling mixed waste streams and multicomponent plastic packaging is challenging because direct melt reprocessing generally results in brittle, immiscible blends. However, separating different types of plastics to prepare them for recycling is difficult because many types of packaging are made from more than one kind of polymer; for example, recycling of water bottles is challenging because they comprise a mixture of PET, PP caps, and packaging materials and labels that include multiple layers of different laminated plastics (e.g., PET and PE).

Block polymers and graft copolymers can compatibilize immiscible polymer blends. ²³⁵ The compatibilized blends exhibit mechanical properties (*i.e.*, toughness) better than blends without compatibilizers. ²³⁶ CSP researchers have exploited compatibilization as a method to recycle mixed plastic waste and improve mechanical properties of polymer blends. **Figure 20** shows that a 70/30 HDPE/*i*PP blend has very poor extensibility (red trace). However, with 1 wt% of a PP/PE multiblock polymer added (green trace), the blend can exceed over 500% strain and has a higher ultimate tensile strength.

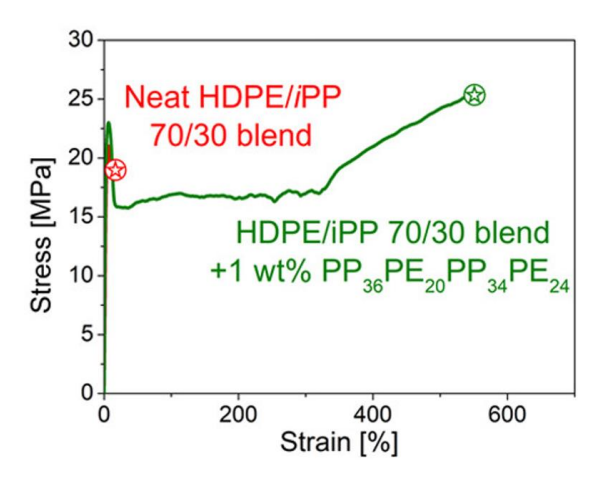


Figure 20. The toughness and extensibility of PE/*i*PP blends (red trace) are significantly enhanced by adding block copolymer compatibilizers (green trace). Adapted from Ref. 239. Copyright 2018 American Chemical Society.

Compatibilized blends usually show mechanical properties that fall between those of the two homopolymers and consist of one phase that is finely dispersed in a second matrix phase. These phases exhibit good interfacial adhesion and steric stabilization. To investigate the degree of compatibilization, typical analytical methods include microscopy techniques such as scanning electron microscopy (SEM) and transmission electron microscopy (TEM). With microscopy, the droplet domain sizes of blends can be measured, with smaller sizes correlating with better compatibilization. Interfacial adhesion can be assessed using methods such as the T-peel test. Failure mode analysis of these materials can give insight into the interfacial adhesion strength and mechanisms of compatibilization.

Reactive compatibilization, where the compatibilizing agent is generated during the melt-blending process, was investigated by Todd *et al.* to improve the properties of PET/HDPE blends.²³⁷ With the addition of only 0.5 wt % loading of a low molar mass amino-telechelic PE (ATPE) (3-17 kg mol⁻¹) elongation at break of the compatibilized blends (PET/HDPE/ATPE 89.5/10/0.5 wt. ratio) increased twelve-fold as compared to the neat blends (PET/HDPE 90/10). Consistent with the notion of compatibilization, domain sizes of the HDPE droplets were reduced eight-fold. The authors proposed that PET and ATPE reacted through amide bond formation during the melt blending process, forming PET-PE multiblock polymer compatibilizers. The semi-crystalline PE block could potentially contribute to compatibilization by co-crystallizing with the PE matrix. Although the exact molecular structures of the polymers generated during these melt mixing experiments were not identified, the putative generation of multiblock polymers indicated a new strategy for compatibilization between polyesters and polyolefins.

Multiblock polymers can also be premade and used as nonreactive compatibilizers for both the PE/*i*PP and PE/PET systems. Eagan *et al.* reported the synthesis of isotactic polypropylene and polyethylene (*i*PP-PE) tetrablock copolymers with precisely controlled molecular masses using a hafnium-based catalyst.²³⁸ By adding 1 wt % *i*PP-PE tetra-block polymer, the strain-at-break of *i*PP/PE blends (70/30 by weight to mimic polyolefin municipal waste) increased from 12% to

450% (which lies between the strain-at-break for *i*PP and PE homopolymers) in uniaxial tensile tests. The diblock polymer with comparable block molecular weight leads to a modest improvement (strain-at-break, 90%). In addition, *i*PP-PE tetrablock polymers displayed better interfacial adhesion between *i*PP and PE films compared to *i*PP-PE diblock polymers.

To gain more insight into the compatibilization of *i*PP and PE, Xu *et al.* explored a series of *i*PP-PE diblock, tetrablock, and hexablock copolymers as compatibilizers in a 70/30 wt % PE-*i*PP blend.²³⁹ The block polymers with a higher number of blocks were able to compatibilize the blend at much lower concentrations than the diblock copolymers. Adding just 1 wt % of tetrablock or hexablock copolymers resulted in optimal strain-at-break. Decreasing the concentration to 0.2 wt % tetra- or hexablock copolymers, the compatibilized blends still achieved significant increase of ductility. In contrast, low molecular mass diblock polymers (ca. 55 kg mol⁻¹) did not improve the strain-at-break as compared to the neat blends, while high molar mass diblock polymers (ca. 140 kg mol⁻¹) resulted in ductile blends after 5 wt % addition.

Droplet sizes decreased with increasing compatibilizer concentrations, which is attributed to the decrease of interfacial tension and better surface coverage. The authors proposed that the tetra-and hexablock polymers mechanically strengthen interfaces between the domains. To study the interfacial adhesion independently, T-peel tests were conducted with block polymer compatibilizers as the adhesive layer between PE and *i*PP films. Cohesive failure was observed when tetra- and hexablock polymers and high molecular weight diblock polymers were used as the adhesive layer, indicating good interfacial adhesion of the block copolymer to both the PE and the *i*PP films. On the other hand, low molar mass diblock polymers exhibited adhesive failure, indicating poor interfacial adhesion. Taken together, these results suggest the following mechanisms of adhesion: high molar mass diblock polymers can co-crystallize with the homopolymers at the interfaces, achieving high interfacial adhesion, while tetra- and hexablock polymers can further form interlocked entanglements (**Figure 21**).

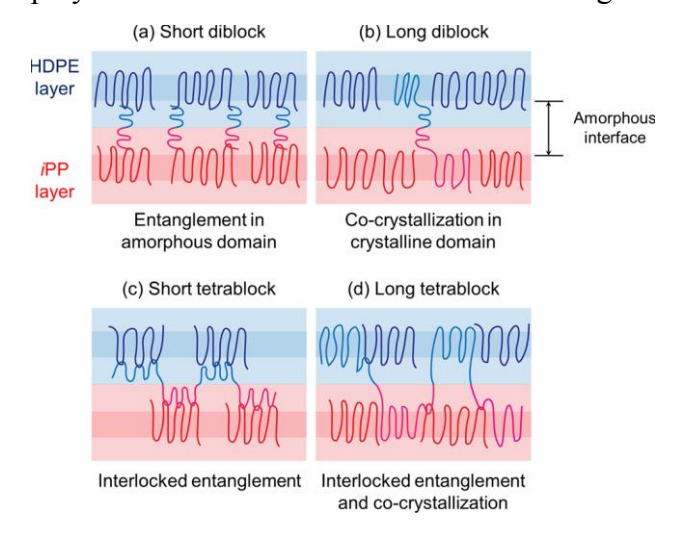


Figure 21. Potential mechanisms of interfacial adhesion and compatibilization using block copolymers. Adapted from Ref. 239. Copyright 2018 American Chemical Society.

This multiblock copolymer strategy has also been employed to compatibilize polyesters and polyolefins. Nomura *et al.* reported novel PET-PE multiblock polymers as adhesive tie-layers in multilayer films and compatibilizer additives for melt-reprocessed blends. PET-PE multiblock polymers were synthesized through a coupling reaction between dihydroxy-terminated PET and PE precursors, with an average of about ten blocks. Interfacial adhesive strength between PET and PE films was increased 600 times by using PET/PE multiblock polymer interlayers (~ 200 nm thickness). Adding only 0.5 wt % of multiblock polymer to PET/PE (80/20 wt/wt) blends significantly reduced the diameter of the PE droplets in the PET matrix from 4 μm to 1.5 μm (**Figure 23**), while the strain-at-break increased from 10% to 333%. Plastic deformation of minority PE domains was observed in SEM images of fractured surfaces, indicating enhanced adhesion.

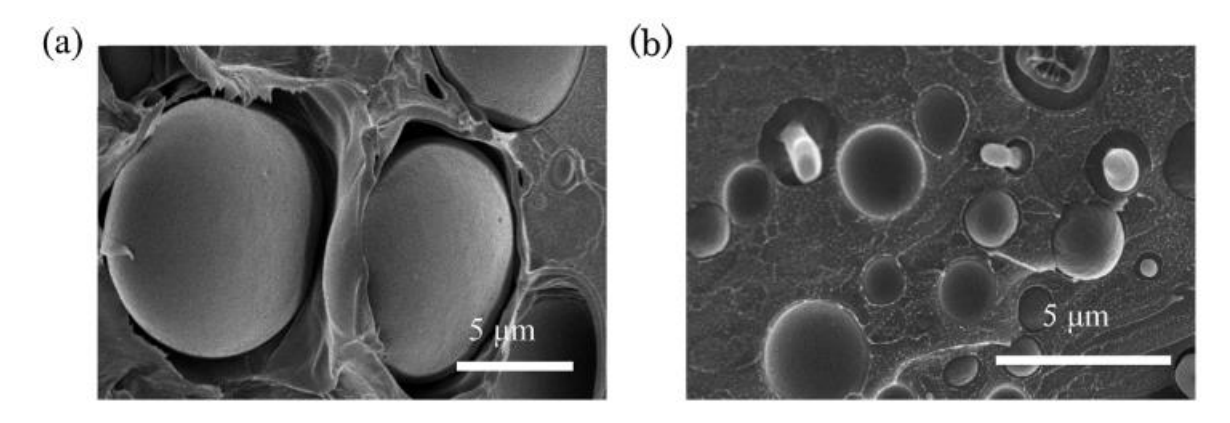


Figure 22. SEM images of cryofractured PE/PET blends (a) without and (b) with a block copolymer compatibilizer present. Notice that the droplet size is larger on the left and that fracturing has produced air gaps between the phases, both contributing to lower interfacial adhesion. Adapted from Ref. 240. Copyright 2020 American Chemical Society.

5.3. Reprocessable Materials

Thermosets are cross-linked polymers typically used in demanding applications such as automobile tires, footwear, and aerospace. In 2019, 14% of all plastics produced in the US were thermosetting resins. ²⁴¹ Because thermosets are permanently cross-linked and therefore topologically fixed, they cannot be recycled by melt reprocessing and are typically, incinerated, landfilled, or downcycled. One way to make thermosets recyclable is to include dynamic covalent cross-links such that network connectivity can change. This change in microscopic topology enables recycling (or remolding). These covalent adaptable networks (CANs) should ideally be similar to traditional thermosets under service conditions. When a stimulus such as heat is applied to the CAN, the cross-links become dynamic, allowing the material to be remolded and reshaped (**Figure 23**). CSP researchers have developed CANs to address the need for reprocessable, cross-linked thermoset- and elastomer-like materials. CANs have received enormous attention from researchers worldwide, and various aspects of the topic have been reviewed extensively elsewhere. ^{242,243,244}

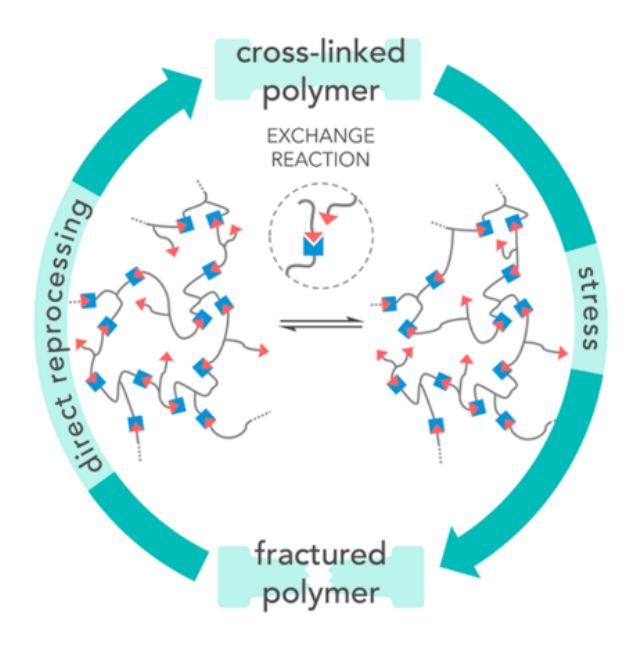


Figure 23. CANs allow network reconfiguration. Adapted from Ref. 242. Copyright 2018 American Chemical Society.

In addition to common mechanical tests such as uniaxial extension and DMTA, stress relaxation analysis (SRA) is often employed to characterize CANs. In classical thermosetting materials, applying an instantaneous stress elicits an elastic response because the strong, permanent crosslinks do not allow for a change in network connectivity; in other words, stress relaxation over short timescales (hundreds to thousands of seconds) is absent in permanently cross-linked networks. In CANs, however, stress relaxation at elevated temperatures implies that connectivity is changing via the dynamic cross-links. Modeling SRA data using an exponential decay function gives relaxation time constants that often follow an Arrhenius-like relationship as a function of temperature. Researchers have looked to these Arrhenius plots to elucidate mechanistic details; parameters such as the activation energy and the Arrhenius pre-exponential factor are believed to correlate with the mechanisms of both molecular exchange and macromolecular motion.²⁴⁵

CSP researchers have developed chemistries that enable CAN reprocessing with a variety of polymer matrices and functional groups. One such dynamic chemistry is transcarbamoylation of urethanes and free alcohols triggered by heat. Polyurethane materials have a variety of applications including footwear, furniture, and construction, and are common thermosets typically synthesized from the condensation of toxic isocyanates and alcohols. Fortman *et al.* described the synthesis of polyhydroxyurethane CANs via the ring opening polymerization of a bis(cyclic carbonate) and a trifunctional amine. ²⁴⁶ Instead of using isocyanates, which are typical precursors of polyurethanes, cyclic carbonates were reacted with multifunctional amines to form the urethane linkages of these thermoset materials. This ring-opening polymerization is designed to liberate alcohols that will later participate in associative exchange processes.

Fortman *et al.*²⁴⁶ performed SRA on polyhydroxyurethanes and analogous *N*-methylated networks, observing similar flow activation energies (111 kJ mol⁻¹ and 101 kJ mol⁻¹, respectively). This similarity suggests that alcohol-mediated associative exchange processes dominate the stress

relaxation mechanism as opposed to dissociative urethane reversion to isocyanates and alcohols (**Scheme 35**); *N*-methylurethanes are unable to undergo dissociation and the thermodynamics of exchange are similar for both bond linkages. Furthermore, acetylation of the free alcohols hindered the polymer reprocessability, which is consistent with the proposed associative exchange mechanism. Fortman *et al.* later studied the use of 5-membered cyclic carbonates,²⁴⁷ which are thermodynamically more stable than their previously-studied 6-membered analogues.²⁴² The networks derived from the 5-membered cyclic carbonate were reprocessed using compression remolding without the need for a catalyst, but decomposed at lower temperatures than the PHUs derived from 6-membered cyclic carbonates.

Associative Urethane Exchange

Dissociative Urethane Reversion

Scheme 38. Urethane cross-links can exchange via an associative mechanism if there are free alcohols present. Dissociative exchange proceeds via reversion to isocyanates and alcohols in the absence of free alcohols.

In contrast to the polyhydroxyurethane system that appears to relax stress by an associative transcarbamoylation process, Brutman *et al.* observed stress relaxation characteristics consistent with partial dissociative urethane reversion to isocyanate and hydroxyl groups in the presence of a tin catalyst.²⁴⁸ They first observed that star polymers with PLA arms had similar stress relaxation activation energies to polymers with polyethylene oxide arms (139–165 kJ mol⁻¹), indicating that bond exchange in this system is not dependent on transesterification chemistry. The ability of urethane bonds to undergo exchange in the absence of alcohol nucleophiles is consistent with several other reports of urethane exchange in cross-linked PLA. These reports indicate that stress relaxation occurs with activation energies (150 kJ mol⁻¹) higher than that of typical transesterification (80 kJ mol⁻¹).^{249,250} Although activation energies were consistent across the urethane linked star polymers synthesized in this study, relaxation rates significantly increased with an increase in the rubbery plateau modulus. This parameter exerted a stronger influence than the effect of free alcohol concentration. Thus, urethane exchange was demonstrated to occur via

both associative and dissociative mechanisms that depended on the polymer composition and reaction conditions. In the absence of free alcohols, urethane reversion occurred with or without catalyst, although the uncatalyzed reaction proceeded 30 times slower. However, free alcohols bound to the tin may deactivate the catalyst and result in negligible urethane reversion reactions.²⁴⁸ Leveraging these insights to the urethane exchange mechanism, researchers further developed end-of-life polyurethane reprocessing strategies.

Recently, cross-linked PU was shown to relax stress in the presence of tin-based catalysts in shapememory materials. ²⁵¹, ²⁵², ²⁵³, ²⁵⁴ However, bulk reprocessing of cross-linked PU has been demonstrated only recently using dynamic covalent bond exchange. Fortman *et al.* studied nontoxic PU carbamate exchange catalysts and found that they enable bulk reprocessability in polyether and polyester cross-linked PUs. ²⁵⁵ Model studies revealed that carbamates exchange at elevated temperatures in the presence of many different catalysts. Likewise, stress relaxation was found to be rapid at elevated temperatures for both polyether and polyester cross-linked PU materials, indicating the exchange process is possible in both types of PU. These materials were subjected to compression molding and experienced moderate recovery of tensile properties after reprocessing (39–67% of original tensile strength). Interestingly, materials reprocessed with the Bi(neo)₃ (neodecanoate-ligated bismuth) catalyst had the highest recovery of tensile strengths and cross-link density among the tested catalysts.

With these results demonstrating bulk reprocessability of PU in hand, Sheppard et al. reported a method to reprocess post-consumer cross-linked PU foams using twin-screw extrusion. 256 This is important because PU foams are ubiquitous in daily life. A common application for PU foams is padding for seat cushions. A urethane exchange catalyst was diffused into PU foam by solution swelling.²⁵⁷ However, compression methods of reprocessing gave films with air voids, attributed to the cellular foam morphology. To circumvent this issue, the researchers employed a microcompounder (a small twin-screw extruder) that effectively mixed foam waste while simultaneously removing air from the material. Microcompounded model PU foams thus had properties similar to newly-synthesized films based on the same monomers, demonstrating removal of air voids from the initial foam morphology. Interestingly, the screw extrusion reprocessing method created films that had significantly higher recovery of mechanical properties compared to the previously reported compression-molded materials. This screw extrusion method was then extended to commercial flexible foam (Figure 24). While Bi(neo)3 was the bestperforming catalyst in compression molding studies, the catalyst showed evidence of degradation during extrusion. Future work includes in-depth studies of the extruded PU films as a function of the various reprocessing catalysts and foam reprocessing from real mixed waste streams.

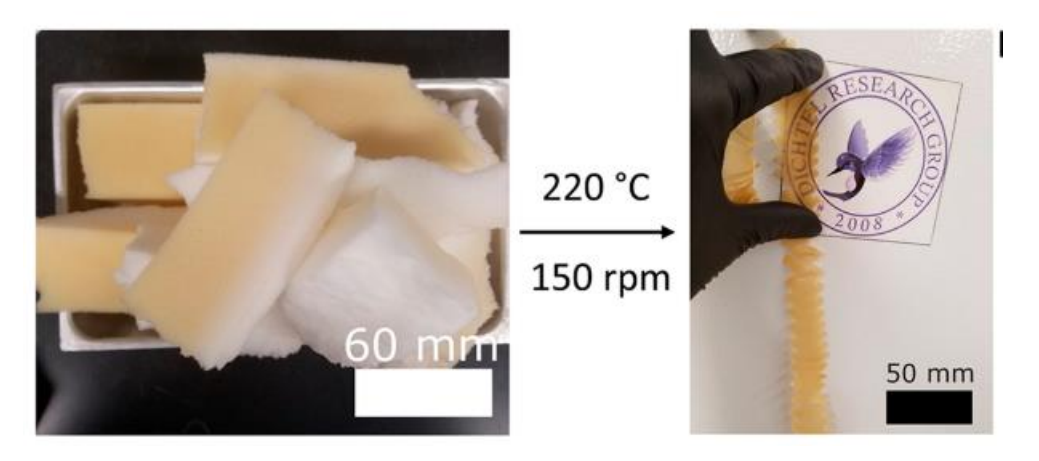


Figure 24. PU foam can be reprocessed into films using a twin-screw extruder after adding a Lewis acidic catalyst by solution swelling. Image adapted from Ref. 256. Copyright 2020 American Chemical Society.

Catalysts can also be used to promote exchange in polycarbonate networks. Snyder *et al.* investigated the use of a Ti(IV) catalyst to reprocess a crosslinked polycarbonate network at elevated temperatures through an associative transcarbonation pathway.²⁵⁸ They investigated the stress relaxation kinetics of these polycarbonate networks as a function of diol stoichiometry and catalyst. Samples with higher catalyst loading and higher diol content exhibited faster stress relaxation. The synthesized polycarbonate materials were subsequently reprocessed at elevated temperatures, displaying varying recovery of rubbery plateau *E* after reprocessing (>72% for all examples). In addition to being reprocessable, these polymers could be degraded in acid. Subsequent liquid-liquid extraction lead to efficient recovery of a precursor to the bis(cyclic carbonate) monomer. This study demonstrated the potential of dynamic covalent cross-linking in adding value to commonly used materials such as polycarbonates.

Much of the CAN literature features the polymerization of specialty monomers to form thermoset-like networks. Ishibashi and Kalow demonstrated that a low-barrier associative conjugate addition-elimination reaction between thiols and Meldrum's acid alkylidene cross-linkers can enable reprocessing of commercially available thiol-containing PDMS. These elastomeric networks exhibit a low T_g value (-108 °C) characteristic of silicones and may be reprocessed via compression remolding (150 °C, 15 min) at least 10 times without a change in mechanical properties. This reprocessability is consistent with robust chemical pathway by which cross-link exchange occurs and furthermore suggests that the polymer backbone is not modified by compression remolding. This idea is further underscored by the fact that de-cross-linking in the presence of a 2-hydroxymercaptan yields a linear polymer that is nearly identical to the original, commercial product by SEC (**Figure 25**). 260

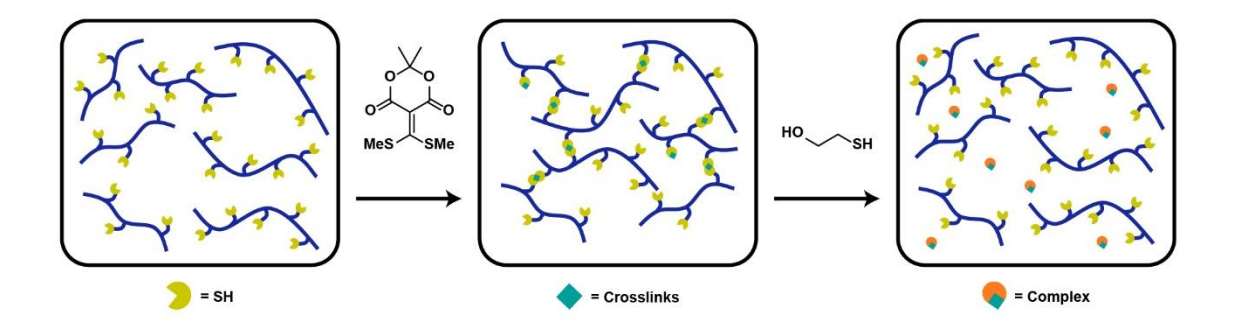


Figure 25. CANs were synthesized through the crosslinking of thiol-functionalized siloxanes using a Meldrum's acid derivative. Networks were disrupted and dissolved in toluene using β-mercaptoethanol, which illustrated the ease of network degradation.

While earlier research on CANs tended to focus on tuning properties by applying new exchange reactions, more recent work is integrating other key phenomena in polymer science with the CAN concept. Snyder et al. explored how a linear prepolymer's sequence affects the properties of resulting cross-linked CANs. 261 Gradient (grad) and statistical (stat) linear polyesters were prepared by ROCOP and included aldehyde handles for imine-based cross-linking. While the DMTA traces of *stat*-derived networks exhibited an extended rubbery plateau, the *grad*-derived networks showed decreasing storage modulus after the glass transition (all T_g values were above 55 °C). This unusual behavior among the grad-CANs was attributed to architecture effects; a dissociative mechanism involving imine hydrolysis was discounted because the networks did not dissolve in neutral pH solutions, even above the T_g . Furthermore, the *stat* networks similarly did not dissolve, underscoring that an associative mechanism is probably operating in these systems. It was therefore hypothesized that the presence of dangling ends in the grad-CANs acts as a plasticizer, leading to the observation of decreasing storage modulus above the glass transition. Because the grad-CANs experienced flow at elevated temperature, stress relaxation could not be accurately assessed. However, the stat-CANs exhibited full stress relaxation between 105 °C and 120 °C in less than 10 s, indicating the potential for reprocessing at elevated temperature. Each of the materials recovered full tensile properties after three iterations of reprocessing and compression remolding at 100 °C for 30 min.

CSP researchers are investigating the incorporation of dynamically cross-linked polymers into non-woven fibers. Non-woven, randomly oriented polymer fiber mats are an important class of polymer products used in a variety of applications such as disposable wipes, face masks, and filtration media. The global market for nonwoven fibers has increased to \$50 billion (USD), and melt-blown fiber products constitute more than 10%, given the high efficiency of the melt-blowing process. Cross-linked melt-blown fibers could be extremely useful because of the improved performance including excellent mechanical properties and good thermal/solvent stability. However, most commodity melt-blown fibers have been made by using thermoplastic feedstocks, and cross-linked materials are generally not used with the process. By employing dynamic cross-linking, the CSP has enabled the production of melt-blown cross-linked fiber systems with the additional benefit of recyclability. Jin *et al.* developed melt-blown thermoset fiber systems using

Diels–Alder reactions between furan and maleimide functional groups as the cross-links (**Scheme 39**).²⁶² The dissociative nature of the classic [4 + 2] cycloaddition enables both melt processing and a solidification mechanism induced by cross-linking. Thermoset melt-blown fibers were produced, which demonstrated that cross-linkable backbones could replace traditional thermoplastics in demanding applications. However, the relatively low dissociation temperature of the furan–maleimide adducts (~100 °C) could be a potential limitation. Jin *et al.* studied another reversible thermoset fiber system, using reversible photodimerization of anthracenes as the dynamic cross-link.²⁶³ Given the higher dissociation temperature of dimerized anthracenes (~160 °C), the resulting cross-linked fibers showed excellent thermal stability. In contrast to the previous example, the melt-blowing and cross-linking processes are decoupled when anthracene dimers are used to cross-link the polymer fibers. The thermoset fibers could be reprocessed at 205 °C into bulk films. These strategies could promote sustainability for nonwoven products.

Diels-Alder Cycloaddition

Anthracene Dimerization

Scheme 39. Dynamic electrocyclic reactions used to reversibly cross-link melt-blown fibers as described by Jin *et al.* ^{262,263}

6. Outreach of CSP

The CSP utilizes its three grand challenges within the sustainable polymer framework to address the growing plastics pollution and sustainability crisis. The research emphasis in the Center is central to our work as highlighted in the preceding sections. As part of our mission, we also emphasize the need for education at all levels. Such education is critical if we want to successfully reach our shared vision of a sustainable future. For example, teaching the public about the importance of sustainable practices will help build an understanding of why the status quo must change. In addition, we prioritize collaboration, inclusivity, diversity, and outreach by seeking better representation of underrepresented minority groups within STEM. Toward achieving these broader impacts, the CSP has focused on increasing scientific critical thinking and literacy among K–12 and undergraduate students through outreach work.

6.1 4-H Partnership

Numerous reports outline the need to grow the STEM workforce, with improvements in K–12 STEM education as a key recommendation for increasing the number of STEM graduates. ^{264,265,266} In studies examining attrition and persistence of students through the STEM pipeline, interest in STEM developed at an early age (*i.e.*, middle school) provides momentum likely to increase participation, level of interest, and success of students in STEM disciplines. ^{267,268,269,270} Inquiry-based projects involving real-world problems further these same goals and outcomes. ^{271,272,273,274}

In 2007, the National 4-H Council recognized the need to engage young learners in STEM and spearheaded the "One Million New Scientists. One Million New Ideas" mandate to engage one million youth in out-of-school STEM learning. ²⁷⁵ 4-H is the largest youth development organization in the United States and is delivered by Cooperative Extension, a feature of all landgrant institutions. Nearly six million youth participate in 4-H programming annually, reaching urban, suburban, and rural audiences. In response to the increased need for STEM programming, the Center has worked with external professionals from the University of California, Davis, Cornell University, and the University of Minnesota to develop a STEM curriculum for 4-H to use nationally. To promote STEM engagement among youth, the CSP began an active collaboration with 4-H in 2014.

The partnership between 4-H professionals and the CSP developed, tested, and published three curricula (Grades K–2, 3–5, and 6–8) following the teaching methods of inquiry and experiential learning. The overarching learning goal of the curricula was to introduce youth to the prevalence and impacts of plastics in everyday life. In addition, the activities were designed to help build the foundational science and engineering skills identified in the Next Generation Science Standards. They also incorporated the SciGirls Strategies for Engaging Girls in STEM. ²⁷⁶ For older youth in grades 6–8, special emphasis was placed on youth-driven community projects to provide real-world applications of STEM. As materials were developed, modules were made available for free download (https://4Hpolymers.org), with the first modules released in 2017. ²⁷⁷ Since their introduction, the modules have been accessed by more than 200 educators from 36 states and 4 countries (**Figure 26**). Based on the information gathered through the website's request form, this curriculum has reached an estimated 16,000 youth. To further dissemination, the modules have

undergone the National 4-H Council's rigorous peer review process and are available for public purchase on the National 4-H shop.



Figure 26. K-2 students examine polymers to practice making scientific observations and exploring material properties.

6.2 Green Chemistry in the Classroom

Polymer science experiments have historically been underrepresented in the undergraduate laboratory curriculum due to the lack of instruction in associated lecture courses, the potentially hazardous nature of traditional experiments, and perceived need for specialized equipment. Considering the size of the polymer industry and the relevance of plastics to society, curricular design focused on modern scientific advances in sustainable polymers represents an opportunity to connect with students and engage their interest in the topic of environmentally friendly plastics. Toward that end, the CSP has developed a portfolio of polymer laboratory experiments tailored for use in both undergraduate and high school curricula. This work leverages the research discoveries of the CSP and translates them to the laboratory classroom environment. Associated curricular materials provide a platform for bringing awareness to the unintended consequences of plastics in society and to inspire students with the opportunity for innovation represented by the mission of "transforming how plastics are made, unmade, and remade."

Polymer experiments that emphasize the principles and techniques of green chemistry 278 are actively sought in the organic chemistry laboratory. One such experiment developed in the Center was inspired by the controlled ROTEP of the renewable monomer δ -decalactone, which proceeds catalytically at room temperature in the absence of solvent. 279 Because this polymerization conforms to many green chemistry principles, it was an excellent starting point for translation into a new laboratory experiment. In step one, the polymerization of δ -decalactone is carried out using an initiator; in step two, a triblock polymer is synthesized, isolated, and transformed into a clear, thin, flexible film easily analyzed by 1 H NMR spectroscopy. 280 Students responded positively to learning about sustainable polymer syntheses and expressed enjoyment in isolating a high molar mass rubbery material compared to the usual small molecule organic liquids and solids of the introductory organic laboratory (

). In an expansion of the experiment to include inquiry-based learning outcomes, groups of students were tasked with synthesizing triblock polymers comparing the use of δ -decalactone and δ -dodecalactone monomers for the midblock and varying proportions of poly(L-lactide) as the endblock. Students designed mechanical testing of the varied triblock copolymers in order to explore their tunable properties. ²⁸¹

poly(L-lactide)-
$$b$$
-poly(δ -decalactone)- b -poly(L-lactide), $x = 4$ poly(L-lactide)- b -poly(δ -dodecalactone)- b -poly(L-lactide), $x = 6$

Figure 27. Structures and image of sustainable triblock polymers prepared in a laboratory designed for undergraduates.

Adapted from the two references, polymer experiment appropriate for both high school and college laboratory classrooms involves the preparation of a biodegradable thermoset polymer using inexpensive, nontoxic, and readily available citric acid and glycerol. ²⁸² This chemistry was integrated with a previous exercise that compared starch-based plastic films containing varying additives and that utilized tensile-testing for incorporation of engineering principles. ²⁸³ In this new "Dyeing to Degrade" experiment by Knutson, *et al.*, combinations of citric acid, glycerol, and tapioca root starch are used to synthesize biofilms colored with a yellow food dye. Students compare and quantify the rates of aqueous basic degradation by following the release of the yellow dye using either ultraviolet spectroscopy or smartphone colorimetry. ²⁸⁴ The versatility of this experiment has resulted in its successful implementation in AP high school classrooms, undergraduate general and honors chemistry laboratory courses, an introductory environmental science course, and a "chemistry for the life sciences" course.

In an adaptable experiment designed for outreach and high school classrooms, students explore threads drawn from poly(ε-caprolactone) samples of different molar masses as absorbable and nonabsorbable medical sutures. The physical and mechanical testing of these threads meet the K–12 Next Generation Science Standards of Engineering Principles and demonstrate the connection of polymer science to society and the real world. These experiments are a major component of a successful "Green & Sustainable Chemistry Workshop" for Minnesota high school teachers and was recognized by the ACS Committee on Environmental Improvements Award for Contributions to Sustainability in Education. Education.

Recently, Gormong *et al.* investigated the emulsion copolymerization of bio-based β-myrcene and dibutyl itaconate (**Figure 28**), first reported by Sarkar and Bhowmick, ²⁸⁸ and successfully developed a new polymer experiment for undergraduate organic and polymer chemistry teaching laboratories. ²⁸⁹ The authors discovered that vigorous stirring of the emulsified reaction mixture produces a tacky, cross-linked elastomer. This network material preferentially swells in nonpolar solvents when exposed to a range of solvents, ordered by dielectric constant, shown in **Figure 29**. An analogous linear/branched copolymer can be prepared by free-radical bulk polymerization of

the same monomers, which is suitable for student estimation of M_n , conversion, and monomer incorporation ratio by ¹H NMR spectroscopy.

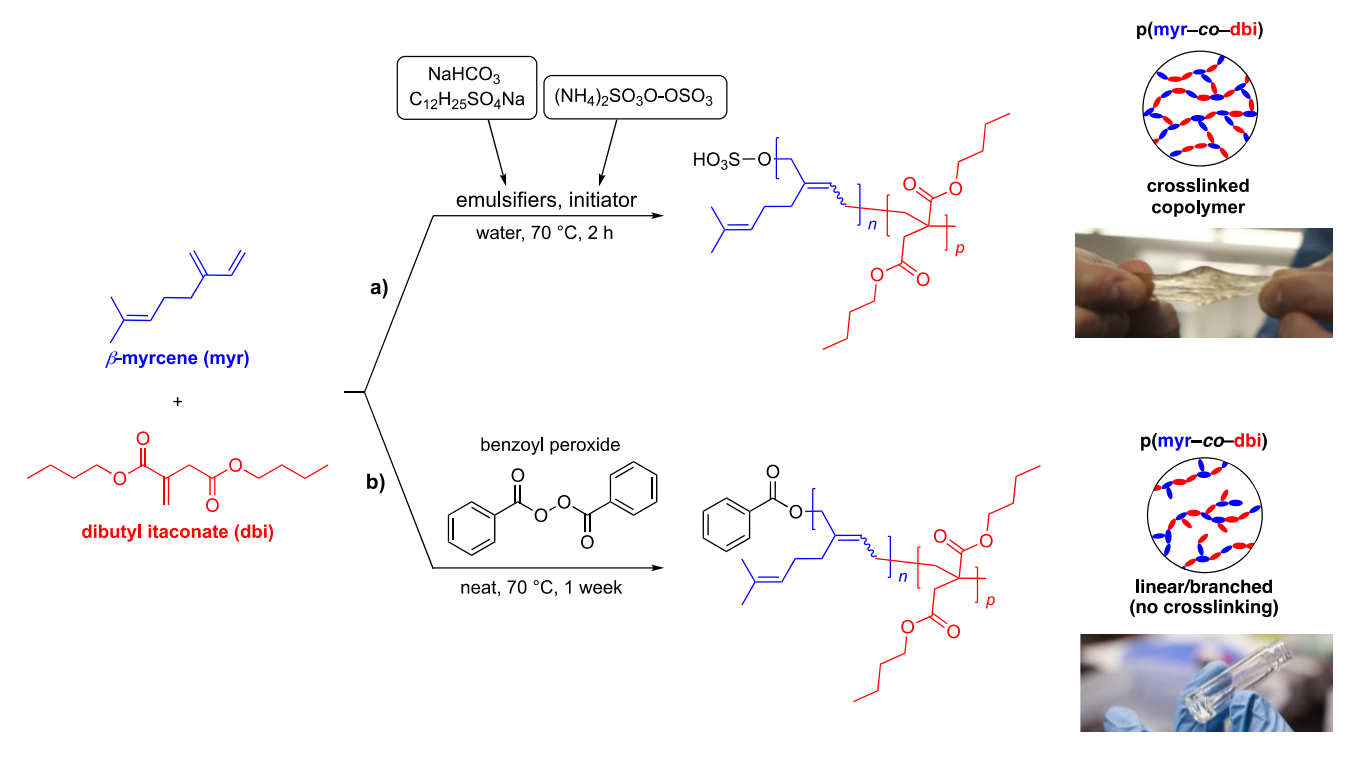


Figure 28. Free-radical copolymerization of β-myrcene and dibutyl itaconate in the teaching laboratory under **a)** emulsion conditions, yielding an elastic copolymer network or **b)** bulk conditions, yielding a viscous linear/branched copolymer. Adapted from Ref. 289. Copyright 2016 American Chemical Society.



Figure 29. Swelling tests of 20–30 mg of cross-linked poly(myr-co-dbi) after ~60 min in a variety of solvents ordered from left to right by ascending dielectric constant. Adapted from Ref. 289. Copyright 2016 American Chemical Society.

6.3 Beyond the Classroom Series

In a collaborative research center, a common language and basic understanding of interdisciplinary topics is necessary to facilitate the research partnerships. In Fall 2014, the CSP initiated a centerwide webinar series called Beyond the Classroom. The original structure of the webinar series was to focus on pertinent topics to sustainable polymers not typically found in regular coursework, such as the chemistry of composting, life cycle analysis, and entrepreneurship. Following assessment gathered in 2015, the Beyond the Classroom series was restructured into an approximately 90 minute "101" introductory course format with presentations by CSP researchers to further facilitate a common knowledge base among participating researchers. Initial topics covered in this restructuring included overviews on biofermentation, polymer processing, and computational chemistry. Each webinar was conducted via videoconference for all Center members to participate in real time. The sessions were also recorded, closed-captioned for accessibility, and archived on the CSP's website, and were then made available to the public on our YouTube channel. ²⁹⁰ A survey of CSP members was overwhelmingly positive for this 101style format that is offered several times per year. Center members valued the opportunity to learn about areas further from their primary research area within the Center and to gain better understanding of the presented topics as a result of the webinar series.

7. Data Management

To improve accessibility to federally funded research, the CSP developed a process for researchers to publish the original, primary data files associated with their ACS manuscripts via a DOI link included within the publication. This process permanently ties the original data files to the manuscript and thereby improves transparency in the scientific publishing process and facilitates data reuse.

The author workflow was developed in collaboration with ACS Publications and the Data Repository for the University of Minnesota (DRUM).²⁹¹ Through the expertise in DRUM, all submitted data files are curated by data curation librarians in the University of Minnesota Library to ensure compliance with FAIR (Findable, Accessible, Interoperable, Reusable) data standards set by the Data Curation Network.²⁹² The process was piloted with multiple manuscript submissions since 2018, to ensure peer reviewers would have anonymous access to the data files during the review process and that the communication process with the journals would be straightforward. All of the Center's curated data sets are also available in a collection within DRUM,²⁹³ and the data files are searchable, crawlable, and citable in their own right.

Prior to submitting their manuscript to the journal, researchers initiate the curation process with DRUM. They organize the primary data files into a logical directory and upload the files associated with the manuscript to DRUM. Critically, they also provide a README.txt file to describe the files, the software needed to open them, and contact information for the data set. The target audience for the data files, organization structure, and the README file are researchers in their same field. The files are uploaded to the data repository under a creative commons license and DRUM then generates an unpublished DOI for the researchers to provide in the manuscript's "Notes" section and protects the files in a secured online location that is provided only to the journal's reviewers. Upon acceptance by the journal, DRUM publishes the DOI.

8. Outlook

This review, representing more than a decade of discoveries published by the NSF Center for Sustainable Polymers, illustrates how integrative efforts across numerous chemical science disciplines contributed to new understandings, materials, processes, and technologies advancing modern polymer science. Transformation of the current landscape for the production and fate of polymers to one that is sustainable in the long term will require fundamental advances of the chemistry of the sustainable polymers and a holistic approach to discovery. A key aspect that distinguishes work from the NSF Center for Sustainable Polymers is the collaborative effort of a diverse group of scientists on these fundamental questions. These collective endeavors become more and more effortless as we establish strong working relationships, shared vision, and a common language that facilitates and fosters innovation. This ecosystem takes time to establish, but the investment is well worth the payoff. When combined with efforts in education, outreach, broadening participation, data management, and corporate engagement, the NSF Center for Sustainable Polymers aspires to have a long-lasting legacy that has a transformative impact on society into our sustainable future.

X. Acknowledgements

We thank the University of Minnesota Initiative for Renewable Energy and the Environment and the National Science Foundation for support of the center (CHE-1901635, CHE-1413862, and CHE-1136607). We recognize the scores of researchers that have contributed to this and other research from the center since its inception. We thank John Beumer for assistance on and generation of graphics.

X. Author Information

Corresponding Author:

*Marc A. Hillmyer, hillmyer@umn.edu

ORCID:

Farihah M. Haque: 0000-0002-5029-7442 Jacob S. A. Ishibashi: 0000-0003-2045-4387 Claire A. L. Lidston: 0000-0002-4541-8190

Huiling Shao: 0000-0001-8007-6408
Frank Bates: 0000-0003-3977-1278
Alice B. Chang: 0000-0001-5036-2681
Geoffrey W. Coates: 0000-0002-3400-2552
Christopher J. Cramer: 0000-0001-5048-1859
Paul J. Dauenhauer: 0000-0001-5810-1953
William R. Dichtel: 0000-0002-3635-6119
Christopher J. Ellison: 0000-0002-0393-2941
Ethan A. Gormong: 0000-0002-6568-2458
Leslie S. Hamachi: 0000-0001-6299-8695
Thomas R. Hoye: 0000-0001-9318-1477

Mengyuan Jin: 0000-0001-8792-3438 Julia A. Kalow: 0000-0002-4449-9566 Hee Joong Kim: 0000-0001-6297-1636 Gaurav Kumar: 0000-0001-7089-6146

Christopher J. LaSalle: 0000-0003-0303-5447 Stephanie Liffland: 0000-0002-9028-2851 Bryce M. Lipinski: 0000-0001-7769-4678 Yutong Pang: 0000-0002-9098-700X Riffat Parveen: 0000-0003-4941-7512 Xiayu Peng: 0000-0002-6216-7493 Yanay Popowski: 0000-0003-1569-0035 Emily A. Prebihalo: 0000-0003-0730-3752 Yernaidu Reddi: 0000-0002-6743-9582 Theresa Reineke: 0000-0001-7020-3450 Jeremy L. Swartz: 0000-0003-0391-8434 William B. Tolman: 0000-0002-2243-6409 Bess Vlaisavljevich: 0000-0001-6065-0732 Jane Wissinger: 0000-0002-9240-3629

Shu Xu: 0000-0002-2713-7897

Marc A. Hillmyer*: 0000-0001-8255-3853

9. References

¹ See: https://csp.umn.edu/spf/

² Wissinger, J. E.; Ellison, C. J.; Dichtel, W. R.; Chang, A. B.; Trotta, J. T.; Yang, A. B.; Bunyard, C. W. Sustainable Polymer Framework, 2020, http://hdl.handle.net/11299/211643.

³ Hillmyer, M. A. The promise of plastics from plants. *Science* **2017**, 358, 868–870.

⁴ Vennestrøm, P. N. R.; Osmundsen, C. M.; Christensen, C. H.; Taarning, E. Beyond Petrochemicals: The Renewable Chemicals Industry. *Angew. Chem., Int. Ed.* **2011**, *50*, 10502–10509.

⁵ Biddy, M. J.; Scarlata, C.; Kinchin, C. Chemicals from Biomass: A Market Assessment of Bioproducts with Near-Term Potential. National Renewable Energy Laboratory, 2016. NREL/TP-5100-65509

⁶ Homer, C. M. Early Days of Harvesting Latex. Chem. Eng. News 2012, 90 (49), 4.

⁷ Tullo, A. H. Tire Makers Try New Rubber Sources. Chem. Eng. News **2012**, 90 (37), 16.

⁸ Bomgardner, M. Dandelions, the scourge of lawns, may be a fount of rubber. *Chem. Eng. News* **2016**, *94* (30), 28–29

⁹ Raber, L. R. Where Rubber Hits the Road. Chem. Eng. News 2004, 82 (37), 12–14.

¹⁰ Greve, H. H. Rubber, 2. Natural. Ullmann's Encyclopedia of Industrial Chemistry; Wiley-VCH: Weinheim, 2000. DOI: 10.1002/14356007.a23 225.

¹¹ Golden, G.; Mann, R. H. Isoprene. Kirk-Othmer Encyclopedia of Chemical Technology, 2nd ed.; Wiley: New York, 200; 64–83. DOI: 10.1002/0471238961.0919151612250201.a01.pub2.

¹² Abdelrahman, O. A.; Park, D. S.; Vinter, K. P.; Spanjers, C. S.; Ren, L.; Cho, H. J.; Zhang, K.; Fan, W.; Tsapatsis, M.; Dauenhauer, P. J. Renewable Isoprene by Sequential Hydrogenation of Itaconic Acid and Dehydra-Decyclization of 3-Methyl-Tetrahydrofuran. *ACS Catal.* **2017**, *7*, 1428–1431.

¹³ Park, D. S.; Abdelrahman, O. A.; Vinter, K. P.; Howe, P. M.; Bond, J. Q.; Reineke, T. M.; Zhang, K.; Dauenhauer, P. J. Multifunctional Cascade Catalysis of Itaconic Acid Hydrodeoxygenation to 3-Methyl-tetrahydrofuran. *ACS Sustainable Chem. Eng.* **2018**, *6*, 9394–9402.

- ¹⁴ Li, S.; Abdelrahman, O. A.; Kumar, G.; Tsapatsis, M.; Vlachos, D. G.; Caratzoulas, S.; Dauenhauer, P. J. Dehydra-Decyclization of Tetrahydrofuran on H-ZSM5: Mechanisms, Pathways, and Role of Transition State Entropy. *ACS Catal.* **2019**, *9*, 10279–10293.
- ¹⁵ Al-Qallaf, F. A. H.; Johnstone, R. A. W.; Liu, J.-Y.; Lu, L.; Whittaker, D. Metal(IV) phosphate catalysed retro-Prins reaction involving an oxetane intermediate. *J. Chem. Soc.*, *Perkin Trans. 2*, **1999**, 1421–1423.
- ¹⁶ Arnold, R. T.; Smolinksy, G. The mechanism of pyrolysis of β-hydroxyolefins. J. Org. Chem., **1960**, 25, 129–130.
- ¹⁷ Arnold, R. T.; Smolinksy, G. Pyrolysis of β-hydroxyolefins. III. A novel method for extending carbon chains. *J. Am. Chem. Soc.*, **1960**, *82*, 4918–4920.
- ¹⁸ Lundberg, D. J.; Lundberg, D. J.; Zhang, K.; Dauenhauer, P. J. Process Design and Economic Analysis of Renewable Isoprene from Biomass via Mesaconic Acid. *ACS Sustainable Chem. Eng.* **2019**, *7*, 5576–5586.
- ¹⁹ Abdelrahman, O. A.; Park, D. S.; Vinter, K. P.; Spanjers, C. S.; Ren, L.; Cho, H. J.; Vlachos, D. G.; Fan, W.; Tsapatsis, M.; Dauenhauer, P. J. Biomass-Derived Butadiene by Dehydra-Decyclization of Tetrahydrofuran. *ACS Sustainable Chem. Eng.* **2017**, *5*, 3732–3736.
- ²⁰ Furukawa, S.; Endo, M.; Komatsu, T. Bifunctional Catalytic System Effective for Oxidative Dehydrogenation of 1-Butene and *n*-Butane Using Pd-Based Intermetallic Compounds. *ACS Catal.* **2014**, *4*, 3533–3542.
- ²¹ Cespi, D.; Passarini, F.; Vassura, I.; Cavani, F. Butadiene from biomass, a life cycle perspective to address sustainability in the chemical industry. *Green Chem.* **2016**, *18*, 1625–1638.
- ²² Bruijnincx, P. C. A.; Weckhuysen, B. M. Shale Gas Revolution: An Opportunity for the Production of Biobased Chemicals? *Angew. Chem., Int. Ed.* **2013**, *52*, 11980–11987.
- ²³ Kuznetsov, A.; Kumar, G.; Ardagh, M. A.; Tsapatsis, M.; Zhang, Q.; Dauenhauer, P. J. On the Economics and Process Design of Renewable Butadiene from Biomass-Derived Furfural. *ACS Sustainable Chem. Eng.* **2020**, *8*, 3273–3282.
- ²⁴ Cho, H. J.; Ren, L.; Vattipailli, V.; Yeh, Y.-H.; Gould, N.; Xu, B.; Gorte, R. J.; Lobo, R.; Dauenhauer, P. J.; Tsapatsis, M; Fan, W. Renewable p-Xylene from 2,5-Dimethylfuran and Ethylene Using Phosphorus-containing Zeolite Catalysts. *ChemCatChem* **2017**, *9*, 398–402.
- ²⁵ Kumar, G.; Liu, D.; Xu, D.; Ren, L.; Tsapatsis, M.; Dauenhauer, P. J. Dehydra-Decyclization of 2-methyltetrahydrofuran to pentadienes on boron-containing zeolites. *Green Chem.* **2020**, *22*, 4147–4160.
- ²⁶ Zhang, X.; Jordan, F.; Szostak, M. Transition-metal-catalyzed decarbonylation of carboxylic acids to olefins: exploiting acyl C-O activation for the production of high value products. *Org. Chem. Front.* **2018**, *5*, 2515–2521.
- ²⁷ Miller, J. A.; Nelson, J. A.; Byrne, M. P. A highly catalytic and selective conversion of carboxylic acids to 1-alkenes of one less carbon atom. *J. Org. Chem.* **1993**, *58*, 18–20.
- ²⁸ Miranda, M.; Pietrandgel, A.; Hillmyer, M. A.; Tolman, W. B. Catalytic decarbonylation of biomass-derived carboxylic acids as efficient route to commodity monomers. *Green Chem.* **2012**, *14*, 490–494.
- ²⁹ Ortuño, M. A.; Dereli, B.; Cramer, C. J. Mechanism of Pd-Catalyzed Decarbonylation of Biomass-Derived Hydrocinnamic Acid to Styrene following Activation as an Anhydride. *Inorg. Chem.* **2016**, *55*, 4124–4131.
- ³⁰ John, A.; Miranda, M. O.; Ding, K.; Dereli, B.; Ortuño, M. A.; LaPointe, A. M.; Coates, G. W.; Cramer, C. J.; Tolman, W. B. Nickel Catalysts for the Dehydrative Decarbonylation of Carboxylic Acids to Alkenes. *Organometallics* **2016**, *35*, 2391–2400.
- ³¹ John, A.; Hogan, L. T.; Hillmyer, M. A.; Tolman, W. B. Olefins from biomass feedstocks: catalytic ester decarbonylation and tandem Heck-type coupling. *Chem. Commun.* **2015**, *51*, 2731–2733.
- ³² John, A.; Dereli, B.; Ortuño, M. A.; Johnson, H. E.; Hillmyer, M. A.; Cramer, C. J.; Tolman, W. B. Selective Decarbonylation of Fatty Acid Esters to Linear α-Olefins. *Organometallics* **2017**, *36*, 2956–2964.
- ³³ Fieser, M. E.; Schimler, S. D.; Mitchell, L. A.; Wilborn, E. G.; John, A.; Hogan, L. T.; Benson, B.; LaPointe, A. M.; Tolman, W. B. Dual-catalytic decarbonylation of fatty acid methyl esters to form olefins. *Chem. Commun.* **2018**, *54*, 7669–7672.
- ³⁴ John, A.; Hillmyer, M. A.; Tolman, W. B. Anhydride-Additive-Free Nickel-Catalyzed Deoxygenation of Carboxylic Acids to Olefins. *Organometallics* **2017**, *36*, 506–509.
- ³⁵ Yee, G. M.; Hillmyer, M. A.; Tonks, I. A. Bioderived Acrylates from Alkyl Lactates via Pd-Catalyzed Hydroesterification. *ACS Sustainable Chem. Eng.* **2018**, *6*, 9579–9584.
- ³⁶Lowe, J. R.; Martello, M. T.; Tolman, W. B.; Hillmyer, M. A. Functional biorenewable polyesters from carvone-derived lactones. *Polym. Chem.* **2011**, *2*, 702–708.

- ³⁷ Xiong, M.; Schneiderman, D. K.; Bates, F. S.; Hillmyer, M. A.; Zhang, K. Scalable production of mechanically tunable block polymers from sugar. *Proc. Natl. Acad. Sci.* **2014**, *111*, 8357–8362.
- ³⁸ Trotta, J. T.; Jin, M.; Stawiasz, K. J.; Michaudel, Q.; Chen, W.-L.; Fors, B. P. Synthesis of Methylene Butyrolactone Polymers from Itaconic Acid. *J. Poly. Sci. Part A Polym. Chem.* **2017**, *55*, 2730–2737.
- ³⁹ Xu, S.; Wang, Y.; Hoye, T. R. Poly(4-ketovalerolactone) from Levulinic Acid: Synthesis and Hydrolytic Degradation. *Macromolecules* **2020**, *53*, 4952–4959.
- ⁴⁰ Kang, S.; Fu, J.; Zhang, G. From lignocellulosic biomass to levulinic acid: A review on acid-catalyzed hydrolysis. Renewable Sustainable Energy Rev. **2018**, *94*, 340–362.
- ⁴¹ Leal Silva, J. F.; Grekin, R.; Mariano, A. P.; Maciel Filho, R. Making levulinic acid and ethyl levulinate economically viable: a worldwide technoeconomic and environmental assessment of possible routes. Energy Technol. **2018**, *6*, 613–639.
- ⁴² Pileidis, F. D.; Titirici, M. M. Levulinic acid biorefineries: new challenges for efficient utilization of biomass. ChemSusChem **2016**, *9*, 562–582.
- ⁴³ Morone, A.; Apte, M.; Pandey, R. A. Levulinic acid production from renewable waste resources: bottlenecks, potential remedies, advancements and applications. Renewable Sustainable Energy Rev. **2015**, *51*, 548–565.
- ⁴⁴ Rackemann, D. W.; Doherty, W. O. The conversion of lignocellulosics to levulinic acid. Biofuels, Bioprod. Biorefin. **2011**, *5*, 198–214.
- ⁴⁵ Hayes, D. J.; Steve, F.; Hayes, M. H. B.; Ross, J. R. H. The Biofine process-production of levulinic acid, furfural, and formic acid from lignocellulosic feedstocks. In Biorefineries-Industrial Processes and Products: Status Quo and Future Directions; Kamm, B., Gruber, P. R., Kamm, M., Eds.; Wiley-VCH Verlag GmbH: Weinheim, Germany, 2008; pp 139–164.
- ⁴⁶ Bozell, J. J.; Moens, L.; Elliott, D. C.; Wang, Y.; Neuenscwander, G. G.; Fitzpatrick, S. W.; Bilski, R. J.; Jarnefeld, J. L. Production of levulinic acid and use as a platform chemical for derived products. Resour. Conserv. Recycl. **2000**, *28*, 227–239.
- ⁴⁷ Lundberg, D. J.; Lundberg, D. J.; Hillmyer, M. A.; Dauenhauer, P. J. Techno-economic Analysis of a Chemical Process to Manufacture Methyl-ε-caprolactone from Cresols. *ACS Sustainable Chem. Eng.* **2018**, *6*, 15316–15324.
- ⁴⁸ Batiste, D. C.; Meyersohn, M. S.; Watts, A.; Hillmyer, M. A. Efficient Polymerization of Methyl-ε-Caprolactone Mixtures To Access Sustainable Aliphatic Polyesters. *Macromolecules* **2020**, *53*, 1795–1808.
- ⁴⁹ Ding, R.; Du, Y.; Goncalves, R. B.; Francis, L. F.; Reineke, T. M. Sustainable near UV-curable acrylates based on natural phenolics for stereolithography 3D printing. *Polym. Chem.* **2019**, *10*, 1067–1077.
- ⁵⁰ Fonseca, L. R.; Dirlam, P. T.; Hillmyer, M. A. Atom-Economical, One-Pot, Self-Initiated Photopolymerization of Lactone Methacrylate for Biobased Hydrogels. *ACS Sustainable Chem. Eng.* **2020**, *8*, 4606–4613.
- ⁵¹ Dairy Products 2017 Summary; National Agricultural Statistics Service, United States Department of Agriculture: Washington, DC, 2018.
- ⁵² Nasiri, M.; Reineke, T. M. Sustainable glucose-based block copolymers exhibit elastomeric and adhesive behavior. *Polym. Chem.* **2016**, 7, 5233–5240.
- ⁵³ Shin, J.; Martello, M. T.; Shrestha, M.; Wissinger, J. E.; Tolman, W. B.; Hillmyer, M. A. Pressure-sensitive adhesives from renewable triblock copolymers. *Macromolecules* **2011**, *44*, 87–94.
- ⁵⁴ Cornforth, J. W.; Cornforth, R. H.; Popják, G.; Gore, I. Y. Studies on the biosynthesis of cholesterol. 5. Biosynthesis of squalene from DL-3-hydroxy-3-methyl-[2-¹⁴C] pentano-5-lactone. *Biochem. J.* **1958**, *69*, 146–155.
- ⁵⁵ Ball-Jones, N. R.; Fahnhorst, G. W.; Hoye, T. R. Poly(isoprenecarboxylates) from Glucose via Anhydromevalonolactone. *ACS Macro Lett.* **2016**, *5*, 1128–1131.
- ⁵⁶ Sajjad, H.; Tolman, W. B.; Reineke, T. M. Block Copolymer Pressure Sensitive Adhesives Derived From Fatty Acids and Triacetic Acid Lactone, *ACS Appl. Polym. Mater.* **2020**, *2*, 2719–2728.
- ⁵⁷ Noweck, K.; Grafahend, W. Fatty Alcohols. *Ullman's Encyclopedia of Industrial Chemistry*; John Wiley & Sons, Inc., 2006; Vol. *14*, pp 114–141.
- ⁵⁸ Wang, S.; Vajjala Kesava, S.; Gomez, E. D.; Robertson, M. L. Sustainable Thermoplastic Elastomers Derived from Fatty Acids. *Macromolecules* **2013**, *46*, 7202–7212.
- ⁵⁹ Xie, D.; Shao, Z.; Achkar, J.; Zha, W.; Frost, J. W.; Zhao, H. Microbial Synthesis of Triacetic Acid Lactone. *Biotechnol. Bioeng.* **2006**, *93*, 727–736.

- ⁶⁰ Goel, A.; Ram, V. J. Natural and Synthetic 2H-Pyran-2-Ones and Their Versatility in Organic Synthesis. *Tetrahedron* **2009**, *65*, 7865–7913.
- ⁶¹ Eckermann, S.; Schröder, G.; Schmidt, J.; Strack, D.; Edrada, R. A.; Helariutta, Y.; Elomaa, P.; Kotilainen, M.; Kilpeläinen, I.; Proksch, P.; Teeri, T. H.; Schröder, J. New Pathway to Polyketides in Plants. *Nature* **1998**, *396*, 387–390.
- ⁶² Collie, J. N. LVI.-The lactone of triacetic acid. J. Chem. Soc., Trans. 1891, 59, 607-617.
- ⁶³ Obydennov, D. L.; El-Tantawy, A. I.; Sosnovskikh, V. Y. Triacetic Acid Lactone as a Bioprivileged Molecule in Organic Synthesis. *Mendeleev Commun.* **2019**, *29*, 1–10.
- ⁶⁴ Shanks, B. H.; Keeling, P. L. Bioprivileged Molecules: Creating Value from Biomass. *Green Chem.* **2017**, *19*, 3177–3185.
- ⁶⁵ Saxon, D. J.; Luke, A. M.; Sajjad, H.; Tolman, W. B.; Reineke, T. M. Next-generation polymers: Isosorbide as a renewable alternative. *Prog. Polym. Sci.* **2020**, *101*, 101196.
- ⁶⁶ Sousa, A. F.; Vilela, C.; Matos, M.; Freire, C. S. R.; Silvestre, A. J. D.; Coelho, J. F. J. Polyethylene Terephthalate: Copolyesters, Composites, and Renewable Alternatives. *Poly(Ethylene Terephthalate) Based Blends, Composites and Nanocomposites* **2015**, 113–141.
- ⁶⁷ Shrotri, A.; Kobayashi, H.; Fukuoka, A. Chapter Two Catalytic Conversion of Structural Carbohydrates and Lignin to Chemicals. *Advances in Catalysis* **2017**, *60*, 59–123.
- ⁶⁸ Roquette launches 'world's largest' isosorbide production unit. Additives for Polymers 2015, 6, 8–9.
- ⁶⁹ Gallagher, J. J.; Hillmyer, M. A.; Reineke, T. M. Isosorbide-based Polymethacrylates. *ACS Sustainable Chem. Eng.* **2015**, *3*, 662–667.
- ⁷⁰ Gallagher, J. J.; Hillmyer, M. A.; Reineke, T. M. Acrylic Triblock Copolymers Incorporating Isosorbide for Pressure Sensitive Adhesives. *ACS Sustain. Chem. Eng.* **2016**, *4*, 3379–3387.
- ⁷¹ Shearouse, W. C.; Lillie, L. M.; Reineke, T. M.; Tolman, W. B. Sustainable Polyesters Derived from Glucose and Castor Oil: Building Block Structure Impacts Properties. *ACS Macro Lett.* **2015**, *4*, 284–288.
- ⁷² Wilbon, P. A.; Swartz, J. L.; Meltzer, N. R.; Brutman, J. P.; Hillmyer, M. A.; Wissinger, J. E. Degradable Thermosets Derived from an Isosorbide/Succinic Anhydride Monomer and Glycerol. *ACS Sustainable Chem. Eng.* **2017**, *5*, 9185–9190.
- ⁷³ Ma, S.; Webster, D. C.; Jabeen, F. Hard and Flexible, Degradable Thermosets from Renewable Bioresources with the Assistance of Water and Ethanol. *Macromolecules* **2016**, *49*, 3780–3788.
- ⁷⁴ Spanjers, C. S.; Schneiderman, D. K.; Wang, J. Z.; Wang, J.; Hillmyer, M. A.; Zhang, K.; Dauenhauer, P. J. Branched Diol Monomers from the Sequential Hydrogenation of Renewable Carboxylic Acids. *Chem. Cat. Chem.* **2016**, *8*, 3031–3035.
- ⁷⁵ Schneiderman, D. K.; Vanderlaan, M. E.; Mannion, A. M.; Panthani, T. R.; Batiste, D. C.; Wang, J. Z.; Bates, F. S.; Macosko, C. W.; Hillmyer, M. A. Chemically Recyclable Biobased Polyurethanes. *ACS Macro Lett.* **2016**, *5*, 515–518.
- ⁷⁶ Mcclintock, M. K.; Fahnhorst, G. W.; Hoye, T. R.; Zhang, K. Engineering the production of dipicolinic acid in E. coli. *Metab. Eng.* **2018**, *48*, 208–217.
- ⁷⁷ Blaisse, M. R.; Dong, H.; Fu, B.; Chang, M. C. Y. Discovery and Engineering of Pathways for Production of α-Branched Organic Acids. *J. Am. Chem. Soc* **2017**, *139*, 14526–14532.
- ⁷⁸ Watanabe, Y.; Ishizuka, K.; Furutate, S.; Abe, H.; Tsuge, T. Biosynthesis and characterization of novel poly(3-hydroxybutyrate-co-3-hydroxy-2-methylbutyrate): thermal behavior associated with α-carbon methylation. *RSC Adv.* **2015**, *5*, 58679–58685.
- ⁷⁹ Tijsma, E. J.; Does, L. V. D.; Bantjes, A.; Vulic, I. Synthesis, Structure, and Properties of Polymers Based on Pivalolactone. *J. Macromol. Sci.*, *Polym. Rev.* **1994**, *34*, 515–553.
- ⁸⁰ Cheng, C.; Watts, A.; Hillmyer, M. A.; Hartwig, J. F. Polysilylether: A Degradable Polymer from Biorenewable Feedstocks. *Angew. Chem., Int. Ed.* **2016**, *55*, 11872–11876.
- ⁸¹ Schneiderman, D. K.; Hillmyer, M. A. 50th Anniversary Perspective: There Is a Great Future in Sustainable Polymers. *Macromolecules*, **2017**, *50*, 3733–3749.
- ⁸² Stößer, T.; Williams, C. K. Selective Polymerization Catalysis from Monomer Mixtures: Using a Commercial Cr-Salen Catalyst To Access ABA Block Polyesters. *Angew. Chem., Int. Ed.* **2018**, *57*, 6337–6341.

- ⁸³ Paul, S.; Zhu, Y.; Romain, C.; Brooks, R.; Saini, P.K.; Williams, C.K. Ring-opening copolymerization (ROCOP): synthesis and properties of polyesters and polycarbonates. Chem. Commun. 2015, 51, 6459–6479.
- 84 Longo, J.M.; Sanford, M.J.; Coates, G.W. Ring-opening copolymerization of epoxides and cyclic anhydrides with discrete metal complexes: structure–property relationships. Chem. Rev. 2016, 116, 15167–15197.
- 85 O'Keefe, B.J.; Hillmyer, M.A.; Tolman, W.B. Polymerization of lactide and related cyclic esters by discrete metal complexes. J. Chem. Soc., Dalton Trans. 2001, 15, 2215-2224.
- ⁸⁶ Hillmyer, M.A.; Tolman, W.B. Aliphatic polyester block polymers: renewable, degradable, and sustainable. Acc. Chem. Res. 2014, 47, 2390-2396.
- 87 Knight, S.C.; Schaller, C.P.; Tolman, W.B.; Hillmyer, M.A. Renewable carvone-based polyols for use in polyurethane thermosets. *RSC Adv.* **2013**, *3*, 20399–20404.

 88 Childers, M.I.; Longo, J.M.; Van Zee, N.J.; LaPointe, A.M.; Coates, G.W. Stereoselective epoxide polymerization
- and copolymerization. Chem. Rev. 2014, 114, 8129-8152.
- ⁸⁹ Chen, Y.; Wilson, J. A.; Petersen, S. R.; Luong, D.; Sallam, S.; Mao, J.; Wesdemiotis, C.; Becker M. L. Ring-Opening Copolymerization of Maleic Anhydride with Functional Epoxides: Poly(propylene fumarate) Analogues Capable of Post-Polymerization Modification. *Angew. Chem., Int. Ed.* **2018**, *57*, 12759 –12764.
- ⁹⁰ Van Zee, N. J.; Coates, G. W. Alternating Copolymerization of Propylene Oxide with Biorenewable Terpene-Based Cyclic Anhydrides: A Sustainable Route to Aliphatic Polyesters with High Glass Transition Temperatures. Angew. Chem., Int. Ed. 2015, 54, 2665–2668.
- ⁹¹ Jing, F.; Hillmyer, M. A. A Bifunctional Monomer Derived from Lactide for Toughening Polylactide. J. Am. Chem. Soc. 2008, 130, 13826-13827.
- 92 Fiore, G. L.; Jing, F.; Young, J. V. G.; Cramer, C. J.; Hillmyer, M. A. High Tg aliphatic polyesters by the polymerization of spirolactide derivatives. *Polym. Chem.* **2010**, *I*, 870–877.

 ⁹³ Van Zee, N. J.; Sanford, M. J.; Coates, G. W. Electronic Effects of Aluminum Complexes in the Copolymerization
- of Propylene Oxide with Tricyclic Anhydrides: Access to Well Defined, Functionalizable Aliphatic Polyesters. J. Am. Chem. Soc. 2016, 138, 2755–2761.
- 94 Sanford, M. J.; Carrodeguas, L. P.; Van Zee N. L.; Kleij, A. W.; Coates G. W. Alternating Copolymerization of Propylene Oxide and Cyclohexene Oxide with Tricyclic Anhydrides: Access to Partially Renewable Aliphatic Polyesters with High Glass Transition Temperatures. *Macromolecules* **2016**, *49*, 6394–6400.
- 95 Winkler, M.; Romain, C.; Meier, M. A. R.; Williams, C. K. Renewable polycarbonates and polyesters from 1,4cyclohexadiene. Green Chem. 2015, 17, 300-306.
- 96 Whiteoak, C. J.; Gjoka, B.; Martin, E.; Belmonte, M. M.; Escudero-Adán, E. C.; Zonta, C.; Licini, G.; Kleij, A. W. Reactivity Control in Iron(III) Amino Triphenolate Complexes: Comparison of Monomeric and Dimeric Complexes. Inorg. Chem. 2012, 51, 10639-10649.
- 97 Saini, P. K.; Romain, C.; Zhu, Y.; Williams, C. K. Di-magnesium and zinc catalysts for the copolymerization of phthalic anhydride and cyclohexene oxide. Polym. Chem. 2014, 5, 6068-6075.
- 98 Zhu, Y.; Romain, C.; Williams, C. K. Selective Polymerization Catalysis: Controlling the Metal Chain End Group to Prepare Block Copolyesters. J. Am. Chem. Soc. 2015, 137, 12179–12182.
- 99 Sanford, M. J.; Van Zee, N. J.; Coates, G. W. Reversible-deactivation anionic alternating ring-opening copolymerization of epoxides and cyclic anhydrides: access to orthogonally functionalizable multiblock aliphatic polyesters. Chem. Sci. 2018, 9, 134-142.
- ¹⁰⁰ Inoue, S. Immortal polymerization: The outset, development, and application. J. Polym. Sci., Part A: Polym. Chem. **2000**, *38*, 2861–2871.
- 101 Fieser, M. E.; Sanford, M. J.; Mitchell, L. A.; Dunbar, C. R.; Mandal, M.; Van Zee, N. J.; Urness, D. M.; Cramer, C. J.; Coates, G. W.; Tolman, W. B. Mechanistic Insights into the Alternating Copolymerization of Epoxides and Cyclic Anhydrides Using a (Salph)AlCl and Iminium Salt Catalytic System. J. Am. Chem. Soc. 2017, 139, 15222-15231.
- ¹⁰² Abel, B.A.; Lidston, C.A.; Coates, G.W. Mechanism-Inspired Design of Bifunctional Catalysts for the Alternating Ring-Opening Copolymerization of Epoxides and Cyclic Anhydrides. J. Am. Chem. Soc. 2019, 141, 12760–12769.
- Noh, E. K.; Na, S. J.; S, S.; Kim, S.-W.; Lee, B. Y. Two Components in a Molecule: Highly Efficient and Thermally Robust Catalytic System for CO₂/Epoxide Copolymerization. J. Am. Chem. Soc. 2007, 129, 8082-8083.

- ¹⁰⁴ S, S.; Min, J. K.; Seong, J. E.; Na, S. J.; Lee, B. Y. A Highly Active and Recyclable Catalytic System for CO₂/Propylene Oxide Copolymerization. *Angew. Chem., Int. Ed.* **2008**, *47*, 7306–7309.
- ¹⁰⁵ Ren, W.-M; Liu, Z.-W.; Wen, Y.-Q.; Zhang, R.; Lu, X.-B. Mechanistic Aspects of Copolymerization of CO₂ with Epoxides Using a Thermally Stable Single-Site Cobalt(III) Catalyst. *J. Am. Chem. Soc.* **2009**, *131*, 11509–11518.
- ¹⁰⁶ Bandar, J. S.; Tanaset, A.; Lambert, T. H. Phase-Transfer Other Types of Catalysis with Cyclopropenium Ions. *Chem.-Eur. J.* **2015**, *21*, 7365–7368.
- ¹⁰⁷ Ren, W.-M.; Liu, Y.; Wu, G.-P.; Liu, J.; Lu, X.-B. Stereoregular Polycarbonate Synthesis: Alternating copolymerization of CO₂ with Aliphatic Terminal Epoxides Catalyzed by Multichiral Cobalt(III) Complexes. *J. Polym. Sci., Part A: Polym. Chem.* **2011**, *49*, 4894–4901.
- ¹⁰⁸ Liu, Y.; Zhou, H.,; Guo, J. Z.; Ren, W.M.; Lu, X. B. Completely recyclable monomers and polycarbonate: approach to sustainable polymers. *Angew. Chem., Int. Ed.* **2017**, *56*, 4862–4866
- ¹⁰⁹ Ellis, W.C.; Jung, Y.; Mulzer, M.; Di Girolamo, R.; Lobkovsky, E.B.; Coates, G.W. Copolymerization of CO₂ and meso epoxides using enantioselective β-diiminate catalysts: a route to highly isotactic polycarbonates. *Chem. Sci.* **2014**, *5*, 4004–4011.
- ¹¹⁰ Nozaki, K.; Nakano, K.; Hiyama, T. Optically Active Polycarbonates: Asymmetric Alternating Copolymerization of Cyclohexene Oxide and Carbon Dioxide. *J. Am. Chem. Soc.* **1999**, *121*, 11008–11009.
- ¹¹¹ Cheng, M.; Darling, N. A.; Lobkovsky, E. B.; Coates, G. W. Enantiomerically-Enriched Organic Reagents via Polymer Synthesis: Enantioselective Copolymerization of Cycloalkene Oxides and CO₂ Using Homogeneous, Zinc-Based Catalysts. *Chem. Commun.* **2000**, 2007–2008.
- ¹¹² Nakano, K.; Nozaki, K.; Hiyama, T. Asymmetric Alternating Copolymerization of Cyclohexene Oxide and CO₂ with Dimeric Zinc Complexes. *J. Am. Chem. Soc.* **2003**, *125*, 5501–5510.
- ¹¹³ Xiao, Y.; Wang, Z.; Ding, K. Copolymerization of Cyclohexene Oxide with CO₂ by Using Intramolecular Dinuclear Zinc Catalysts. *Chem. Eur. J.* **2005**, *11*, 3668–3678.
- ¹¹⁴ Abbina, S.; Du, G. Chiral Amido-Oxazolinate Zinc Complexes for Asymmetric Alternating Copolymerization of CO₂ and Cyclohexene Oxide. *Organometallics* **2012**, *31*, 7394–7403.
- ¹¹⁵ Cheng, M.; Lobkovsky, E. B.; Coates, G. W. Catalytic Reactions Involving C₁ Feedstocks: New High-Activity Zn(II)-Based Catalysts for the Alternating Copolymerization of Carbon Dioxide and Epoxides. *J. Am. Chem. Soc.* **1998**, *120*, 11018–11019.
- ¹¹⁶ Cheng, M.; Moore, D. R.; Reczek, J. J.; Chamberlain, B. M.; Lobkovsky, E. B.; Coates, G. W. Single-Site β-Diiminate Zinc Catalysts for the Alternating Copolymerization of CO₂ and Epoxides: Catalyst Synthesis and Unprecedented Polymerization Activity. *J. Am. Chem. Soc.* **2001**, *123*, 8738–8749.
- ¹¹⁷ Moore, D. R; Coates, G. W. Electronic and Steric Effects on Catalysts for CO₂/Epoxide Polymerization: Subtle Modifications Resulting in Superior Activities. *Angew. Chem., Int. Ed.* **2002**, *41*, 2599–2602.
- ¹¹⁸ Kim, J. G.; Cowman C. D.; LaPointe, A. M.; Wiesner, U.; Coates, G. W. Tailored Living Block Copolymerization: Multiblock Poly(cyclohexene carbonate)s with Sequence Control. *Macromolecules*, **2011**, *44*, 1110–1113.
- ¹¹⁹ Moore, D.R.; Cheng, M.; Lobkovsky, E.B.; Coates, G.W. Mechanism of the alternating copolymerization of epoxides and CO2 using β-diiminate zinc catalysts: evidence for a bimetallic epoxide enchainment. *J. Am. Chem. Soc.* **2003**, *125*, 11911–11924.
- ¹²⁰ Shao, H.; Reddi, Y.; Cramer C. J. Modeling the mechanism of CO₂/cyclohexene oxide copolymerization catalyzed by chiral zinc β-diiminates: factors affecting reactivity and isotacticity. *ACS Catal.* **2020**, *10*, 8870–8879.
- ¹²¹ Dechy-Cabaret, O.; Martin-Vaca, B.; Bourissou, D. Controlled ring-opening polymerization of lactide and glycolide. *Chem Rev.* **2004**, *104*, 6147–6176.
- Ding, K.; Miranda, M. O.; Moscato-Goodpaster, B.; Ajellal, N.; Breyfogle, L. E.; Hermes, E. D.; Schaller, C. P.; Roe, S. E.; Cramer, C. J.; Hillmyer, M. A.; Tolman, W. B. Roles of Monomer Binding and Alkoxide Nucleophilicity in Aluminum-Catalyzed Polymerization of ε-Caprolactone. *Macromolecules* **2012**, *45*, 5387–5396.
- ¹²³Miranda, M. O.; Deporre, Y.; Vazquez-Lima, H.; Johnson, M. A.; Marell, D. J.; Cramer, C. J.; Tolman, W. B. Understanding the Mechanism of Polymerization of ε-Caprolactone Catalyzed by Aluminum Salen Complexes. *Inorg. Chem.* **2013**, *52*, 13692–13701.
- ¹²⁴Marenich, A. V.; Jerome, S. V.; Cramer, C. J.; Truhlar, D. G. Charge Model 5: An Extension of Hirshfeld Population Analysis for the Accurate Description of Molecular Interactions in Gaseous and Condensed Phases. *J. Chem. Theory. Comput.* **2012**, *8*, 527–541

- ¹²⁵ Marlier, E. E.; Macaranas, J. A.; Marell, D. J.; Dunbar, C. R.; Johnson, M. A.; DePorre, Y.; Miranda, M. O.; Neisen, B. D.; Cramer, C. J.; Hillmyer, M. A.; Tolman, W. B. Mechanistic studies of ε-caprolactone polymerization by (salen) alor complexes and a predictive model for cyclic ester polymerizations. *ACS Catal.* **2016**, *6*, 1215–1224.
- ¹²⁶ Stasiw, D. E.; Mandal, M.; Neisen, B. D.; Mitchell, L. A.; Cramer, C. J.; Tolman, W. B. Why So Slow? Mechanistic Insights from Studies of a Poor Catalyst for Polymerization of ε-Caprolactone. *Inorg. Chem.* **2017**, *56*, 725–728.
- ¹²⁷ Huang, Y.-T.; Wang, W.-C.; Hsu, C.-P.; Lu, W.-Y.; Chuang, W.-J.; Chiang, M. Y.; Lai, Y.-C.; Chen, H.-Y. The ring-opening polymerization of ε-caprolactone and l-lactide using aluminum complexes bearing benzothiazole ligands as catalysts. *Polym. Chem.* **2016**, *7*, 4367–4377.
- ¹²⁸ Zhang, Y.; Gao, A.; Zhang, Y.; Xu, Z.; Yao, W. Aluminum complexes with benzoxazolphenolate ligands: Synthesis, characterization and catalytic properties for ring-opening polymerization of cyclic esters. *Polyhedron* **2016**, *112*, 27–33.
- ¹²⁹ Macaranas, J.A.; Luke, A.M.; Mandal, M.; Neisen, B.D.; Marell, D.J.; Cramer, C.J.; Tolman, W.B. Sterically Induced Ligand Framework Distortion Effects on Catalytic Cyclic Ester Polymerizations. *Inorg. Chem.* **2018**, *57*, 3451–3457.
- ¹³⁰ Mandal, M.; Luke, A. M.; Dereli, B.; Elwell, C. E.; Reineke, T. M.; Tolman, W. B.; Cramer, C. J. Computational Prediction and Experimental Verification of ε-Caprolactone Ring-Opening Polymerization Activity by an Aluminum Complex of an Indolide/Schiff-Base Ligand. *ACS Catal.* **2018**, *9*, 885–889.
- ¹³¹ Fahnhorst, G.W.; Stasiw, D.E.; Tolman, W.B.; Hoye, T.R. Isomerization of Linear to Hyperbranched Polymers: Two Isomeric Lactones Converge via Metastable Isostructural Polyesters to a Highly Branched Analogue. *ACS Macro Lett.* **2018**, *7*, 1144–1148.
- ¹³² Fahnhorst, G.W.; Hoye, T.R. A carbomethoxylated polyvalerolactone from malic acid: synthesis and divergent chemical recycling. *ACS Macro Lett.* **2018**, *7*, 143–147.
- ¹³³ Amador, A.G.; Watts, A.; Neitzel, A.E.; Hillmyer, M.A. Entropically driven macrolide polymerizations for the synthesis of aliphatic polyester copolymers using titanium isopropoxide. *Macromolecules* **2019**, 52, 2371-2383.
- ¹³⁴ Fox, T. G. Influence of Diluent and of Copolymer Composition on the Glass Temperature of a Polymer System. *Bull. Am. Phys. Soc.* **1956**, *1*, 123.
- ¹³⁵ Gurusamy-Thangavelu, S. A.; Emond, S. J.; Kulshrestha, A.; Hillmyer, M. A.; Macosko, C. W.; Tolman, W. B.; Hoye, T. R. Polyurethanes based on renewable polyols from bioderived lactones. *Polym. Chem.* **2012**, *3*, 2941–2948. ¹³⁶ Jensen, T. R.; Breyfogle, L. E.; Hillmyer, M. A.; Tolman, W. B. Stereoelective polymerization of D, L-lactide using N-heterocyclic carbene based compounds. *Chem. Commu.* **2004**, *21*, 2504–2505.
- ¹³⁷ Pietrangelo, A.; Hillmyer, M. A.; Tolman, W. B. Stereoselective and controlled polymerization of D,L-lactide using indium(iii) trichloride. *Chem. Commun.* **2009**, 2736–2737.
- ¹³⁸ Stasiw, D. E.; Luke, A. M.; Rosen, T.; League, A. B.; Mandal, M.; Neisen, B. D.; Mitchell, L. A.; Cramer, C. J.; Kol, M.; Tolman, W. B. Mechanism of the Polymerization of rac-Lactide by Fast Zinc Alkoxide Catalysts. *Inorg. Chem.* **2017**, *56*, 14366–14372.
- ¹³⁹ Luke, A.M.; Peterson, A.; Chiniforoush, S.; Mandal, M.; Popowski, Y.; Sajjad, H.; Bouchey, C.J.; Shopov, D.Y.; Graziano, B.J.; Yao, L.J.; Cramer, C.J. Mechanism of Initiation Stereocontrol in Polymerization of rac-Lactide by Aluminum Complexes Supported by Indolide–Imine Ligands. *Macromolecules* **2020**, *53*, 1809–1818.
- ¹⁴⁰ Ahmed, S.M.; Poater, A.; Childers, M.I.; Widger, P.C.B.; LaPointe, A.M.; Lobkovsky, E.B.; Coates, G.W, Cavallo, L. Enantioselective Polymerization of Epoxides Using Biaryl-Linked Bimetallic Cobalt Catalysts: A Mechanistic Study. *J. Am. Chem. Soc.* 2013, *135*, 18901–18911.
- ¹⁴¹ Lillie, L.M.; Tolman, W.B.; Reineke, T.M. Structure/property relationships in copolymers comprising renewable isosorbide, glucarodilactone, and 2, 5-bis (hydroxymethyl) furan subunits. *Polym. Chem.* **2017**, *8*, 3746–3754.
- ¹⁴² Kim, S. S., Lau, C. M., Lillie, L. M., Tolman, W. B., Reineke, T. M., Ellison, C. J. Degradable Thermoset Fibers from Carbohydrate-Derived Diols via Thiol-ene Photopolymerization, *ACS Appl. Polym. Mater.* **2019**, *1*, 2933–2942
- ¹⁴³ Strietholt, W.A.; Thiem, J.; Howele , U.F. Synthesis and ring-opening polymerization of 1, 4: 2, 5: 3, 6-trianhydro-d-mannitol and structure studies by MNDO calculations. *Die Makromolekulare Chemie* **1991**, *192*, 317–331.
- ¹⁴⁴ Saxon, D. J.; Nasiri, M.; Mandal, M.; Maduskar, S.; Dauenhauer, P. J.; Cramer, C. J.; LaPointe, A. M.; Reineke, T. M. Architectural Control of Isosorbide-Based Polyethers via Ring-Opening Polymerization. *J. Am. Chem. Soc.* **2019**, *141*, 5107–5111.

- ¹⁴⁵ Penczek, S. Cationic ring-opening polymerization (CROP) major mechanistic phenomena. *J. Polym. Sci. Pol. Chem.* **2000**, *38*, 1919–1933.
- ¹⁴⁶ Schneiderman, D. K.; Ting, J. M.; Purchel, A. A.; Miranda Jr., R.; Tirrell, M. V.; Reineke, T. M.; Rowan, S. J. Open-to-air RAFT polymerization in complex solvents: from whisky to fermentation broth. *ACS Macro Lett.* **2018**, *7*, 406–411.
- ¹⁴⁷ Thuronyi, B. W.; Privalsky, T. M.; Chang, M. C. Y. Engineered Fluorine Metabolism and Fluoropolymer Production in Living Cells. *Angew. Chem., Int. Ed.* **2017**, *56*, 13637–13640.
- ¹⁴⁸ Matsen, M. W.; Thompson, R. B. Equilibrium Behavior of Symmetric ABA Triblock Copolymer Melts. *J. Chem. Phys.* **1999**, *111*, 7139–7146.
- ¹⁴⁹ Holden, G.; Kricheldorf, H. R.; Quirk, R. P. *Thermoplastic Elastomers*, 3rd ed.; Holden, G., Kricheldorf, H. R., Quirk, R. P., Eds.; Hanser Gardner Publications, Inc.: Cincinnati, 2004.
- ¹⁵⁰ Watts, A.; Kurokawa, N.; Hillmyer, M. A. Strong, Resilient, and Sustainable Aliphatic Polyester Thermoplastic Elastomers. *Biomacromolecules* **2017**, *18*, 1845–1854.
- ¹⁵¹ Han, C. D.; Kim, J.; Kim, J. K. Determination of the Order—Disorder Transition Temperature of Block Copolymers. *Macromolecules* **1989**, *22*, 383–394.
- ¹⁵² Reisch, M. S. Thermoplastic Elastomers Target Rubber And Plastics Markets. *Chemical & Engineering News*. August 1996, pp 10–14.
- 153 Kraton Corporation. Kraton Corporation http://kraton.com/ (accessed Sep 12, 2018).
- ¹⁵⁴ Groot, W.; van Krieken, J.; Sliekersl, O.; de Vos, S. Production and Purification of Lactic Acid and Lactide. In Poly(Lactic Acid): Synthesis, Structures, Properties, Processing, and Application; Auras, R., Lim, L.-K., Selke, S. E. M., Tsuji, H., Eds.; John Wiley & Sons, Inc.: Hoboken, NJ, 2010.
- ¹⁵⁵ Martello, M. T.; Hillmyer, M. A. Polylactide-Poly(6-Methyl-ε-Caprolactone)-Polylactide Thermoplastic Elastomers. *Macromolecules* **2011**, *44*, 8537–8545.
- ¹⁵⁶ Martello, M. T.; Schneiderman, D. K.; Hillmyer, M. A. Synthesis and Melt Processing of Sustainable Poly(ε-Decalactone)-Block-Poly(Lactide) Multiblock Thermoplastic Elastomers. *ACS Sustain. Chem. Eng.* **2014**, *2*, 2519–2526.
- 157 Schneiderman, D. K.; Hill, E. M.; Martello, M. T.; Hillmyer, M. A. Poly(Lactide)-Block-Poly(ε-Caprolactone-Co-ε-Decalactone)-Block-Poly(Lactide) Copolymer Elastomers. *Polym. Chem.* **2015**, *6*, 3641–3651.
- ¹⁵⁸ Watts, A.; Hillmyer, M. A. Aliphatic Polyester Thermoplastic Elastomers Containing Hydrogen-Bonding Ureidopyrimidinone Endgroups. *Biomacromolecules* **2019**, *20*, 2598–2609.
- ¹⁵⁹ Kim, H. J.; Jin, K.; Shim, J.; Dean, W.; Hillmyer, M. A.; Ellison, C. J. Sustainable Triblock Copolymers as Tunable and Degradable Pressure Sensitive Adhesives. *ACS Sustain. Chem. Eng.* **2020**, *8*, 12036-12044.
- ¹⁶⁰ Ding, K.; John, A.; Shin, J.; Lee, Y.; Quinn, T.; Tolman, W. B.; Hillmyer, M. A. High-Performance Pressure-Sensitive Adhesives from Renewable Triblock Copolymers. *Biomacromolecules* **2015**, *16*, 2537–2539.
- ¹⁶¹ Muro, T.; Takeda, M. US Patent 5059487, **1991**.
- ¹⁶² Nasiri, M.; Saxon, D.; Reineke, T. M. Enhanced Mechanical and Adhesion Properties in Sustainable Triblock Copolymers via Non-covalent Interactions. *Macromolecules* **2018**, *51*, 2456–2465.
- ¹⁶³ Spencer, R. K. W.; Matsen, M. W. Domain Bridging in Thermoplastic Elastomers of Star Block Copolymer. *Macromolecules* **2017**, *50*, 1681–1687.
- ¹⁶⁴Roberge, D. M.; Buhl, D.; Niederer, J. P.; Hölderich, W. F. Catalytic Aspects in the Transformation of Pinenes to p-Cymene. *Appl. Catal. A Gen.* **2001**, *215*, 111–124.
- ¹⁶⁵ Linnekoski, J. A.; Asikainen, M.; Heikkinen, H.; Kaila, R. K.; Räsänen, J.; Laitinen, A.; Harlin, A. Production of p-Cymene from Crude Sulphate Turpentine with Commercial Zeolite Catalyst Using a Continuous Fixed Bed Reactor. *Org. Process Res. Dev.* **2014**, *18*, 1468–1475.
- ¹⁶⁶ Geyer, R.; Jambeck, J. R.; Law, K. L. Production, use, and fate of all plastics ever made. *Science Advances* **2017**, *3*, e1700782.
- ¹⁶⁷ Ruzette, A.-V.; Leibler, L. Block copolymers in tomorrow's plastics. *Nat. Mater.* **2005**, *4*, 19–31.
- ¹⁶⁸ Bates, F. S.; Hillmyer, M. A.; Lodge, T. P.; Bates, C. M.; Delaney, K. T.; Fredrickson, G. H. Multiblock polymers: Panacea or Pandora's box? *Science* **2012**, *336*, 434–440.
- ¹⁶⁹ Dealy, J. M.; Read, D. J.; Larson, R. G.: Structure and Rheology of Molten Polymers From Structure to Flow Behavior and Back Again. 2nd ed.; Hanser Publishers.

- ¹⁷⁰ Lohse, D. J.; Milner, S. T.; Fetters, L. J.; Xenidou, M.; Hadjichristidis, N.; Mendelson, R. A.; García-Franco, C. A.; Lyon, M. K. Well-Defined, Model Long Chain Branched Polyethylene. 2. Melt Rheological Behavior. *Macromolecules* **2002**, *35*, 3066–3075.
- ¹⁷¹ Lim, L. S.; Harada, T.; Hillmyer, M. A.; Bates, F. S. High Strength Polyolefin Block Copolymers. *Macromolecules* **2004**, *37*, 5847–5850.
- ¹⁷² Childers, C. W.; Kraus, G. Properties of Random and Block Copolymers of Butadiene and Styrene. III. Three Sequence Styrene-Butadiene-Styrene Block Polymers. *Rubber Chem. Technol.* **1967**, *40*, 1183–1199.
- ¹⁷³ Hermel, T. J.; Hahn, S. F.; Chaffin, K. A.; Gerberich, W. W.; Bates, F. S. Role of Molecular Architecture in Mechanical Failure of Glassy/Semicrystalline Block Copolymers: CEC vs CECEC Lamellae. *Macromolecules* **2003**, *36*, 2190–2193.
- ¹⁷⁴ Lee, I.; Panthani, T. R.; Bates, F. S. Sustainable Poly(lactide-b-butadiene) Multiblock Copolymers with Enhanced Mechanical Properties. *Macromolecules* **2013**, *46*, 7387–7398.
- Panthani, T. R.; Bates, F. S. Crystallization and Mechanical Properties of Poly(l-lactide)-Based Rubbery/Semicrystalline Multiblock Copolymers. *Macromolecules* **2015**, *48*, 4529–4540.
- ¹⁷⁶ Cochran, E. W.; Morse, D. C.; Bates, F. S. Design of ABC triblock copolymers near the ODT with the random phase approximation. *Macromolecules* **2003**, *36*, 782–792.
- ¹⁷⁷ Zhang, J.; Li, T.; Mannion, A. M.; Schneiderman, D. K.; Hillmyer, M. A.; Bates, F. S. Tough and Sustainable Graft Block Copolymer Thermoplastics. *ACS Macro Letters* **2016**, *5*, 407–412.
- ¹⁷⁸ Maher, M. J.; Jones, S. D.; Zografos, A.; Xu, J.; Schibur, H. J.; Bates, F. S. The Order–Disorder Transition in Graft Block Copolymers. *Macromolecules* **2018**, *51*, 232–241.
- ¹⁷⁹ Zhang, J.; Schneiderman, D. K.; Li, T.; Hillmyer, M. A.; Bates, F. S. Design of Graft Block Polymer Thermoplastics. *Macromolecules* **2016**, *49*, 9108–9118.
- ¹⁸⁰ Mannion, A. M.; Bates, F. S.; Macosko, C. W. Synthesis and Rheology of Branched Multiblock Polymers Based on Polylactide. *Macromolecules* **2016**, *49*, 4587–4598.
- ¹⁸¹ Haugan, I. N.; Maher, M. J.; Chang, A. B.; Lin, T.-P.; Grubbs, R. H.; Hillmyer, M. A.; Bates, F. S. Consequences of Grafting Density on the Linear Viscoelastic Behavior of Graft Polymers. *ACS Macro Letters* **2018**, *7*, 525.
- ¹⁸² Haugan, I. N.; Lee, B.; Maher, M. J.; Zografos, A.; Schibur, H. J.; Jones, S. D.; Hillmyer, M. A.; Bates, F. S. Physical Aging of Polylactide-Based Graft Block Polymers. *Macromolecules* **2019**, *52*, 8878–8894.
- ¹⁸³ Aeschelmann, F.; Carus, M. Biobased Building Blocks and Polymers in the World: Capacities, Production, and Applications–Status Quo and Trends Towards 2020. *Industr. Biotechnol.* **2015**, *11*, 154–159.
- ¹⁸⁴ Sudesh, K.; Iwata, T. Sustainability of Biobased and Biodegradable Plastics. *CLEAN Soil, Air, Water* **2008**, *36*, 433–442.
- ¹⁸⁵ Haider, T.; Völker, C.; Kramm, J.; Landfester, K.; Wurm, F. R. Plastics of the future? The impact of biodegradable polymers on the environment and on society. *Angew. Chem., Int. Ed.* **2019**, *58*, 50.
- polymers on the environment and on society. *Angew. Chem., Int. Ed.* **2019**, *58*, 50.

 186 Lipinski, B. M.; Morris, L. S.; Silberstein, M. N.; Coates, G. W. Isotactic Poly(Propylene Oxide): A Photodegradable Polymer with Strain Hardening Properties. *J. Am. Chem. Soc.* **2020**, *142*, 6800–6806.
- ¹⁸⁷ Widger, P. C. B.; Ahmed, S. M.; Coates, G. W. Exploration of Cocatalyst Effects on a Bimetallic Cobalt Catalyst System: Enhanced Activity and Enantioselectivity in Epoxide Polymerization. *Macromolecules* **2011**, *44* (14), 5666–5670.
- ¹⁸⁸ Childers, M. I.; Vitek, A. K.; Morris, L. S.; Widger, P. C. B.; Ahmed, S. M.; Zimmerman, P. M.; Coates, G. W. Isospecific, Chain Shuttling Polymerization of Propylene Oxide Using a Bimetallic Chromium Catalyst: A New Route to Semicrystalline Polyols. *J. Am. Chem. Soc.* **2017**, *139* (32), 11048–11054.
- ¹⁸⁹ Kawai, F. Microbial Degradation of Polyethers. *Appl. Microbiol. Biotechnol.* **2002**, *58* (1), 30–38 DOI: 10.1007/s00253-001-0850-2.
- ¹⁹⁰ Fahnhorst, G. W.; De Hoe, G. X.; Hillmyer, M. A.; Hoye, T. R. 4-Carboalkoxylated Polyvalerolactones from Malic Acid: Tough and Degradable Polyesters. *Macromolecules* **2020** DOI: 10.1021/acs.macromol.0c00212.
- ¹⁹¹ Yu, X.; Jia, J.; Xu S.; Lao, K. U.; Sanford, M. J.; Ramakrishnan, R. K.; Nazarenko, S. I.; Hoye, T. R.; Coates, G. W.; DiStasio Jr, R. A. Unraveling substituent effects on the glass transition temperatures of biorenewable polyesters. *Nat. Commun.* **2018**, *9*, 2880.
- ¹⁹² Dlubek, G.; Bamford, D.; Rodriguez-Gonzalez, A.; Bornemann, S.; Stejny, J.; Schade, B.; Alam, M. A.; Arnold, M.

- Free volume, glass transition, and degree of branching in metallocene-based propylene/alpha-olefin copolymers: positron lifetime, density, and differential scanning calorimetric studies. *J. Polym. Sci. B.* **2002**, *40*, 434–453.
- ¹⁹³ Kilburn, D.; Dlubek, G.; Pionteck, J.; Alam, M. A. Free volume in poly (nalkyl methacrylate)s from positron lifetime and PVT experiments and its relation to the structural relaxation. *Polymer* **2006**, 47, 7774–7785.
- ¹⁹⁴ Odian, G. Principles of Polymerization 4th edn, John Wiley & Sons Inc., Hoboken, NJ, 2004.
- ¹⁹⁵ Xu, Z., Hadjichristidis, N., Fetters, L. J.; Mays, J. W. Physical Properties of Polymers. Springer, Heidelberg, 1995.
- ¹⁹⁶ Hristov, H.; Bolan, B.; Yee, A.; Xie, L.; Gidley, D. Measurement of Hole Volume in Amorphous Polymers Using Positron Spectroscopy. *Macromolecules* **1996**, *29* (26), 8507-8516.
- ¹⁹⁷ White, R. and Lipson, J. Free Volume in the Melt and How It Correlates with Experimental Glass Transition Temperatures: Results for a Large Set of Polymers. *ACS Macro Lett.* **2015**, *4* (5), 588-592.
- ¹⁹⁸ Zhang, Q.; Molenda, M.; Reineke, T. M. Epoxy resin thermosets derived from trehalose and β-cyclodextrin. *Macromolecules* **2016**, *49*, 8397–8406.
- ¹⁹⁹ Zhang, Q.; Phillips, H. R.; Purchel, A.; Hexum, J. K.; Reineke, T. M. Sustainable and Degradable Epoxy Resins from Trehalose, Cyclodextrin, and Soybean Oil Yield Tunable Mechanical Performance and Cell Adhesion. *ACS Sustain. Chem. Eng.* **2018**, *6* (11), 14967–14978.
- ²⁰⁰ Petrović, Z. S., Polyurethanes from Vegetable Oils. *Polymer Reviews* **2008**, 48 (1), 109-155.
- ²⁰¹ P. Krol, Linear Polyurethanes: Synthesis Methods, Chemical Structures, Properties and Applications, VSP, Boston, 2008
- ²⁰² Oprea, S. The effect of chain extenders structure on properties of new polyurethane elastomers. *Polym. Bull.* **2010**, *65*, 753–766 (2010).
- ²⁰³ Vlad, S.; Cristea, M.; Ciobanu, C.; Macocinschi, D.; Filip, D.; Nistor, A.; Gradinaru, L. M. *J. Optoelectron. Adv. Mater.* **2010**, *12*, 2278–2287
- ²⁰⁴ C. Prisacariu, E. Scortanu and V. A. Prisacariu, Rev. Roum. Chim. **2011**, *56*, 425–431.
- ²⁰⁵ Kojio, K.; Furukawa, M.; Nonaka, Y.; Nakamura, S. Control of Mechanical Properties of Thermoplastic Polyurethane Elastomers by Restriction of Crystallization of Soft Segment. *Materials* **2010**, *3*, 5097–5110
- ²⁰⁶ Oprea, S. Synthesis and characterization of linear and crosslinked poly(urethane urea) elastomers with triazine moieties in the main chain. *Polym. Bull.* **2012**, *68*, 1271–1285.
- ²⁰⁷ Campos, L. M.; Killops, K. L.; Sakai, R.; Paulusse, J. M. J.; Damiron, D.; Drockenmuller, E.; Messmore, B. W.; Hawker, C. J. Development of Thermal and Photochemical Strategies for Thiol–Ene Click Polymer Functionalization, *Macromolecules* **2008**, *41*, 7063–7070.
- ²⁰⁸ Trotta, J. T.; Watts, A.; Wong, A. R.; Lapointe, A. M.; Hillmyer, M. A.; Fors, B. P. Renewable Thermosets and Thermoplastics from Itaconic Acid. *ACS Sustain. Chem. Eng.* **2019**, *7*, 2691–2701...
- ²⁰⁹ Brutman, J. P.; De Hoe, G. X.; Schneiderman, D. K.; Le, T. N.; Hillmyer, M. A. Renewable, Degradable, and Chemically Recyclable Cross-Linked Elastomers. *Ind. Eng. Chem. Res.* **2016**, *55*, 11097–11106.
- ²¹⁰ De Hoe, G. X.; Zumstein, M. T.; Tiegs, B. J.; Brutman, J. P.; McNeill, K.; Sander, M.; Coates, G. W.; Hillmyer, M. A. Sustainable Polyester Elastomers from Lactones: Synthesis, Properties, and Enzymatic Hydrolyzability. *J. Am. Chem. Soc.* **2018**, *140*, 963–973.
- ²¹¹ Schutyser, W.; Van Den Bosch, S.; Dijkmans, J.; Turner, S.; Meledina, M.; Van Tendeloo, G.; Debecker, D. P.; Sels, B. F. Selective Nickel-Catalyzed Conversion of Model and Lignin-Derived Phenolic Compounds to CyclohexanoneBased Polymer Building Blocks, *Chem. Sus. Chem.* **2015**, *8*, 1805–1818.
- ²¹² Klemes, M. J.; Ling, Y.; Chiapasco, M.; Alsbaiee, A.; Helbling, D. E.; Dichtel, W. R. Phenolation of Cyclodextrin Polymers Controls Their Lead and Organic Micropollutant Adsorption. *Chem. Sci.* **2018**, *9*, 8883–8889.
- ²¹³ Klemes, M. J.; Ling, Y.; Ching, C.; Wu, C.; Xiao, L.; Helbling, D. E.; Dichtel, W. R. Reduction of a Tetrafluoroterephthalonitrile-β-Cyclodextrin Polymer to Remove Anionic Micropollutants and Perfluorinated Alkyl Substances from Water. *Angew. Chem., Int. Ed.* **2019**, *58*, 12049–12053.
- ²¹⁴ Alsbaiee, A.; Smith, B. J.; Xiao, L.; Ling, Y.; Helbling, D. E.; Dichtel, W. R. Rapid Removal of Organic Micropollutants from Water by a Porous β-Cyclodextrin Polymer. *Nature* **2016**, *529*, 190–194.
- ²¹⁵ Xiao, L.; Ling, Y.; Alsbaiee, A.; Li, C.; Helbling, D. E.; Dichtel, W. R. β-Cyclodextrin Polymer Network Sequesters Perfluorooctanoic Acid at Environmentally Relevant Concentrations. *J. Am. Chem. Soc.* **2017**, *139*, 7689–7692.

- ²¹⁶ Xiao, L.; Ching, C.; Ling, Y.; Nasiri, M.; J. Klemes, M.; M. Reineke, T.; E. Helbling, D.; R. Dichtel, W. Cross-Linker Chemistry Determines the Uptake Potential of Perfluorinated Alkyl Substances by β-Cyclodextrin Polymers. *Macromolecules* **2019**, *52*, 3747–3752.
- ²¹⁷ Alzate-Sánchez, D. M.; Ling, Y.; Li, C.; P. Frank, B.; Bleher, R.; Howard Fairbrother, D.; E. Helbling, D.; R. Dichtel, W. β-Cyclodextrin Polymers on Microcrystalline Cellulose as a Granular Media for Organic Micropollutant Removal from Water. *ACS Appl. Mater. & Comp. Interfaces* **2019**, *11*, 8089–8096.
- ²¹⁸ Cyclopure. https://cyclopure.com/ (accessed 2020-12-20).
- ²¹⁹ Tokiwa, Y.; Calabia, B. P.; Ugwu, C. U.; Aiba, S. Biodegradability of Plastics. *Int. J. Mol. Sci.* **2009**, *10*, 3722–3742.
- ²²⁰ Woodward, L. N.; Grunlan, M. A. Hydrolytic Degradation and Erosion of Polyester Biomaterials. *ACS Macro Lett.* **2018**, *7*, 976.
- ²²¹ Xiong, M.; Schneiderman, D. K.; Bates, F. S.; Hillmyer, M. A.; Zhang, K. Scalable Production of Mechanically Tunable Block Polymers from Sugar. *Proc. Natl. Acad. Sci. U. S. A.* **2014**, *111*, 8357–8362.
- ²²² Yang, W.; Dong, Q.; Liu, S.; Xie, H.; Liu, L.; Li, J. Recycling and Disposal Methods for Polyurethane Foam Wastes. *Procedia Environ. Sci.* **2012**, *16*, 167–175.
- ²²³ Al-Salem, S. M.; Lettieri, P.; Baeyens, J. Recycling and Recovery Routes of Plastic Solid Waste (PSW): A Review. *Waste Management*. October 2009, pp 2625–2643.
- ²²⁴ Starkweather, H. W.; Zoller, P.; Jones, G. A. The Heat of Fusion of Poly(Ethylene Terephthalate). *J. Polym. Sci. Polym. Phys. Ed.* **1983**, *21*, 295–299.
- ²²⁵ Yui, N.; Ooya, T. Biodegradable Polymers. In *Supramolecular Design for Biological Applications*; 2002; Vol. 23, pp 169–190. https://doi.org/10.1201/9781420041187.sec2.
- ²²⁶ Tokiwa, Y.; Suzuki, T. Hydrolysis of Polyesters by Lipases. *Nature* **1977**, 270, 76–78.
- ²²⁷ Tang, D.; Chen, Z.; Correa-Netto, F.; Macosko, C. W.; Hillmyer, M. A.; Zhang, G. Poly(Urea Ester): A Family of Biodegradable Polymers with High Melting Temperatures. *J. Polym. Sci. Part A Polym. Chem.* **2016**, *54*, 3795–3799.
- ²²⁸ Albertsson, A. C.; Varma, I. K. Aliphatic Polyesters: Synthesis, Properties and Applications. In *Advances in Polymer Science*; Springer, Berlin, Heidelberg, 2002; Vol. 157, pp 1–40. https://doi.org/10.1007/3-540-45734-8_1.
- ²²⁹ Kim, H. J.; Reddi, Y.; Cramer, C. J.; Hillmyer, M. A.; Ellison, C. J. Readily Degradable Aromatic Polyesters from Salicylic Acid. *ACS Macro Letters* **2020**, *9*, 96-102.
- ²³⁰ Neitzel, A. E.; Barreda, L.; Trotta, J. T.; Fahnhorst, G. W.; Haversang, T. J.; Hoye, T. R.; Fors, B. P.; Hillmyer, M. A. Hydrolytically-Degradable Homo- and Copolymers of a Strained Exocyclic Hemiacetal Ester. *Polym. Chem.* **2019**, *10*, 4573–4583.
- ²³¹ Murphy, C. A.; Cameron, J. A.; Huang, S. J.; Vinopal, R. T. Fusarium polycaprolactone depolymerase is cutinase. Appl. Environ. Microbiol. 1996, 62, 456–460.
- ²³² Gallagher, J. J.; Hillmyer, M. A.; Reineke, T. M. Degradable Thermosets from Sugar-Derived Dilactones. *Macromolecules* **2014**, *47*, 498–505.
- ²³³ Hashimoto, K.; Wibullcksanakul, S.; Okada, M. Macromolecular Synthesis from Saccharic Lactones. Polyaddition of D-glucaro- and D-mannaro- 1,4:6, 3-dilactones with Diisocyanates and Hydrolyzability of the Resulting Polyurethanes Having Dilactone Rings in the Main Chains. *J. Polym. Sci., Part A: Polym. Chem.* **1995**, *33*, 1495–1503.
- ²³⁴ Lillie, L. M.; Tolman, W. B.; Reineke, T. M. Degradable and Renewably-Sourced Poly(ester-thioethers) by Photo-initiated Thiol-ene Polymerization. *Polym. Chem.* **2018**, *9*, 3272–3278.
- ²³⁵ Ajji, A.; Utracki, L. A. Interphase and Compatibilization of Polymer Blends. **1996**, 36 (12), 1574–1585.
- ²³⁶ Kaiser, K.; Schmid, M.; Schlummer, M. Recycling of Polymer-Based Multilayer Packaging: A Review. *Recycling* **2017**, *3*, 1.
- ²³⁷ Todd, A. D.; McEneany, R. J.; Topolkaraev, V. A.; Macosko, C. W.; Hillmyer, M. A. Reactive Compatibilization of Poly(Ethylene Terephthalate) and High-Density Polyethylene Using Amino-Telechelic Polyethylene. *Macromolecules* **2016**, *49*, 8988–8994.
- ²³⁸ Eagan, J. M.; Xu, J.; Di Girolamo, R.; Thurber, C. M.; Macosko, C. W.; La Pointe, A. M.; Bates, F. S.; Coates, G. W. Combining Polyethylene and Polypropylene: Enhanced Performance with PE/IPP Multiblock Polymers. *Science* **2017**, *355*, 814–816.
- ²³⁹ Xu, J.; Eagan, J. M.; Kim, S. S.; Pan, S.; Lee, B.; Klimovica, K.; Jin, K.; Lin, T. W.; Howard, M. J.; Ellison, C. J.;

- LaPointe, A. M.; Coates, G, W.; Bates, F, S. Compatibilization of Isotactic Polypropylene (*i*PP) and High-Density Polyethylene (HDPE) with *i*PP-PE Multiblock Copolymers. *Macromolecules* **2018**, *51*, 8585–8596.
- ²⁴⁰ Nomura, K.; Peng, X.; Kim, H.; Jin, K.; Kim, H. J.; Bratton, A. F.; Bond, C. R.; Broman, A. E.; Miller, K. M.; Ellison, C. J. Multiblock Copolymers for Recycling Polyethylene–Poly(Ethylene Terephthalate) Mixed Waste. *ACS Appl. Mater. Interfaces* **2020**, *12*, 9726–9735.
- American Chemistry Council. U.S. Resin Production and Sales, May 2020; https://plastics.americanchemistry.com/Year-End-Resin-Stats.pdf
- ²⁴² Fortman, D. J.; Brutman, J. P.; De Hoe, G. X.; Snyder, R. L.; Dichtel, W. R.; Hillmyer, M. A. Approaches to Sustainable and Continually Recyclable Cross-Linked Polymers. *ACS Sustain. Chem. Eng.* **2018**, *6*, 11145–11159.
- ²⁴³ Chakma, P.; Konkolewicz, D. Dynamic Covalent Bonds in Polymeric Materials. *Angew. Chem., Int. Ed.* **2019**, *58*, 9682–9695.
- ²⁴⁴ Scheutz, G. M.; Lessard, J. J.; Sims, M. B.; Sumerlin, B. S. Adaptable Crosslinks in Polymeric Materials: Resolving the Intersection of Thermoplastics and Thermosets. *J. Am. Chem. Soc.* **2019**, *141*, 16181–16196.
- ²⁴⁵ A recent review: Winne, J. M.; Leibler, L.; Du Prez, F. E. Dynamic Covalent Chemistry in Polymer Networks: A Mechanistic Perspective. *Polym. Chem.* **2019**, *10*, 6091–6108.
- ²⁴⁶ Fortman, D. J.; Brutman, J. P.; Cramer, C. J.; Hillmyer, M. A.; Dichtel, W. R. Mechanically Activated, Catalyst-Free Polyhydroxyurethane Vitrimers. *J. Am. Chem. Soc.* **2015**, *137*, 14019–14022.
- ²⁴⁷ Fortman, D. J.; Brutman, J. P.; Hillmyer, M. A.; Dichtel, W. R. Structural effects on the reprocessability and stress relaxation of crosslinked polyhydroxyurethanes. *J. Appl. Polym. Sci.* **2017**, *134*, 44984–44994.
- ²⁴⁸ Brutman, J. P.; Fortman, D. J.; De Hoe, G. X.; Dichtel, W. R.; Hillmyer, M. A. Mechanistic Study of Stress Relaxation in Urethane-Containing Polymer Networks. *J. Phys. Chem. B* **2019**, *123*, 1432–1441.
- ²⁴⁹ Brutman, J. P.; Delgado, P. A.; Hillmyer, M. A. Polylactide Vitrimers. ACS Macro Lett. **2014**, *3*, 607–610.
- ²⁵⁰ Yu, Y.; Storti, G.; Morbidelli, M. Kinetics of Ring-Opening Polymerization of L,L-Lactide. *Ind. Eng. Chem. Res.* **2011**, *50*, 7927–7940.
- ²⁵¹ Zheng, N.; Fang, Z.; Zou, W.; Zhao, Q.; Xie, T. Thermoset Shape-Memory Polyurethane with Intrinsic Plasticity Enabled by Transcarbamoylation. *Angew. Chem., Int. Ed.* **2016**, *55*, 11421–11425...
- ²⁵² Heo, Y.; Sodano, H. A. Self-Healing Polyurethanes with Shape Recovery. *Adv. Funct. Mater.* **2014**, *24*, 5261–5268.
- ²⁵³ Offenbach, J. A.; Tobolsky, A. V. Chemical Relaxation of Stress in Polyurethane Elastomers. *J. Colloid Sci.* **1956**, *11*, 39–47
- ²⁵⁴ Yan, P.; Zhao, W.; Fu, X.; Liu, Z.; Kong, W.; Zhou, C.; Lei, J. Multifunctional Polyurethane-Vitrimers Completely Based on Transcarbamoylation of Carbamates: Thermally-Induced Dual-Shape Memory Effect and Self-Welding. *RSC Adv.* **2017**, *7*, 26858–26866..
- ²⁵⁵ Fortman, D. J.; Sheppard, D. T.; Dichtel, W. R. Reprocessing Cross-Linked Polyurethanes by Catalyzing Carbamate Exchange. *Macromolecules* **2019**, *52*, 6330–6335.
- ²⁵⁶ Sheppard, D. T.; Jin, K.; Hamachi, L. S.; Dean, W.; Fortman, D. J.; Ellison, C. J.; Dichtel, W. R. Reprocessing Postconsumer Polyurethane Foam Using Carbamate Exchange Catalysis and Twin-Screw Extrusion. *ACS Cent. Sci.* **2020**, *6*, 921–927.
- ²⁵⁷ Yue, L.; Bonab, V. S.; Yuan, D.; Patel, A.; Karimkhani, V.; Manas-Zloczower, I. Vitrimerization: A Novel Concept to Reprocess and Recycle Thermoset Waste via Dynamic Chemistry. *Glob. Challenges* **2019**, *3*, 1800076.
- ²⁵⁸ Snyder, R. L.; Fortman, D. J.; De Hoe, G. X.; Hillmyer, M. A.; Dichtel, W. R. Reprocessabel Acid-Degradable Polycarbonate Vitrimers. *Macromolecules* **2018**, *51*, 389–397.
- ²⁵⁹ İshibashi, J. S. A.; Kalow, J. A. Vitrimeric Silicone Elastomers Enabled by Dynamic Meldrum's Acid-Derived Cross-Links. *ACS Macro Lett.* **2018**, *7*, 482–486.
- ²⁶⁰ Sun, X.; Anslyn, E. V. An Auto-Inductive Cascade for the Optical Sensing of Thiols in Aqueous Media: Application in the Detection of a VX Nerve Agent Mimic. *Angew. Chem., Int. Ed.* **2017**, *56*, 9522–9526.
- ²⁶¹ Snyder, R. L.; Lidston, C. A. L.; De Hoe, G. X.; Parvulescu, M. J. S.; Hillmyer, M. A.; Coates, G. W. Mechanically Robust and Reprocessable Imine Exchange Networks from Modular Polyester Pre-Polymers. *Polym. Chem.* **2020**, *11*, 5346–5355.
- ²⁶² Jin, K.; Kim, S.-S.; Xu, J.; Bates, F. S.; Ellison, C. J. Melt-Blown Cross-Linked Fibers from Thermally Reversible Diels—Alder Polymer Networks, *ACS Macro Letters* **2018**, *7*, 1339–1345.

- ²⁶³ Jin, K.; Benerji, A.; Kitto, D.; Bates, F. S.; Ellison, C. J. Mechanically Robust and Recyclable Cross-Linked Fibers from Melt Blown Anthracene-Functionalized Commodity Polymers ACS Appl. Mater. Interfaces 2019, 11, 12863-12870.
- ²⁶⁴ Tapping America's Potential: The Education for Innovation Initiative. *Business Roundtable* 1–21.
- ²⁶⁵ prepared by, P. K. The Science and Engineering Workforce: Realizing America's Potential.
- ²⁶⁶ Rising above the Gathering Storm Energizing and Employing America for a Brighter Economic Future; Committee on Prospering in the Global Economy of the 21st Century (U.S.), Committee on Science, E., Eds.; National Academies Press: Washington, D.C., 2007.
- ²⁶⁷ Cleaves, A. The Formation of Science Choices in Secondary School, *International Journal of Science Education* 27, 471–486.
- ²⁶⁸ Kidd, G.; Naylor, F. The Predictive Power of Measured Interests in Tertiary Course Choice: The Case of Science. Australian Journal of Education 1991, 35, 261–272.
- ²⁶⁹ Maltese, A. V.; Tai, R. H. Eveballs in the Fridge: Sources of Early Interest in Science. *International Journal of* Science Education 2009, 32, 669-685.
- ²⁷⁰ Tai, R. H.; Liu, C. Q.; Maltese, A. V.; Fan, X. Planning Early for Careers in Science. Science 2006, 312, 1143– 1144.
- ²⁷¹ Marks, H. M. Student Engagement in Instructional Activity: Patterns in the Elementary, Middle, and High School Years. American Educational Research Journal 2000, 37, 153–184.
- ²⁷² Bouillion, L. M.; Gomez, L. M. Connecting School and Community with Science Learning; Real World Problems and School-Community Partnerships as Contextual Scaffolds. Journal of Research in Science Teaching **2001**, 38, 878–898...
- ²⁷³ Rivet, A. E.; Krajcik, J. S. Contextualizing Instruction: Leveraging Students' Prior Knowledge and Experiences to Foster Understanding of Middle School Science. Journal of Research in Science Teaching 2007, 45, 79-100.
- ²⁷⁴ Maltese, A. v.; Tai, R. H. Pipeline Persistence: Examining the Association of Educational Experiences with Earned Degrees in STEM among U.S. Students. Science Education 2011, 95, 877-907.
- ²⁷⁵ See: https://4-h.org
- ²⁷⁶ SciGirls CONNECT. SciGirls Strategies: How to Engage Girls in STEM http://www.scigirlsconnect.org/scigirlsstrategies-engage-girls-stem/ (accessed May 14, 2020).
- ²⁷⁷ Be a 4-H Scientist 4hpolymers.org (accessed May 13, 2020).
- ²⁷⁸ Anastas, P. T. Green Chemistry: Theory and Practice; Warner, J. C., Ed.; Oxford University Press: Oxford [England]; New York, 2000.

 279 Martello, M. T.; Burns, A.; Hillmyer, M. Bulk Ring-Opening Transesterification Polymerization of the
- Renewable δ-Decalactone Using an Organocatalyst. ACS Macro Letters 2012, 1, 131–135.
- ²⁸⁰ Schneiderman, D. K.; Gilmer, C.; Wentzel, M. T.; Martello, M. T.; Kubo, T.; Wissinger, J. E. Sustainable Polymers in the Organic Chemistry Laboratory: Synthesis and Characterization of a Renewable Polymer from δ-Decalactone and L-Lactide. *Journal of Chemical Education* **2014**, *91*, 131–135.
- ²⁸¹ Fahnhorst, G.; Swingen, Z.; Schneiderman, D.; Blaquiere, C.; Wentzel, M.; Wissinger, J. Synthesis and Study of Sustainable Polymers in the Organic Chemistry Laboratory: An Inquiry-Based Experiment Exploring the Effects of Size and Composition on the Properties of Renewable Block Polymers; 2016; pp 123–147. https://doi.org/10.1021/bk-2016-1233.ch008.
- ²⁸² Halpern, J. M.; Urbanski, R.; Weinstock, A. K.; Iwig, D. F.; Mathers, R. T.; von Recum, H. A. A Biodegradable Thermoset Polymer Made by Esterification of Citric Acid and Glycerol. Journal of Biomedical Materials Research Part A 2014, 102, 1467–1477.
- ²⁸³ Harris, R.; Ahrenstorff, C.; Theryo, G.; Johnson, A.; Wissinger, J. E. Make it and Break it: Bioplastics from Plant Starch with Incorporation of Engineering Practices https://csp.umn.edu/wp-content/uploads/2017/03/Make-it-and-Break-it.pdf (accessed May 19, 2020).
- ²⁸⁴ Knutson, C. M.; Hilker, A. P.; Tolstyka, Z. P.; Anderson, C. B.; Wilbon, P. A.; Mathers, R. T.; Wentzel, M. T.; Perkins, A. L.; Wissinger, J. E. Dyeing to Degrade: A Bioplastics Experiment for College and High School Classrooms. Journal of Chemical Education 2019, 96, 2565–2573.

- ²⁸⁵ Knutson, C. M.; Schneiderman, D. K.; Yu, M.; Javner, C. H.; Distefano, M. D.; Wissinger, J. E. Polymeric Medical Sutures: An Exploration of Polymers and Green Chemistry. Journal of Chemical Education 2017, 94, 1761-1765.
- ²⁸⁶ National Research Council, 2013, Next generation science standards for states by states: Appendix J. Science, technology, society and the environment. Retrieved from http://www.nextgenscience. org/sites/ngss/files/APPENDIX% 20J, 204, 13.
- ²⁸⁷ Wissinger, J. E.; Knutson, C. M.; Javner, C. H. Designing Impactful Green and Sustainable Chemistry Workshops for High School Teachers. In Chemistry Education for a Sustainable Future, Vol. 1: High School, Outreach, and Global Perspectives; Obare, S., Peterman, K., Middlecamp, C., Eds.; ACS Symposium Series, 2020;
- pp 1–14.
 ²⁸⁸ Sarkar, P.; Bhowmick, A. K. Green Approach toward Sustainable Polymer: Synthesis and Characterization of Poly(Myrcene-Co-Dibutyl Itaconate). ACS Sustainable Chem. Eng. 2016, 4, 2129–2141.
- ²⁸⁹ Gormong, E. A.; Wentzel, M. T.; Cao, B.; Kundel, L. N.; Reineke, T. M.; Wissinger, J. E. Exploring Divergent Green Reaction Media for the Copolymerization of Biobased Monomers in the Teaching Laboratory. J. Chem. Educ.
- ²⁹⁰ NSF Center for Sustainable Polymers. Beyond the Classroom https://csp.umn.edu/beyond-the-classroom/ (accessed May 13, 2020).
- ²⁹¹ Data Repository for U of M (DRUM) https://conservancy.umn.edu/handle/11299/166578 (accessed May 18,
- ²⁹² Data Curation Network A shared staffing model for digital data repositories https://datacurationnetwork.org/
- (accessed May 15, 2020). ²⁹³ Center for Sustainable Polymers (CSP) https://conservancy.umn.edu/handle/11299/193178 (accessed December 13, 2020).